ITERATED REGULARIZATION METHODS FOR SOLVING INVERSE PROBLEMS

by

Nathaniel Mays

B.S. in Mathematics, West Virginia University, 2005

B.S. in Mechanical Engineering, West Virginia University, 2005

Submitted to the Graduate Faculty of

Arts and Sciences in partial fulfillment

of the requirements for the degree of

Doctor of Philosophy in Mathematics

University of Pittsburgh

2011

UNIVERSITY OF PITTSBURGH

ARTS AND SCIENCES

This dissertation was presented

by

Nathaniel Mays

It was defended on

May 24, 2011

and approved by

W. Layton, Ph. D., Professor

P. Smolinski, Ph. D., Associate Professor

C. Trenchea, Ph. D., Assistant Professor

I. Yotov, Ph. D., Professor

Dissertation Director: W. Layton, Ph. D., Professor

ITERATED REGULARIZATION METHODS FOR SOLVING INVERSE PROBLEMS

Nathaniel Mays, PhD

University of Pittsburgh, 2011

Typical inverse problems are ill-posed which frequently leads to difficulties in calculating numerical solutions. A common approximation method to solve ill-posed inverse problems is iterated Tikhonov-Lavrentiev regularization.

We examine iterated Tikhonov-Lavrentiev regularization and show that, in the case that regularity properties are not globally satisfied, certain projections of the error converge faster than the theoretical predictions of the global error. We also explore the sensitivity of iterated Tikhonov regularization to the choice of the regularization parameter. We show that by calculating higher order sensitivities we improve the accuracy. We present a simple to implement algorithm that calculates the iterated Tikhonov updates and the sensitivities to the regularization parameter. The cost of this new algorithm is one vector addition and one scalar multiplication per step more than the standard iterated Tikhonov calculation.

In considering the inverse problem of inverting the Helmholz-differential filter (with filter radius δ), we propose iterating a modification to Tikhonov-Lavrentiev regularization (with regularization parameter α and J iteration steps). We show that this modification to the method decreases the theoretical error bounds from $\mathcal{O}(\alpha(\delta^2+1))$ for Tikhonov regularization to $\mathcal{O}((\alpha\delta^2)^{J+1})$. We apply this modified iterated Tikhonov regularization method to the Leray deconvolution model of fluid flow. We discretize the problem with finite elements in space and Crank-Nicolson in time and show existence, uniqueness and convergence of this solution.

We examine the combination of iterated Tikhonov regularization, the L-curve method,

a new stopping criterion, and a bootstrapping algorithm as a general solution method in brain mapping. This method is a robust method for handling the difficulties associated with brain mapping: uncertainty quantification, co-linearity of the data, and data noise. We use this method to estimate correlation coefficients between brain regions and a quantified performance as well as identify regions of interest for future analysis.

TABLE OF CONTENTS

LIST OF TABLES

LIST OF FIGURES

PREFACE

Many people helped directly and indirectly with the completion of this thesis.

Firstly, I'd like to thank my advisor, Dr. Layton, for his near infinite amount of patience in my education. He always told me exactly what I needed to hear even if it is not what I wanted to hear. He encouraged me to see the big picture and the implications beyond the current problem, which increased my appreciation of mathematics. Thanks to him, I will always appreciate that the more red there is on a paper, the closer it is to completion.

I'd like to thank my wife, Eva, for her patience and understanding that some months need to be dedicated completely to Math (in particular the months around preliminary exams, comprehensive exams, my overview and this thesis). I'd like to thank her for her love, support, and encouragement to persevere through the difficult times of graduate school. She has always been willing to patiently listen to a presentation whenever I needed to practice a talk.

I'd like to thank my instructors Prof. Ivan Yotov and Prof. Catalin Trenchea for their valuable feedback in classes and on this thesis, Prof. Lothar Reichel for his time and conversations about inverse problems and the Swedish language, and Dr. Myron Sussman for the most important lesson in programming that I ever learned (**always** have a way of verifying that your code is correct). Thanks go to my entire committee for all of their help and comments.

I'd also like to acknowledge everyone who has helped with particular parts of this thesis. Chapter 2 is based on a joint paper with Prof. William Layton and Dr. Ross Ingram. Chapter 3 is based on a joint paper with Ming Zhong. Chapter 4 is based on a joint paper with Dr. Ross Ingram, Prof. Carolina Manica, and Prof. Iuliana Stanculescu. Chapter 5 is based on a joint paper with Dr. Caterina Rosano, Dr. Howard Aizenstein, Dr. Robert

Boudreau, Dr. Elisabeta Marai, Adrian Maries, Dr. Kim Wong and Dr. S. Levent Yilmaz.

Lastly, I'd like to thank my family for their love and for supporting and encouraging me to follow whatever direction I chose.

1.0 INTRODUCTION

"Most people, if you describe a train of events to them, will tell you what the result would be. They can put those events together in their minds, and argue from them that something will come to pass. There are few people, however, who, if you told them a result, would be able to evolve from their own inner consciousness what the steps were which led up to that result." (Sherlock Holmes)

Inverse problems (complementing direct problems) are ubiquitous. Any observable physical phenomenon (direct problem) has the associated inverse problem, "What caused this effect?" Specific examples of inverse problems are: parameter identification - given a model with tuning parameters and measurements of the output of the model, what values of the parameters best correspond to the measurements; image processing - given an image that has been blurred, find the original image; wave scattering - given a source of vibration on the surface and measurements of the returning waves, determine the underlying structure that the waves pass through.

Hadamard defined a well-posed problem to be a problem with the existence of a unique solution that depends continuously on the problem data, and an ill-posed problem is one that violates one or more of those conditions. Inverse problems are typically ill-posed. Many methods, see [23], have been proposed to give approximate solutions when no solution exists.

Two archetypical examples are the linear and non-linear inverse problems.

Problem 1.0.1 (Linear inverse problem)**.** *Given Hilbert spaces X and Y, linear operator $A : X \to Y$, data $y \in Range(A)$, and noise $e \in Y$, we denote $b = y + e$. The linear inverse*

problem is to find x satisfying

$$Ax = b. \tag{1.1}$$

Problem 1.0.2 (Non-linear inverse problem)**.** *Given Hilbert spaces X and Y, non-linear operator $F : X \to Y$, data $y \in Range(F)$, and noise $e \in Y$, we denote $b = y + e$. The non-linear inverse problem is to find x satisfying*

$$F(x) = b. \tag{1.2}$$

Definition 1.0.3 (Condition number)**.** *The condition number $\kappa(A)$ of a linear operator A with respect to an operator norm $\|\cdot\|$ is*

$$\kappa(A) = \begin{cases} \|A^{-1}\|\|A\| & A \text{ is nonsingular} \\ \infty & A \text{ is singular.} \end{cases} \tag{1.3}$$

An operator is said to be perfectly conditioned if $\kappa(A) = 1$, well-conditioned if $\kappa(A)$ is small, and ill-conditioned if $\kappa(A)$ is large.

A discussion on the ill-conditioning of non-linear equations can be found in [75].

Proposition 1.0.4. *Let $x^*, b, e \in \mathbb{R}^n$ and $A \in \mathbb{R}^{n\times n}$. If $Ax^* = b$ with $b \neq 0$ and $\tilde{x}$ is a calculated solution to $Ax = b + e$, then the relative error is bounded.*

$$\frac{\|x^* - \tilde{x}\|}{\|x^*\|} \leq \kappa(A)\frac{\|e\|}{\|b\|}. \tag{1.4}$$

Proof. This is a well-known result, see [46, 75]. □

Definition 1.0.5 (Argmin)**.** *The argmin of a functional $f : X \to \mathbb{R}$ is the set of values in X defined by*

$$\underset{x\in X}{\operatorname{argmin}} f(x) = \{x \in X | f(x) \leq f(y), \quad \forall y \in X\}.$$

If $\underset{x\in X}{\operatorname{argmin}} f(x)$ contains a single element, then let $\underset{x\in X}{\operatorname{argmin}} f(x)$ denote that element.

One method of solving inverse problems is ordinary least squares (OLS).

Algorithm 1.0.6 (Ordinary Least Squares)**.** *The least squares solution to Problem 1.0.1 is found by solving the minimization problem*

$$x_{OLS} = \underset{x \in X}{\operatorname{argmin}} \|Ax - b\|^2.$$

An equivalent formulation for the least squares solution to Problem 1.0.1 is to solve for x_{OLS} in

$$A^T A x_{OLS} = A^T b,$$

where A^T denotes the transpose of the operator A. The least squares solution to Problem 1.0.2 is found by solving the minimization problem (if the minimum exists)

$$x_{OLS} \in \underset{x \in X}{\operatorname{argmin}} \|F(x) - b\|^2.$$

Remark 1.0.7. *In the special case of the spectral norm and if A is a normal operator ($A^T A = AA^T$), then $\kappa(A^T A) = (\kappa(A))^2$. Therefore, in the case that A is normal and ill-conditioned, then ordinary least squares becomes a more difficult problem to solve.*

One method for approximating the solution to an ill-posed problem is Tikhonov regularization.

Definition 1.0.8 (Tikhonov Regularization - linear)**.** *For a given regularization parameter $\alpha > 0$, the Tikhonov solution x_α to Problem 1.0.1 is calculated by solving*

$$(A^T A + \alpha I) x_0 = A^T b. \tag{1.5}$$

Solving (1.5) for x_α is equivalent to solving the minimization problem

$$x_0 = \underset{x \in X}{\operatorname{argmin}} \|Ax - b\|^2 + \alpha \|x\|^2. \tag{1.6}$$

Equation (1.6) shows that Tikhonov regularization and the choice of α is a balance between minimizing the residual (accuracy) and minimizing the size of the solution (stability). In another method, iterated Tikhonov regularization, the regularization parameter α is chosen for stability and iterates to regain accuracy.

Definition 1.0.9 (Iterated Tikhonov regularization)**.** *For a given regularization parameter $\alpha > 0$ and stopping parameter $J \in \mathbb{N}$, the iterated Tikhonov solutions x_j for $j = 1, \ldots, J$ to Problem 1.0.1 are calculated by solving*

$$\begin{aligned}(A^TA + \alpha I)x_0 &= A^Tb \\ (A^TA + \alpha I)(x_j - x_{j-1}) &= A^T(b - Ax_{j-1}).\end{aligned} \tag{1.7}$$

Solving (1.7) for x_j for $j = 1, \ldots, J$ is equivalent to solving the minimization problem

$$\begin{aligned}x_0 &= \underset{x \in X}{\operatorname{argmin}} \|Ax - b\|^2 + \alpha\|x\|^2 \\ x_j &= \underset{x \in X}{\operatorname{argmin}} \|Ax - b\|^2 + \alpha\|x - x_{j-1}\|^2.\end{aligned} \tag{1.8}$$

The defect correction method (Algorithm 1.0.10 and [97]) is an iterative method to find the solution to Problem 1.0.1 (and generalized to non-linear problems in [97]).

Algorithm 1.0.10 (Defect Correction Method)**.** *Let A, x, and b be as in Problem 1.0.1. Let G be an approximate inverse of A. Then calculate the approximation x_0 by*

$$x_0 = Gb.$$

Given x_{j-1}, the next approximation x_j is calculated by

$$x_j - x_{j-1} = x_0 - GAx_{j-1}$$

Remark 1.0.11 (Connection of iterated Tikhonov regularization to the defect correction method)**.** *The defect correction method is an iterative method for finding an approximation to the solution of Problem 1.0.1. Choosing $G = (A^TA + \alpha I)^{-1}A^T$, the defect correction method reduces to iterated Tikhonov regularization.*

Equations (1.5) and (1.7) are valid only for the linear Problem 1.0.1, but (1.6) and (1.8) are generalizable to the nonlinear Problem 1.0.2. The Tikhonov solution to Problem 1.0.2 is found by solving the minimization problem

$$x_\alpha = \underset{x \in X}{\operatorname{argmin}} \|F(x) - b\|^2 + \alpha \|x\|^2,$$

and the iterated Tikhonov solution is found by taking $x_{-1} = 0$ and solving

$$x_i = \underset{x \in X}{\operatorname{argmin}} \|F(x) - b\|^2 + \alpha \|x - x_{i-1}\|^2.$$

Algorithm 1.0.12 (Iterated Tikhonov-Lavrentiev regularization)**.** *If the operator A in Problem 1.0.1 is symmetric and non-negative definite, then for a given regularization parameter $\alpha > 0$ and stopping parameter $J \in \mathbb{N}$, the iterated Tikhonov-Lavrentiev solutions x_j for $j = 1, \ldots, J$ to Problem 1.0.1 are calculated by solving*

$$\begin{aligned} (A + \alpha I)x_0 &= A^T b \\ (A + \alpha I)(x_j - x_{j-1}) &= b - Ax_{j-1}. \end{aligned} \tag{1.9}$$

Proposition 1.0.13 (Error bound for iterated Tikhonov-Lavrentiev regularization)**.** *Let A, b, α and x_j be as in Algorithm 1.0.12. Suppose that $e = 0$, that is $b = Ax$ for some $x \in X$. If $x \in \mathrm{Range}(A^\beta)$ for some $\beta \geq 0$ (regularity condition), then, for any $J \leq \beta$, there exists a constant $C(J)$ such that*

$$\|x - x_J\| \leq C(J)\alpha^{J+1}. \tag{1.10}$$

Furthermore, for any $J > \beta$, there exists a constant $C(J)$ such that

$$\|x - x_J\| \leq C(J)\alpha^{\beta+1}. \tag{1.11}$$

Proof. This is a summary of results from [21, 23, 51, 107]. □

Chapter 2 presents a new superconvergence property for iterated Tikhonov-Lavrentiev regularization. Previous work [23] has shown that given sufficient regularity of the solution ($x \in \text{Range}(A^J)$ in Proposition 1.0.13), then the error bound to the problem with $e = 0$ is $\|x - x_J\| = \mathcal{O}(\alpha^{J+1})$ for Tikhonov-Lavrentiev regularization. However, when the regularity condition is violated ($x \in \text{Range}(A^\beta)$ for $\beta < J$), then further iterations will not improve the error bound ($\|x - x_J\| = \mathcal{O}(\alpha^{\beta+1})$). Theorem 2.2.11 shows that if the regularity properties are not globally satisfied, then there exists a projection P such that $\|P(x - x_J)\| = \mathcal{O}(\alpha^{J+1})$.

We also explore the sensitivity of iterated Tikhonov-Lavrentiev regularization to the choice of the regularization parameter chosen. We show that higher order sensitivities correct for accuracy. Algorithm 2.3.2 is a simple-to-implement procedure that calculates the iterated Tikhonov-Lavrentiev updates and the sensitivities to the regularization parameter at the cost of one vector addition and one scalar multiplication per step beyond that of the standard iterated Tikhonov-Lavrentiev calculation.

Chapter 3 examines the problem of deconvolving the Helmholz differential filter (with filter radius δ). In [67], it was shown that the error in the solution when using Tikhonov-Lavrentiev regularization was $\mathcal{O}(\alpha(1 + \delta^2))$, but the error could be reduced to $\mathcal{O}(\alpha\delta^2)$ by using a modified Tikhonov-Lavrentiev regularization that exploits the properties of the filter. Algorithm 3.3.1 is an extension of the algorithm presented in [67] to an iterated method, and we show that for J iteration steps, the error is $\mathcal{O}((\alpha\delta^2)^{J+1})$. Theorem 3.4.2 is a stopping criteria of the iteration process to prevent convergence to a noisy solution. We provide numerical examples to verify these error bounds and the stopping condition.

Chapter 4 presents a general theory for regularization models of the Navier-Stokes equations based on the Leray deconvolution model with a general deconvolution operator designed to fit a few important key properties listed in Assumption 4.2.4. We study the mathematical properties of these operators and show that the modified iterated Tikhonov-Lavrentiev operator from Chapter 3 satisfies Assumption 4.2.4. An existence theory is derived for the family of models, and a rigorous convergence theory is derived for the resulting algorithms. Numerical experiments supporting our theoretical results are presented for the case of the modified iterated Tikhonov-Lavrentiev operator mentioned above.

Chapter 5 applies iterated Tikhonov regularization and the L-curve method in Algorithm

5.1.1, the Brain-Gait Correlator, a useful tool for examining the problem of brain mapping. There is consistent evidence that smaller brain volume is associated with slowing gait in older adults. Finding a reliable, precise and localized spatial correlation of neuroimaging data with gait data is a challenging problem. This is difficult due to the uncertainty, co-linearity, and sparsity. The challenge increases as the spatial description becomes more localized.

This chapter gives a reliable and accurate algorithm for dealing with the uncertainty, approximate co-linearity and data noise in this problem. We propose Algorithm 5.1.1, the Brain-Gait Correlator, which combines iterated Tikhonov regularization and the L-curve method. Algorithm 5.1.9 is a new stopping criterion that we show prevents iterated Tikhonov regularization from converging to the noisy solution. As a first test of the algorithm, we validate our initial findings of the spatial distribution of volumetric brain loss in relationship with gait speed. Next, we compare and present results of a combination of iterated Tikhonov regularization with the L-curve method applied to real data derived from two cohorts of older adults. We demonstrate that the L-curve method automatically chooses additional regularization for enhanced stability, which will dampen the effects of ill conditioning. Finally, the analysis indicates that smaller volume of the dorsolateral prefrontal cortex in the left hemisphere is associated with slower gait consistent with prior studies. This algorithm is more robust with increased levels of noise than least squares regression. The algorithm produces reliable results when least squares regression fails, as shown by an example where least squares regression is not a sufficiently robust solution method by adding 10% noise into a problem and observing 9,324,000% error in the solution.

2.0 ITERATED TIKHONOV REGULARIZATION

"[Paradoxes] can be traced to the use of plausible arguments. Among these are the arguments that 'small causes produce small effects' and that 'symmetric causes produce symmetric effects'." (G. Birkhoff)

2.1 INTRODUCTION

Inverse problems and other ill-posed problems arise in application areas in material, environmental, and energy research and development [23, 45, 53, 57, 103].

Problem 2.1.1 (Noisy inverse problem)**.** *Let X be a Hilbert space and $G : X \to X$ a linear, compact operator. Suppose that $\phi_{true} \in X$ and $G\phi_{true} = \bar{\phi}$, however only noisy data $y = \bar{\phi} + noise$ is known. As accurately as possible, determine the noise-free solution $\phi_{true} \in X$ $\phi_{true} \in X$ satisfying $G\phi_{true} = \bar{\phi}$:*

$$G\phi = \bar{\phi} + noise. \tag{2.1}$$

In the case of multiple solutions to (2.1), the minimum norm solution is chosen.

Our motivation for considering Problem 2.1.1, arises in parameter identification [22, 23], deconvolution in image processing [11], and the closure problem in turbulence modeling [10, 28, 59]. An example of the type of operator from Problem 2.1.1 is the differential filter in Example 2.1.2 [19, 27].

Example 2.1.2. *An operator satisfying Problem 2.1.1 is the Helmholz differential filter. Let* Ω *be a regular, bounded, polyhedral domain. The differential filter* $G : L^2(\Omega) \to L^2(\Omega)$ *is defined by* $G\phi_{true} = \bar{\phi}$ *where*

$$-\delta^2 \Delta \bar{\phi} + \bar{\phi} = \phi.$$

One family of solution methods to Problem 2.1.1, regularization methods, require a source condition on the true solution to obtain error estimates.

Definition 2.1.3 (Source condition)**.** *We say that the true solution* ϕ_{true} *to Problem 2.1.1 satisfies a source condition if for some* $\beta > 0$*,*

$$\phi_{true} \in Range(G^\beta). \tag{2.2}$$

If the solution satisfies the source condition for $\beta \geq 1$, then iteration of the regularization methods yields better error bounds. However, if the source condition is not satisfied for a large enough β and an iterative method is applied, then traditional error analysis methods predict worse global errors with the number of iterations. We show that even without the source condition, some projections of the error decrease with further iterations.

The fundamental difficulties in solving Problem 2.1.1 are that (i) G is not generally stably invertible and (ii) the best estimate of $\bar{\phi}$ is generally not in Range(G) due to noise contamination.

When ϕ_{true} is smooth in the sense of satisfying a source condition, $\phi_{true} \in$ Range(G^β) for some $\beta > 0$, highly effective methods are known for solving Eq. (2.1). We focus our analysis on the case of low regularity solutions. Examples of this are using the differential filter applied to solutions of the Navier-Stokes equations [25,54] or applying a Gaussian filter to a discontinuous L^2 image [11, 88].

A full theory of the global error under the source condition given above for various regularization schemes is known, see e.g. [1,4,23,41,70,86,106,109]. We present herein several extensions to the error analysis for a family of iterative regularization schemes including

- superconvergence in large scales of solution space *without source conditions* and
- characterization of sensitivity in parameter selection.

A particular iterated regularization method considered is the iterated Tikhonov-Lavrentiev regularization method.

Definition 2.1.4 (Iterated Tikhonov-Lavrentiev regularization)**.** *For operator $G : X \to X$, we define $\phi_j := D_j y$ for $j = 0, 1, \ldots$ by*

$$\phi_0 = (G + \alpha I)^{-1} y, \qquad \phi_j - \phi_{j-1} = (G + \alpha I)^{-1}(y - G\phi_{j-1}). \tag{2.3}$$

However, this generalizes into a family of iterated regularization operators. Let $D_0 : X \to X$ denote a particular regularization operator (e.g. $D_0 = (G + \alpha I)^{-1}$ for Tikhonov-Lavrentiev or $D_0 = (G^*G + \alpha I)^{-1}G^*$ for Tikhonov). For $j = 0, 1, \ldots$, define the iterated regularization $D_j : X \to X$ (derived from D_0) by $\phi_j := D_j y$ through:

$$\phi_0 = D_0 y, \qquad \phi_j - \phi_{j-1} = D_0(y - G\phi_{j-1}). \tag{2.4}$$

See Condition 2.1.10 in Section 2.1.2 for a precise setting for the operators G and D_0.

Practical problems having limited regularity are problematic when obtaining error estimates for iterated regularization methods. For example, it is well known (see [51] and Section 2.1.2 that follows) that if ϕ_j represents the j-th iterated Tikhonov regularization approximation, $\phi_{true} \in \text{Range}(G^*G)^\beta$ for some $0 < \beta \leq J$ (source condition), and the noise is bounded by $\|\epsilon\|_X \leq \epsilon_0 < \infty$, then

$$\|\phi_{true} - \phi_J\|_X \leq \alpha^{-1/2}(J + 1)\epsilon_0 + \alpha^{\beta+1}C(J).$$

Consequently, if $\beta < 1$, the present global error theory for iterated Tikhonov gives a worse error bound for each step beyond $J = 0$. However, we show that even in the case of limited regularity, iterated Tikhonov regularization continues to improve the approximation for some components of the approximate solution. Results of this type are often called *superconvergence* because they show a greater rate of convergence by some components of the approximation than predicted by the global theory [90].

In Section 2.1.1, we provide a brief description of our main motivation, the closure problem in turbulence modeling, because the solution does not satisfy the regularity conditions necessary for applying iterated deconvolution methods [54]. In Section 2.1.2, we introduce several approximate deconvolution operators satisfying Eq. (2.4) and Condition 2.1.10. In

Section 2.2, we present and prove our main result – recovery of optimal accuracy of iterated regularization methods defined by Eq. (2.4) and Condition 2.1.10 when the source condition is not satisfied.

In Section 2.3.1, we extend results by Leonov [62] from Tikhonov regularization to iterated Tikhonov-Lavrentiev. In particular, we prove that each step of iterated Tikhonov-Lavrentiev computes the sensitivity of the approximation with respect to the regularization parameter α. There are two approaches to the interpretation: either the sensitivity are computed and used to update the approximations, or the updates are computed and generate the sensitivities. We propose an associated algorithmic modification to iterated Tikhonov-Lavrentiev regularization. In Section 2.3.2, by direct calculation for our motivating problem of the deconvolution of turbulent velocities, we confirm the classical, global error estimate for iterated Tikhonov-Lavrentiev and the optimal convergence in large scales consistent with superconvergence theory presented in Section 2.2.3. The theoretical predictions are confirmed with a numerical test in Section 2.4.

2.1.1 Approximate deconvolution in turbulence modeling

We are motivated by the closure problem in modeling turbulent fluid flow with the Navier-Stokes equations [10, 28, 59]. Accuracy for this application improves with additional deconvolution steps (minimally one per time step) inside a numerically intensive calculation (small time steps and long time calculations are required for computing turbulent flows) [16]. The solutions are not generally regular [25, 54]. Moreover, the noise ϵ includes the error in the turbulence model used as well as numerical errors and their successive accumulation through time evolution. Consequently, an exact characterization of the noise is not feasible. We show that iterated Tikhonov-Lavrentiev is particularly well adapted for this type of situation.

Definition 2.1.5 (Fourier series)**.** *Let $u(x,t) : (0,\pi)^3 \times [0,T] \to \mathbb{R}^3$ be a π-periodic velocity field. Denote $\hat{u}(\boldsymbol{k},t) = \pi^{-3}\int u(x,t)e^{i\boldsymbol{k}\cdot x}dx$ to be the Fourier coefficients where $\boldsymbol{k} = (k_1,k_2,k_3)$ is the wave number vector and $k = |\boldsymbol{k}|$ is the magnitude of $\boldsymbol{k}$. Then*

$$u(x,t) = \sum_{\boldsymbol{k}\in\mathbb{Z}^3} \hat{u}(\boldsymbol{k},t)e^{-i\boldsymbol{k}\cdot x} = \sum_{k}\left(\sum_{k-1<|\boldsymbol{k}|\le k} \hat{u}(\boldsymbol{k},t)e^{-i\boldsymbol{k}\cdot x}\right). \tag{2.5}$$

Definition 2.1.6 (Space of large scales)**.** *For a length scale δ, define the space of large scales to be*

$$X_{large} := span\left\{e^{i\boldsymbol{k}\cdot x} : |\boldsymbol{k}| \leq 1/\delta\right\}. \tag{2.6}$$

According to the well accepted K41 theory of turbulence (a phenomenological theory in good agreement with experimental data [73]), most of the kinetic energy of the flow resides in the large scales corresponding to small wave numbers. See Section 2.3.2 for more details. Consequently, we consider a filter G with filter radius $\delta > 0$ and associated cutoff frequency $1/\delta$. The *resolved or large scales* in a turbulent flow are those length scales above δ or equivalently, those with frequencies below $1/\delta$. As a specific example, we consider the differential filter.

Definition 2.1.7 (Differential Filter)**.** *The differential filter $G : L^2((0,\pi)^3) \to L^2((0,\pi)^3)$ for a filter radius δ is defined as $G = (-\delta^2\Delta + 1)^{-1}$. For any $u \in L^2((0,\pi)^3)$*

$$Gu = \sum_k \left(\sum_{|\boldsymbol{k}|=k} (\delta^2 k^2 + 1)^{-1} \hat{u}(\boldsymbol{k}, t) e^{-i\boldsymbol{k}\cdot x} \right).$$

It is well-known that G defined here is a linear, compact operator [59].

Definition 2.1.8 (Large scale projection)**.** *Define the L^2- orthogonal projection into the large scales $P : L^2(\Omega) \to X_{large}$ by*

$$P\left(\sum_{\boldsymbol{k}\in\mathbb{Z}^3} \widehat{u}(\boldsymbol{k},t) e^{i\boldsymbol{k}\cdot x} \right) = \sum_{|\boldsymbol{k}|\leq \boldsymbol{1/\delta}} \widehat{u}(\boldsymbol{k},t) e^{i\boldsymbol{k}\cdot x}.$$

The superconvergence result proved in Theorem 2.3.12 for iterated Tikhonov-Lavrentiev regularization states

$$\|P(\phi_{true} - \phi_J)\|_X \leq 2\sqrt{2}\epsilon_0 + \alpha^{J+1} C(J).$$

That is, the error in the energetically important resolved scales, $k < 1/\delta$, is $\mathcal{O}(\alpha^{J+1})$, and the influence of noise in the large scales *does not* grow with increased iterations.

2.1.2 Approximation by regularization

We consider a family of iterated regularization operators for the approximation of Eq. (2.1). Following this, we provide a brief overview of one well-known method fitting this framework, Tikhonov-Lavrentiev regularization.

Definition 2.1.9. *For $G : X \to X$, we say that $G \geq 0$ if G is self-adjoint and*

$$(Gv, v)_X \geq 0, \qquad \forall v \in X. \tag{2.7}$$

Condition 2.1.10. (*Iterated regularization approximations*) *Let $G : X \to X$ be compact, self-adjoint, non-negative definite linear operator. Let $f : \mathbb{R} \to \mathbb{R}$ be a continuous function and $D_0 : X \to X$ be a regularization operator such that $D_0 = f(G)$ is self adjoint, positive definite, bounded and it satisfies*

$$\|G - D_0^{-1}\|_{\mathcal{L}(X,X)} \leq \alpha, \qquad \lambda(D_0) \leq \alpha^{-1}, \qquad \lambda(GD_0) \leq 1. \tag{2.8}$$

The spectral theorem implies that G and D_0 commute, because D_0 is a continuous function of the self-adjoint operator G. Hence, $\lambda(GD_0) = \lambda(G)\lambda(D_0) = \lambda(G)f(\lambda(G))$. The approximation operator associated with iterated Tikhonov-Lavrentiev regularization, developed and analyzed in [21, 51, 106, 107], satisfies these conditions (as shown in Section 2.2.1).

Iterated Tikhonov-Lavrentiev regularization, corresponding to $J > 0$ and $D_0 = (G + \alpha I)^{-1}$, decouples the stability from accuracy by allowing for conservatively large $\alpha > 0$ selection to ensure stability and successive defect correction updates to recover accuracy.

Algorithm 2.1.11 (Iterated Tikhonov-Lavrentiev)**.** *Select $\alpha > 0$ and fix $J \in \mathbb{N}$.*

1. *Solve for ϕ_0 satisfying*

$$(G + \alpha I)\phi_0 = y \tag{2.9}$$

2. *For $j = 1, \ldots, J$, solve for ϕ_j satisfying*

$$(G + \alpha I)(\phi_j - \phi_{j-1}) = y - G\phi_{j-1} \tag{2.10}$$

Note that in the iterated Tikhonov-Lavrentiev method, j is necessarily terminated at a moderate value. The important question is thus convergence as $\alpha \to 0$, and not with respect to J. There is a complete theory of the global error under source conditions, e.g [51]. We summarize results from [21, 23, 51, 107] here.

Theorem 2.1.12 (Global error estimate)**.** *Suppose that G is non-negative definite. Fix $\alpha > 0$. Let $e_J := \phi_{true} - \phi_J$. Suppose, for some $\beta \geq 0$ that $\phi_{true} \in Range(G^\beta)$ and the noise is bounded $\|\epsilon\|_X \leq \epsilon_0 < \infty$. Then, there exists a constant $C(J) < \infty$ such that, for any $0 \leq J \leq \beta$,*

$$\|e_J\|_X \leq \alpha^{-1}(J+1)\epsilon_0 + \alpha^{J+1}C(J). \tag{2.11}$$

Moreover, if $\alpha = \alpha(\epsilon_0) = C\epsilon_0^{1/(J+2)}$ we have that $\|e_J\|_X \leq C\epsilon_0^{1-1/(J+2)}$.

Theorem 2.1.12 shows that a judicious choice of α reduces the error in the approximation $e_j = \phi_{true} - \phi_j$ to the noise level ϵ_0 at each iterated Tikhonov-Lavrentiev update. However, the error increases after a limit is reached which is determined by the smoothness of the underlying solution $J \leq \beta$.

For Tikhonov (-Lavrentiev) selection of the regularization parameter α large enough to ensure stability but small enough to preserve accuracy in approximating ϕ_{true} is a central problem. Several methods for selecting J and α a posteriori are known for iterated Tikhonov (-Lavrentiev) including the L-curve method [40, 42], monotone error rule, using sensitivities [62], and the discrepancy principle. Extrapolation methods based on varying α inside iterated Tikhonov is explored in depth in the work of Hämarik, Palm and Raus [36] and Brezinski, Redivo-zaglia, Rodriguez, and Seatzu [14]. See the work of Engl [21], Hämarik, Palm, and Raus [37], Hämarik and Tautenhahn [38], Gfrerer [29], Leonov [62], Hanke and Groetsch [39], among others.

Also, the sensitivity of the Tikhonov (-Lavrentiev) approximation $s_0(\alpha) := \frac{d\phi}{d\alpha}$ has been studied in detail by Tikhonov and Arsenin [104] and Leonov [62]. In particular, Leonov showed that a pseudo-optimal choice of regularization parameter for Tikhonov regularization can be characterized using sensitivities via the smallest minimizer of $\alpha \mapsto \|\alpha s_0(\alpha)\|_X + \alpha^{-1/2}\epsilon_0$. Theorem 2.3.5 shows that this sensitivity and higher order sensitivities can be used to increase the accuracy of Tikhonov-Lavrentiev approximation in an algorithmically simple

way.

2.2 ERROR ESTIMATION OF LOW-REGULARITY SOLUTIONS

We show in this section that the approximation when $\phi_{true} \in \text{Range}(G^\beta)$ contains hidden accuracy for small β. Indeed, some components of the error can converge faster than the global error.

2.2.1 Error estimates

We derive the error equation for the regularization approximations $\phi_j = D_j y$ satisfying Eq. (2.4) and Condition 2.1.10. Fix j between 0 and $J \in \mathbb{N}$, and let $G \geq 0$. Eliminating intermediate steps in the definition of the iterated regularization approximations in Algorithm 2.1.11 gives

$$D_j = D_0 \sum_{i=0}^{j} (FD_0)^i, \qquad F = F(G, \alpha) := D_0^{-1} - G. \tag{2.12}$$

To derive the error equation for the general iterated regularization approximations, first note that $G\phi_{true} = \bar{\phi}$ so that we can write

$$\phi_{true} - \phi_0 = \phi_{true} - D_0(G\phi_{true} + \epsilon) = -D_0\epsilon + D_0 F \phi_{true},$$

and

$$\begin{aligned} \phi_{true} - \phi_j &= \phi_{true} - D_j(G\phi_{true} + \epsilon) \\ &= -D_0\epsilon - \phi_{j-1} - D_0\left(G\phi_{true} + \epsilon - G\phi_{j-1}\right) = -D_0\epsilon + D_0 F e_{j-1}. \end{aligned}$$

We summarize via elimination of intermediate quantities without further proof:

Proposition 2.2.1. (*Error equation for $G \geq 0$*) *The j-th iterated deconvolution error $e_j := \phi_{true} - \phi_j$ satisfies*

$$e_j = -D_0 \left(\sum_{k=0}^{j} (FD_0)^k \right) \epsilon + (FD_0)^{j+1} \phi_{true}. \tag{2.13}$$

Suppose G is symmetric and non-negative. The general regularity assumption to prove error estimates for regularization schemes is, for some $\beta \geq 0$

$$\phi_{true} \in \text{Range}(G^\beta), \quad \text{(source condition)}. \tag{2.14}$$

We show in this section that the source condition implies the additional Regularity Condition (in Proposition 2.2.2) for iterated regularization operators using Condition 2.1.10. This condition is necessary for the approximation theory of regularization methods.

Proposition 2.2.2. *Suppose that the source condition $\phi_{true} \in \text{Range}(G^\beta)$ is satisfied for some $\beta \geq 0$. Then, (ϕ_{true}, D_0) satisfies*

$$\|D_0^\beta \phi_{true}\|_X \leq C(\beta) < \infty, \quad \textit{(Regularity Condition)}. \tag{2.15}$$

Proof. Recall that we assume $\|D_0\| \leq \alpha^{-1}$. Since G is compact, self-adjoint, and non-negative definite, then the spectral theorem implies the existence of non-negative, real eigenvalues $(\lambda_k(G))_{1\leq k<\infty}$ and corresponding complete, orthonormal set of eigenvectors $(x_k)_{1\leq k<\infty}$ satisfying $Gx_k = \lambda_k(G)x_k$ for $k = 1, 2, \ldots, \infty$. Denote $\hat{\phi}(k) := (\phi_{true}, x_k)_X$ so that $\phi_{true} = \sum_k \hat{\phi}(k)x_k$ and $\|\phi_{true}\|_X^2 = \sum_k |\hat{\phi}(k)|^2$. Furthermore, since $\phi_{true} \in \text{Range}(G^\beta)$ there exists $\psi \in X$ such that $\phi_{true} = G^\beta \psi$. Then,

$$\sum_k |\lambda_k(G)|^{-2\beta} |\hat{\phi}(k)|^2 = \|\psi\|_X^2 < \infty.$$

Note that we can identify $\lambda_k(D_0) = f(\lambda_k(G))$ as a continuous function $f : \mathbb{R} \to \mathbb{R}$ of the self-adjoint operator G. Thus, by direct calculation, we see that

$$\begin{aligned}
\|D_0^\beta\|_X^2 &= \sum_k |\lambda_k(D_0)|^{-2\beta} |\hat{\phi}(k)|^2 \\
&= \sum_k \frac{|\lambda_k(D_0)|^{2\beta}}{|\lambda_k(G)|^{2\beta}} \left(|\lambda_k(G)|^{-2\beta} |\hat{\phi}(k)|^2 \right) \\
&\leq \left(\sup_k |\lambda_k(G)||\lambda_k(D_0)| \right)^{2\beta} \sum_k |\lambda_k(G)|^{-2\beta} |\hat{\phi}(k)|^2 \leq \|\psi\|_X^2 < \infty.
\end{aligned}$$

Here we applied Condition 2.1.10 so that $|\lambda_k(G)||\lambda_k(D_0)| \leq 1$ for all k. □

2.2.2 Superconvergence in interpolation spaces

Before stating and proving the main result, note that the assumption below that $\|G^{J-\beta}\epsilon\|_X \leq \epsilon_0$ follows from $\|\epsilon\|_X \leq \epsilon_0$. However, when G is a smoothing operator, it is possible to get a stronger bound since we often have that $\|G^{J-\beta}\epsilon\|_X << \|\epsilon\|_X$.

Lemma 2.2.3 (Superconvergence of iterated regularization methods)**.** *Let $G \geq 0$ and fix $\alpha > 0$. Let G and $D_0 : X \to X$ satisfy Condition 2.1.10. Suppose that $\phi_{true} \in Range(G^\beta)$ for some $0 \leq \beta < J$ and that the noise satisfies $\|G^{J-\beta}\epsilon\|_X \leq \epsilon_0 < \infty$. Then there exists a constant $C(J) < \infty$ such that*

$$\|G^{J-\beta}(\phi_{true} - \phi_J)\|_X \leq \frac{(J+1)\epsilon_0}{\alpha} + C(J)\alpha^{J+1}. \tag{2.16}$$

Proof. Let $F = D_0^{-1} - G$. First, consider $\beta = J$ so that $\phi_{true} \in \text{Range}(G^J)$. Fix $j \leq J$. Then starting with the error equation (2.13),

$$\begin{aligned}
\|e_j\|_X &= \left\| -D_0 \left(\sum_{k=0}^{j} (FD_0)^k \right) \epsilon + (FD_0)^{j+1} \phi_{true} \right\|_X \\
&\leq \|D_0\|_{\mathcal{L}(X,X)} \left[\sum_{k=0}^{j} \left(\|F\|_{\mathcal{L}(X,X)} \|D_0\|_{\mathcal{L}(X,X)} \right)^k \right] \|\epsilon\|_X \\
&\quad + \|F\|_{\mathcal{L}(X,X)}^{j+1} \|D_0^{j+1} \phi_{true}\|_X.
\end{aligned}$$

From the regularity condition on ϕ_{true} proved in Proposition 2.2.2, we have that

$$\|D^{j+1}\phi_{true}\|_X \leq C(j).$$

From Condition 2.1.10 we can then conclude

$$\|e_j\|_X \leq \frac{(j+1)\epsilon_0}{\alpha} + C(j)\alpha^{j+1}. \tag{2.17}$$

The general result for lower regularity $\phi_{true} \in \text{Range}(G^\beta)$ for $\beta < J$ follows from a change of variables. Indeed, multiply $G\phi_{true} = y$ by $G^{J-\beta}$ to get

$$G\tilde{\phi}_{true} = \tilde{y},$$

where $\tilde{\phi}_{true} = G^{J-\beta}$, and $\tilde{y} = G^{J-\beta}y$. Then, if $\phi_{true} \in \text{Range}(G^\beta)$, it follows that $\tilde{\phi}_{true} \in \text{Range}(G^J)$. Similarly, multiplying the equation for ϕ_j by $G^{J-\beta}$ results in

$$\tilde{\phi}_j - \tilde{\phi}_{j-1} = D_0(\tilde{y} - G\tilde{\phi}_{j-1}),$$

where $\tilde{\phi}_j = G^{J-\beta}\phi_j$ for all $j \leq J$. With noise $\tilde{\epsilon} = G^{J-\beta}\epsilon$, the error estimate for the tilde-problem $\tilde{e}_J = \tilde{\phi}_{true} - \tilde{\phi}_J$ takes the form of Equation (2.17)

$$\|\tilde{e}_J\|_X \leq \frac{(J+1)\epsilon_0}{\alpha} + C(J)\alpha^{J+1}.$$

Therefore, since $\tilde{e}_J = G^{J-\beta}e_J$, the main result follows. □

To put this superconvergence result in its appropriate framework, we further restrict our problem.

Assumption 2.2.4. *X is a separable Hilbert space and $G : X \to X$ compactly and is self adjoint and positive.*

Let $(x_k)_{1\leq k<\infty} \subset X$ be the complete, orthonormal basis for X of eigenvectors of G so that $Gx_k = \lambda_k x_j$ where

$$\lambda_1 \geq \lambda_2 \geq \ldots \lambda_k \geq \lambda_{k+1} \to 0, \quad \text{as } k \to \infty.$$

Furthermore, for any $u \in X$, we can expand u and Gu by

$$u = \sum_{1\leq k<\infty} \widehat{u}_k x_k, \qquad Gu = \sum_{1\leq k<\infty} \lambda_k(G)\widehat{u}_k x_k, \qquad \widehat{u}_k = (u, x_k)_X.$$

We first develop an estimate via negative norms and then use this theory to provide an optimal error estimate in $\|\cdot\|_X$ on large scales.

Definition 2.2.5. *For any $u \in Span\{x_k : k \geq 1\}$,*

$$\|u\|^2_{X_{-s}} := \sum_{k=1}^{\infty} \lambda_k^s |\widehat{u}_k|^2. \tag{2.18}$$

We note that in Eq. (2.18), convergence is not an issue since $\widehat{u}_k$ is only finitely nonzero because $u \in \text{Span}\{x_k : k \geq 1\}$.

Definition 2.2.6. *Suppose that Assumption 2.2.4 holds. Then*

$$X_{-s} = \text{ closure of } X \text{ under } \|\cdot\|_{X_{-s}}. \tag{2.19}$$

Remark 2.2.7. *The parameter $s > 0$ in Eqs. (2.18) and (2.19) is chosen to correspond to the usual Sobolev spaces when $G = (-\delta^2\Delta + I)^{-1}$ under periodic boundary conditions. We observe that $u \in X_{-s}$ with decreasing s corresponds to increasing smoothness since*

$$u \in X_{-s} \quad \Leftrightarrow \quad G^{s/2}u \in X \quad \Leftrightarrow \quad u \in Range(G^{-s/2}).$$

Theorem 2.2.8 (Error estimate in interpolation spaces)**.** *Under the assumptions of Lemma 2.2.3 and Assumption 2.2.4*

$$\|\phi_{true} - \phi_J\|_{X_{-(J-\beta)}} \leq \frac{(J+1)\epsilon_0}{\alpha} + C(J)\alpha^{J+1}. \tag{2.20}$$

Proof. We apply Lemma 2.2.3 to $\|\phi_{true} - \phi_J\|_{X_{-(J-\beta)}}$ to obtain the result. □

Thus, even when the global error in X is not optimal as in the sense of Theorem 2.2.3, the error in a negative norm X_{-s} ($s > 0$) in the scale of Hilbert spaces is much smaller than in $X = X_0$. Theorem 2.2.8 connects superconvergence on large scales to the work of [90] on functionals.

Corollary 2.2.9. *If $\phi \mapsto (\phi, l)_X$ defines a bounded, linear functional, e.g. $l \in X_{J-\beta}$, then*

$$|(l, \phi_{true})_X - (l, \phi_J)_X| \leq \|l\|_{X_{J-\beta}} \left\{ \frac{J+1}{\alpha}\epsilon_0 + \alpha^{J+1}C(J) \right\}.$$

2.2.3 Superconvergence - large scale error estimation

We connect the above abstract result to the application of deconvolution of turbulent velocities. Fix a cutoff $N_0 > 0$ and define a subspace associated with the large scales:

$$X_{N_0} := \text{Span}\left\{x_k : \forall k < N_0\right\}, \quad \text{(truncated function space)}. \tag{2.21}$$

Then we can define the projection operator $P : X \to X_{N_0}$ onto the large scales by

$$Pu := \sum_{1 \le k < N_0} \hat{u}_k x_k. \tag{2.22}$$

Corollary 2.2.10. *Under the assumptions of Lemma 2.2.3 and Assumptions 2.2.4,*

$$\|P(\phi_{true} - \phi_J)\|_X \le C(N_0)\frac{(J+1)\epsilon_0}{\alpha} + C(J)\alpha^{J+1}, \tag{2.23}$$

where $C(N_0) = \lambda_{N_0}^{-(J-\beta)/2} > 0$.

Proof. Note that

$$\|Pu\|_X^2 \le \lambda_{N_0}^{J-\beta} \sum_{k=1}^{N_0} \lambda_k^{-(J-\beta)} |\widehat{u}_k|^2 \le \lambda_{N_0}^{J-\beta} \sum_{k=1}^{\infty} \lambda_k^{-(J-\beta)} |\widehat{u}_k|^2 = \lambda_{N_0}^{J-\beta} \|u\|_{X_{-(J-\beta)}}^2.$$

Now apply the result of Theorem 2.2.8. □

An even more refined result is presented in Section 2.3.2 where, in large scales, the estimate on the noisy contribution, does not grow with J, and additionally, we retain optimal convergence in the noise-free part of the estimate $\mathcal{O}(\alpha^{J+1})$. Motivated by turbulence phenomenology [54] (see Condition 2.3.9), we consider the following spectral property of solutions u.

Theorem 2.2.11. *Suppose that G and D_0 satisfy Condition 2.1.10 and that the true solution u satisfies for any $k \ge 0$*

$$|\widehat{u}_k|^2 = (u, x_k)_X^2 \le Ck^m,$$

for some fixed m and $C > 0$. Then the error in the large (resolved) scales satisfies

$$\|P(u - D_J \bar{u}_\epsilon)\|_X \le C_0(N_0)\|P\epsilon\|_X + \alpha^{J+1} C_1(N_0, J),$$

for some constant $C_0 > 0$ independent of J and α, and $C_1 > 0$.

Proof. Let $\|\cdot\| = \|\cdot\|_X$. We first notice that

$$\|P\left(u - D_J(\bar{u} + \epsilon)\right)\| \leq \|P(u - D_J\bar{u})\| + \|PD_J\epsilon\|\,.$$

We first consider the noisy part of the estimate

$$\begin{aligned}\|PD_J\epsilon\|^2 &= \sum_{1\leq k<N_0} (\lambda_k(D_J))^2 |\widehat{\epsilon}_k|^2 \\ &\leq \sup_{1\leq k<N_0} (\lambda_k(D_J))^2 \sum_{1\leq k<N_0} |\widehat{\epsilon}_k|^2 \\ &= \sup_{1\leq k<N_0} (\lambda_k(D_J))^2 \|P\epsilon\|^2.\end{aligned}$$

Therefore,

$$\|PD_J\epsilon\| \leq \sup_{1\leq k<N_0} (\lambda_k(D_J)) \|P\epsilon\|.$$

Furthermore, by summing the geometric series for $D_J = D_0 \sum_{j=0}^{J} (FD_0)^j$, recalling that $F = D_0^{-1} - G$, we obtain

$$\begin{aligned}\lambda_k(D_J) &= \lambda_k(D_0) \frac{1 - (\lambda_k(D_0)\lambda_k(F))^{J+1}}{1 - (\lambda_k(D_0)\lambda_k(F))} \\ &= \lambda_k(G)^{-1} \left[1 - (\lambda_k(D_0)\lambda_k(F))^{J+1}\right].\end{aligned}$$

Since

$$\begin{aligned}\lambda_k(D_0)\lambda_k(F) &= \lambda_k(D_0)\lambda_k(D_0^{-1} - G) \\ &= \lambda_k(D_0)\left(\lambda_k(D_0^{-1}) - \lambda_k(G)\right) = 1 - \lambda_k(D_0)\lambda_k(G),\end{aligned}$$

and $|\lambda_k(D_0)||\lambda_k(G)| \leq 1$ from Condition 2.1.10, it follows that $|\lambda_k(D_J)| \leq |\lambda_k(G)|^{-1}$. Therefore,

$$\|PD_J\epsilon\| \leq \sup_{1\leq k<N_0} \lambda_k(G)^{-1} \|P\epsilon\|.$$

Now for the non-noisy part of the estimate. Let $Q_J = 1 - \lambda_k(D_J)\lambda_k(G)$. From above we conclude that

$$Q_J = (\lambda_k(D_0)\lambda_k(F))^{J+1} \leq \sup_{1\leq k<N_0} (\lambda_k(D_0)\alpha)^{J+1}$$

Now we enforce the velocity condition $|\widehat{u}_k|^2 \leq Ck^m$ to obtain

$$\begin{aligned}
\|P(u - D_J\bar{u})\|^2 &= \sum_{1\leq k<N_0} |1 - \lambda_k(D_J)\lambda_k(G)|^2 |\widehat{u}_k|^2 \\
&\leq C \sup_{1\leq k<N_0} \left[|1 - \lambda_k(D_J)\lambda_k(G)|^2\right] \sum_{1\leq k<N_0} k^m \\
&\leq C \sup_{1\leq k<N_0} \lambda_k(D_0)^{2J+2}\alpha^{2J+2} \sum_{1\leq k<N_0} k^m \\
&\leq C(N_0) \sup_{1\leq k<N_0} \lambda_k(D_0)^{2J+2}\alpha^{2J+2} \\
&\leq C(N_0) \sup_{1\leq k<N_0} \lambda_k(G)^{-2J-2}\alpha^{2J+2}.
\end{aligned}$$

The last inequality follows from Condition 2.1.10. Combining the results, we prove the claim.

□

The constant in the deconvolution error term in Theorem 2.2.11 can be improved in the case that $m < -1$, as is the case in Condition 2.3.9. If $m < -1$ then the dependence of C on N_0 can be removed. We use the integral comparison test to obtain

$$\begin{aligned}
\|P(u - D_J\bar{u})\|^2 &\leq C \sup_{1\leq k<N_0} \lambda_k(D_0)^{2J+2}\alpha^{2J+2} \sum_{1\leq k<N_0} k^m \\
&\leq C \sup_{1\leq k<N_0} \lambda_k(D_0)^{2J+2}\alpha^{2J+2}(1 + \int_1^\infty z^m dz) \\
&\leq C \sup_{1\leq k<N_0} \lambda_k(D_0)^{2J+2}\alpha^{2J+2}
\end{aligned}$$

The last inequality follows since $m < -1$.

2.3 APPLICATIONS

First, we consider the sensitivity of iterated Tikhonov-Lavrentiev regularization approximation to regularization parameter selection α. Then, we verify the predicted (worst case) error bounds for the application of turbulent velocities.

2.3.1 Sensitivity analysis of Tikhonov-Lavrentiev regularization

It is important to be able to quantify the accuracy of the regularization scheme used. Sensitivities give information about the reliability of predictions, e.g. [2,12,34,64,95]. Sensitivities are also required when the output of an algorithm is optimized over the algorithm's inputs, e.g. [34].

Definition 2.3.1. *The sensitivity with respect to α of the j-th regularized approximation $\phi_j = \phi_j(\alpha)$ is denoted*

$$s_j = s_j(\alpha) := \frac{d}{d\alpha}\phi_j(\alpha). \tag{2.24}$$

Higher order steps of iterated Tikhonov-Lavrentiev approximations ϕ_j implicitly compute higher order the sensitivities of ϕ_j. The following alternate algorithm for iterated Tikhonov-Lavrentiev regularization is presented in terms of the sensitivities. The calculation of sensitivities requires solving for the updates, so this form of the iterated Tikhonov-Lavrentiev algorithm is enticing from a numerical efficiency and programmatic infrastructure point of view.

Algorithm 2.3.2 (Iterated Tikhonov-Lavrentiev via sensitivities)**.** *Select $\alpha > 0$ and fix $J \in \mathbb{N}$.*

1. *Solve for ϕ_0, s_0, ϕ_1 satisfying*

$$(G + \alpha I)\phi_0 = y, \qquad (G + \alpha I)s_0 = -\phi_0, \qquad \phi_1 = \phi_0 - \alpha s_0. \tag{2.25}$$

2. *For $j = 1, \ldots, J$, solve for ϕ_j satisfying*

$$(G + \alpha I)(s_j - s_{j-1}) = -(\phi_j - \phi_{j-1}) - Gs_{j-1}.$$

If $j < J$, then compute update

$$\phi_{j+1} = \phi_j - \alpha s_j + \alpha^2 D_0 s_{j-1}.$$

Since ϕ_0 is a function of α, its Taylor polynomial expansion at α as a function of $\tilde{\alpha}$ is

$$T_j(\phi_0(\alpha))(\tilde{\alpha}) := \phi_0(\alpha) + (\tilde{\alpha} - \alpha)\frac{d}{d\alpha}\phi_0(\alpha) + \ldots + \frac{(\tilde{\alpha} - \alpha)^j}{j!}\frac{d^j}{d\alpha^j}\phi_0(\alpha).$$

Then the Maclaurin polynomial M_j is

$$M_j(\phi_{true}) := T_j(\phi_0(\alpha))(\tilde{\alpha})|_{\tilde{\alpha}=0} = \phi_0(\alpha) - \alpha\frac{d}{d\alpha}\phi_0(\alpha) + \ldots + \alpha^j\frac{(-1)^j}{j!}\frac{d^j}{d\alpha^j}\phi_0(\alpha).$$

Next we show that $M_j(\phi_{true})$ is exactly the j-th iterated Tikhonov-Lavrentiev approximation ϕ_j. Thus, updates implicitly compute higher order sensitivities of $\phi_0(\alpha)$ and use them to correct the approximation.

Lemma 2.3.3. *For $G \geq 0$, $\alpha > 0$, $1 \leq j \leq J$, the Tikhonov-Lavrentiev approximations satisfy*

$$\phi_{j+1}(\alpha) - \phi_j(\alpha) = -\alpha s_j(\alpha) + \alpha^2 D_0 s_{j-1}(\alpha), \tag{2.26}$$

$$\phi_j(\alpha) - \phi_{j-1}(\alpha) = \alpha^{j-1} D_0^{j-1}(\phi_1 - \phi_0), \tag{2.27}$$

$$\frac{d^{j-1}s_0(\alpha)}{d\alpha^{j-1}} = (-1)^{j-1}\frac{k!}{2\alpha}D_0^{k-2}s_1(\alpha). \tag{2.28}$$

Proof. The iterated Tikhonov-Lavrentiev approximation updates are given by

$$(G + \alpha I)(\phi_j - \phi_{j-1}) = y - G\phi_{j-1}.$$

Hence,

$$-\alpha\phi_{j-2} = y - (G + \alpha I)\phi_{j-1} \quad \text{and,} \tag{2.29}$$

$$-\alpha\phi_{j-1} = y - (G + \alpha I)\phi_j. \tag{2.30}$$

On the other hand, implicit differentiation of the update equation with respect to α produces

$$(G + \alpha I)s_{j-1} = -(\phi_{j-1} - \phi_{j-2}) + \alpha s_{j-2}. \tag{2.31}$$

Subtracting (2.29) and (2.30) and substituting into (2.31) proves the first identity, (2.26). The next identity follows by subtracting (2.29) and (2.30) again and rearranging to get

$$(G + \alpha I)(\phi_j - \phi_{j-1}) = \alpha(\phi_{j-1} - \phi_{j-2}).$$

Backward induction proves (2.27). In (2.36) we show that $\phi_1(\alpha) - \phi_0(\alpha) = -\alpha s_0(\alpha)$. Implicit differentiation of (2.36) shows

$$\frac{ds_0(\alpha)}{d\alpha} = -\alpha^{-1} s_1(\alpha). \tag{2.32}$$

On the other hand, starting with $(G + \alpha I)\phi_0(\alpha) = y$ and differentiating j times with respect to α, we get

$$\frac{d^{j-1} s_0(\alpha)}{d\alpha^{j-1}} = -j D_0 \frac{d^{j-2} s_0(\alpha)}{d\alpha^{j-2}}.$$

Using backward induction with the relation (2.32), we prove (2.28). □

Lemma 2.3.4. *For $G \geq 0$, $\alpha > 0$, the sensitivity $s_1(\alpha)$ and Tikhonov-Lavrentiev approximations ϕ_0 and ϕ_1 satisfy*

$$(G + \alpha I) s_1(\alpha) = -2(\phi_1(\alpha) - \phi_0(\alpha)). \tag{2.33}$$

Proof. The claim is proved by applying $s_0(\alpha) = -\frac{\phi_1(\alpha) - \phi_0(\alpha)}{\alpha}$ from (2.25) to (2.31). □

Theorem 2.3.5 (Higher order sensitivities correct for accuracy)**.** *Suppose $G \geq 0$ and fix $\alpha > 0$. Then, in the absence of noise and when $\phi_{true} \in Range(G^J)$*

$$\phi_{true} = M_k(\phi_{true}) + \mathcal{O}(\alpha^{k+1}). \tag{2.34}$$

In the general case of noisy data, the k-th Tikhonov-Lavrentiev approximation satisfies

$$\phi_k = M_k(\phi_{true}). \tag{2.35}$$

Proof. First note that $\phi_0(\alpha) = (G + \alpha I)^{-1} y$ is a smooth function of $\alpha > 0$. Therefore, if $y = \bar{\phi}$ (no-noise), then $\phi_{true} = \phi_0(\alpha = 0)$ (properly defined as a limit when the source condition is satisfied as shown by considering the error equation and estimate), and so by Taylor's Theorem we prove the first claim. Next, by Lemma 2.3.3, (2.26),

$$\phi_k(\alpha) = \phi_{k-1} - \alpha s_{k-1}(\alpha) + \alpha^2 D_0 s_{k-2}(\alpha).$$

We proceed by induction to show that $\phi_k = M_k(\phi_{true})$. The base case $k = 1$ is concluded by implicitly differentiating (2.9) to obtain

$$s_0 = -(G + \alpha I)^{-1} \phi_0,$$

and then rearranging terms in (2.10) and using the above formula gives

$$\begin{aligned} \phi_1 - \phi_0 &= (G + \alpha I)^{-1}((G + \alpha I)\phi_0 - G\phi_0) \\ &= (G + \alpha I)^{-1}(\alpha \phi_0) \\ &= -\alpha s_0. \end{aligned} \tag{2.36}$$

For the inductive step, assume that $\phi_{k-1} = M_{k-1}(\phi_{true})$. We must show that

$$\alpha^k \frac{(-1)^k}{k!} \frac{d^k \phi_0(\alpha)}{d\alpha^k} = \alpha s_{k-1}(\alpha) + \alpha^2 D_0 s_{k-2}(\alpha). \tag{2.37}$$

Using Lemma 2.3.3, equations (2.26) and (2.28) imply that (2.37) is equivalent to showing

$$\phi_k(\alpha) - \phi_{k-1}(\alpha) = -\frac{\alpha^{k-1}}{2} D_0^{k-2} s_1(\alpha). \tag{2.38}$$

Multiplying (2.38) by $-2\alpha^{-k+1}(G + \alpha I)^{k-1}$, we get

$$(G + \alpha I) s_1(\alpha) = -\frac{2}{\alpha^{k-1}} (G + \alpha I)^{k-1} (\phi_k(\alpha) - \phi_{k-1}(\alpha)). \tag{2.39}$$

From (2.27) and (2.28), it follows that (2.39) is equivalent to

$$(G + \alpha I) s_1(\alpha) = -2(\phi_1(\alpha) - \phi_0(\alpha)). \tag{2.40}$$

Since we prove the identity (2.40) in Lemma 2.3.4, we are done. □

2.3.2 Deconvolution of turbulent velocities

We now show a specific example of turbulent velocities satisfying the theory of Section 2.2.3. To develop this result we must first summarize some features of the time-averaged energy spectrum of homogeneous, isotropic turbulence and the decomposition of energy into wave numbers via Fourier series, see [58]. Consider notation as introduced in Section 2.1.1.

Definition 2.3.6 (Long time average)**.** *Let $\langle\cdot\rangle$ denote long time averaging, given by*

$$\langle\psi\rangle := \limsup_{T\to\infty} \frac{1}{T}\int_0^T \psi(t)dt.$$

Definition 2.3.7 (Kinetic energy)**.** *The kinetic energy distribution functions are defined by*

$$\widehat{E}(k,t) = \frac{1}{2}\sum_{k-1<|\boldsymbol{k}|\leq k} |u(x,t)|^2 dx, \quad \textit{and}$$
$$\widehat{E}(k) = \left\langle \widehat{E}(k,t)\right\rangle.$$

Remark 2.3.8. *Parseval's equality implies that the time averaged kinetic energy of the given velocity $u(x,t)$ can be written as*

$$\widehat{E}(k) = \left\langle \frac{1}{2}\sum_{k-1<|\boldsymbol{k}|\leq k} |\widehat{u}(\boldsymbol{k},t)|^2 \right\rangle.$$

Let $\nu > 0$ represent fluid viscosity and ε_{edr} the time averaged energy dissipation rate given by

$$\varepsilon_{edr} = \left\langle \int \nu|\nabla u(x,t)|^2 dx \right\rangle.$$

If U represents a global velocity scale of the flow's large structures, the K41 theory of turbulence [3, 33, 54] (a phenomenological theory with good agreement in the large with experimental data [82, 83]) states that there is a range of wave numbers, known as the *inertial range*, satisfying $0 < U\nu^{-1} \leq k \leq \varepsilon_{edr}^{1/4}\nu^{-3/4} < \infty$ over which $\widehat{E}(k) \simeq 1.6\varepsilon_{edr}^{2/3}k^{-5/3}$. Consistent with the K41 theory, we make the following assumption.

Condition 2.3.9 (K41 Compatible Velocity)**.** *Over all $0 < k < \infty$,*

$$\widehat{E}(k) \leq 1.6\varepsilon_{edr}^{2/3}k^{-5/3}.$$

Recall from Section 2.1.1 the discussion of projections into large scales.

Definition 2.3.10 (Large scale projection)**.** *Fix the filter radius $\delta > 0$, cutoff frequency $1/\delta$, and large scale solution space X_{large}. Let $P : L^2(\Omega) \to X_{large}$ be the L^2 orthogonal projection into X_{large}. Then*

$$P\left(\sum_{\boldsymbol{k}\in\mathbb{Z}^3} \widehat{u}(\boldsymbol{k},t)e^{i\boldsymbol{k}\cdot x}\right) = \sum_{|\boldsymbol{k}|\leq 1/\delta} \widehat{u}(\boldsymbol{k},t)e^{i\boldsymbol{k}\cdot x}.$$

For a specific example, we consider the Pao filter [73, 84].

Definition 2.3.11 (Pao filter)**.** *The Pao filter G acting on $u \in L^2([0,\pi]^3)$ is defined by*

$$Gu(x) = \sum_{\boldsymbol{k}} \frac{1}{1+\delta^2|\boldsymbol{k}|^2}\widehat{u}(\boldsymbol{k})e^{i\boldsymbol{k}\cdot x}.$$

We write the transfer function of G as

$$\widehat{G}(\boldsymbol{k}) = \frac{1}{1+\delta^2|\boldsymbol{k}|^2}.$$

This is the transfer function for the differential filter $G = (-\delta^2\triangle + 1)^{-1}$. Even though the turbulent velocity is not smooth, Theorem 2.2.11 implies that the rate of convergence coincides with the smooth case.

Theorem 2.3.12. *Suppose that a velocity u is K41 compatible. The time averaged deconvolution error for iterated Tikhonov-Lavrentiev deconvolution applied to the Pao filter in the large (resolved) scales, as defined in Definition 2.3.10, satisfies*

$$\left\langle ||P(u - D_J\bar{u}_\epsilon)||^2_{L^2(\Omega)} \right\rangle^{1/2} \leq 2\sqrt{2}||P\epsilon||_{L^2(\Omega)} + \alpha^{J+1}\varepsilon_{edr}^{1/3}C(J).$$

The method of proof is similar to that applied in Theorem 2.2.11. The key difference is that Theorem 2.3.12 is studying Fourier expansions in a particular case as opposed to spectral decomposition for a general filter and deconvolution. Recall that for the Pao filter, $\widehat{G}(\boldsymbol{k}) = (\delta^2|\boldsymbol{k}|^2+1)^{-1}$ and $\widehat{D_0}(\boldsymbol{k}) = ((\delta^2|\boldsymbol{k}|^2+1)^{-1} + \alpha)^{-1}$ (Tikhonov-Lavrentiev).

Proof. Denote $\|\cdot\| = \|\cdot\|_{L^2(\Omega)}$. Expanding the error term gives

$$\begin{aligned}\|P(u - D_J(Gu+\epsilon))\|^2 &= \|P(u - D_JGu) + P(D_J\epsilon))\|^2 \\ &\le 2\|P(u - D_JGu)\|^2 + 2\|PD_J\epsilon\|^2 \\ &\le 2\sum_{|\boldsymbol{k}|\le 1/\delta} |1 - \widehat{D_J}(\boldsymbol{k})\widehat{G}(\boldsymbol{k})|^2|\widehat{u}(\boldsymbol{k},t)|^2 + 2\sum_{|\boldsymbol{k}|\le 1/\delta} |\widehat{D_J}(\boldsymbol{k})|^2|\widehat{\epsilon}(\boldsymbol{k},t)|^2.\end{aligned}$$

Recall from (2.12) that

$$D_J = D_0\sum_{j=0}^{J}[(D_0^{-1} - G)D_0]^j = D_0\sum_{j=0}^{J}(I - GD_0)^j.$$

Calculating the transfer function, we obtain

$$\begin{aligned}\widehat{D_J}(\boldsymbol{k}) &= \frac{1}{(\delta^2|\boldsymbol{k}|^2+1)^{-1} + \alpha}\sum_{j=0}^{J}\left[1 - \frac{(\delta^2|\boldsymbol{k}|^2+1)^{-1}}{(\delta^2|\boldsymbol{k}|^2+1)^{-1} + \alpha}\right]^j \\ &= \frac{\delta^2|\boldsymbol{k}|^2+1}{1+\alpha(\delta^2|\boldsymbol{k}|^2+1)}\sum_{j=0}^{J}\left[\frac{\alpha(\delta^2|\boldsymbol{k}|^2+1)}{1+\alpha(\delta^2|\boldsymbol{k}|^2+1)}\right]^j \\ &= \frac{\delta^2|\boldsymbol{k}|^2+1}{1+\alpha(\delta^2|\boldsymbol{k}|^2+1)}\frac{1 - \left[\frac{\alpha(\delta^2|\boldsymbol{k}|^2+1)}{1+\alpha(\delta^2|\boldsymbol{k}|^2+1)}\right]^{J+1}}{1 - \frac{\alpha(\delta^2|\boldsymbol{k}|^2+1)}{1+\alpha(\delta^2|\boldsymbol{k}|^2+1)}} \\ &= (\delta^2|\boldsymbol{k}|^2+1)\left(1 - \left[\frac{\alpha(\delta^2|\boldsymbol{k}|^2+1)}{1+\alpha(\delta^2|\boldsymbol{k}|^2+1)}\right]^{J+1}\right) \\ &\le 2.\end{aligned}$$

The last inequality follows from $|\boldsymbol{k}| \le 1/\delta$. This inequality implies the bound on the noisy term.

$$\begin{aligned}\|P(D_J\epsilon))\|^2 &= \sum_{|\boldsymbol{k}|\le 1/\delta} |\widehat{D_J}(\boldsymbol{k})|^2|\widehat{\epsilon}(\boldsymbol{k},t)|^2 \\ &\le \sup_{|\boldsymbol{k}|\le 1/\delta} |\widehat{D_J}(\boldsymbol{k})|^2 \sum_{|\boldsymbol{k}|\le 1/\delta} |\widehat{\epsilon}(\boldsymbol{k},t)|^2 \\ &\le 4\|P\epsilon\|^2.\end{aligned}$$

Recalling that $F = D_0^{-1} - G$, we calculate

$$\widehat{F}(\boldsymbol{k}) = \widehat{D_0}(\boldsymbol{k})^{-1} - \widehat{G}(\boldsymbol{k}) = \left(\frac{1}{\delta^2|\boldsymbol{k}|^2+1} + \alpha\right) - \frac{1}{\delta^2|\boldsymbol{k}|^2+1} = \alpha.$$

This implies that

$$\begin{aligned}
\|P(u - D_J G u)\|^2 &= \sum_{|\boldsymbol{k}|\leq 1/\delta} |1 - \widehat{D_J}(\boldsymbol{k})\widehat{G}(\boldsymbol{k})|^2 |\widehat{u}(\boldsymbol{k},t)|^2 \\
&= \sum_{|\boldsymbol{k}|\leq 1/\delta} \left|1 - \left(1 - (\widehat{D_0}(\boldsymbol{k})\widehat{F}(\boldsymbol{k}))^{J+1}\right)\right|^2 |\widehat{u}(\boldsymbol{k},t)|^2 \\
&= \sum_{|\boldsymbol{k}|\leq 1/\delta} (\frac{1}{(\delta^2|\boldsymbol{k}|^2 + 1)^{-1} + \alpha)}\alpha))^{2J+2} |\widehat{u}(\boldsymbol{k},t)|^2 \\
&\leq 2^{2J+2}\alpha^{2J+2} \sum_{|\boldsymbol{k}|\leq 1/\delta} |\widehat{u}(\boldsymbol{k},t)|^2.
\end{aligned}$$

Imposing the K41 compatibility condition, we obtain (via integral comparison)

$$\begin{aligned}
\left\langle ||P(u - D_J G u)||^2 \right\rangle &\leq 2^{2J+3}\alpha^{2J+2} \left\langle \frac{1}{2} \sum_{|\boldsymbol{k}|\leq 1/\delta} |\widehat{u}(\boldsymbol{k},t)|^2 \right\rangle \\
&\leq 2^{2J+3}\alpha^{2J+2} \sum_{k\leq 1/\delta} 1.6\epsilon_{edr}^{2/3} k^{-5/3} \\
&\leq 2^{2J+3}\alpha^{2J+2} 1.6\epsilon_{edr}^{2/3} \left(1 + \int_1^\infty k^{-5/3}\right) \\
&\leq C(J)\alpha^{2J+2}\epsilon_{edr}^{2/3}.
\end{aligned}$$

The claim is proved by combining the results and taking the square root. □

The main difference between Theorem 2.3.12 and the error bound on Tikhonov-Lavrentiev regularization, Theorem 2.1.12 is that the noise in the small scales is not amplified. The bound on $\|P(D_J\epsilon))\|$ depends directly on $\sup_{|\boldsymbol{k}|\leq 1/\delta} |\widehat{D_J}(\boldsymbol{k})|^2$, which is bounded. However, $\sup_{|\boldsymbol{k}|\in\mathbb{R}} |\widehat{D_J}(\boldsymbol{k})|^2$ which is needed for the estimate in Theorem 2.1.12 is unbounded as $\alpha \to 0$.

2.4 NUMERICAL EXPERIMENTS

2.4.1 Superconvergence of turbulent velocities

Theorem 2.3.12 implies that the noise is not amplified by $\frac{1}{\alpha}$ in the projection of the error, as is the case for Tikhonov-Lavrentiev regularization. We verify this error bound with a calculation. We construct a synthetic velocity field $u_{M,N} : (0, 2\pi)^2 \to \mathbb{R}^2$ representative of the time-averaged turbulent velocities discussed in Section 2.3.2. For $m = 1, 2, \ldots, M < \infty$ and $n = 1, 2, \ldots, N < \infty$ and basis functions $A_{m,n}$, define

$$u_{M,N}(x, y) = \sum_{n=1}^{N} \sum_{m=1}^{M} (m^2 + n^2)^{-7/6} A_{m,n}(x, y). \tag{2.41}$$

Desiring $u_{M,N}$ to be 2π-periodic with $\nabla \cdot u_{M,N} = 0$, we chose

$$A_{m,n}(x, y) := (n \sin(mx) \cos(ny), -m \cos(mx) \sin(ny)) .$$

Thus, (2.41) provides a decomposition of $u_{M,N}$ in terms of its Fourier spectrum. Let

$$Q(k) := \left\{(m, n) \in [1, M] \times [1, N] : (k - 1)^2 < m^2 + n^2 \leq k^2, \quad m \leq M, n \leq N\right\} .$$

Then with $M = N$ and writing $u_{N,N} := u_N$, we calculate

$$\|u_N\|^2 = \sum_{k=1}^{N} \pi^2 E(k), \qquad E(k) := \sum_{(m,n)\in Q(k)} (m^2 + n^2)^{-7/3}(m^2 + n^2).$$

Since each sum over $(m, n) \in Q(k)$ contains of order $\mathcal{O}(k)$ terms, we conclude that the constructed u_N satisfies

$$E(k) \leq \mathcal{O}(k^{-5/3}).$$

We are interested in analyzing the effect of iterated Tikhonov regularization on the large-scale approximations $u_{M,N}(x, y)$. Let $G = (-\delta^2\Delta + I)^{-1}$ and write $G\phi = \bar{\phi}$. Since $\Delta A_{m,n} = -(m^2 + n^2)A_{m,n}$, we calculate

$$\overline{A}_{m,n} = \frac{1}{1 + \delta^2(m^2 + n^2)} A_{m,n}$$

Lemma 2.4.1. *The transfer function for G on functions from Span$(A_{m,n})$ is*

$$\hat{G}(m,n) = (1+\delta^2(m^2+n^2))^{-1}.$$

Moreover, letting $D_0 = (G+\alpha I)^{-1}$, then

$$\hat{D}_J = \frac{1}{\hat{G}}\left(1-\alpha^{J+1}\hat{D}_0^{J+1}\right).$$

Proof. Note that $\Delta A_{m,n} = -(m^2+n^2)A_{m,n}$ and calculate

$$GA_{m,n} = \frac{1}{1+\delta^2(m^2+n^2)}A_{m,n},$$

to obtain $\widehat{G}(m,n)$.

Equation (2.12) implies that

$$\widehat{D_J}(m,n) = \widehat{D_0}(m,n)\sum_{k=0}^{J}(\widehat{F}(m,n)\widehat{D_0}(m,n))^k,$$

where $\widehat{F}(m,n) = \alpha$. This implies that

$$\begin{aligned}\widehat{D_J}(m,n) &= \widehat{D_0}(m,n)\frac{1-(\alpha\widehat{D_0}(m,n))^{J+1}}{1-\alpha\widehat{D_0}(m,n)}\\ &= \frac{1-(\alpha\widehat{D_0}(m,n))^{J+1}}{\widehat{D_0}(m,n)^{-1}-\alpha}\\ &= \frac{1}{\widehat{G}(m,n)}(1-(\alpha\widehat{D_0}(m,n))^{J+1}),\end{aligned}$$

as claimed. □

Lemma 2.4.2. *The noise-free error in the large scales, $e_{N,J} = u_N - D_J(\bar{u}_N)$, is*

$$E_0^2 := \|e_{N,J}\|^2 = \pi^2\alpha^{2J+2}\sum_{m,n=1}^{N}\frac{\left[1+\delta^2(m^2+n^2)\right]^{2J+2}(m^2+n^2)^{-8/6}}{\left[1+\alpha(1+\delta^2(m^2+n^2))\right]^{2J+2}}.$$

Proof.

$$\|e_{N,J}\|^2 = (e_{N,J}, e_{N,J}) = ((I - D_J G)u_N, (I - D_J G)u_N) \tag{2.42}$$

$$= (\sum_{m,n=1}^{N} (1 - \widehat{D_J}(m,n)\widehat{G}(m,n))(m^2+n^2)^{-7/6} A_{m,n}, \tag{2.43}$$

$$\sum_{m,n=1}^{N} (1 - \widehat{D_J}(m,n)\widehat{G}(m,n))(m^2+n^2)^{-7/6} A_{m,n}).$$

We note that

$$(A_{m,n}, A_{i,j}) = \begin{cases} \pi^2(m^2+n^2), & m = i > 0 \text{ and } n = j > 0 \\ 0 & otherwise \end{cases},$$

because of the orthogonality of $\sin(n_i x)$ for integer values $n_i \neq n_j$, and apply this and Lemma 2.4.1 to (2.42) to obtain the result. □

Proposition 2.4.3. *The error to the noisy problem in the large scales, $e^{\epsilon}_{N,J} = u_N - D_J(\bar{u}_N + \epsilon)$, is*

$$E^2_\epsilon := \|e^{\epsilon}_{N,J}\|^2 = \|e_{N,J}\|^2 + \sum_{j,k=0}^{J} \alpha^{j+k} \left(D_0^{j+1}\epsilon, D_0^{k+1}\epsilon\right)$$

$$- 2\sum_{k=0}^{J}\sum_{m,n=1}^{N} \alpha^{k+J+1} \frac{[1+\delta^2(m^2+n^2)]^{J+1}\,(m^2+n^2)^{-7/6}}{[1+\alpha(1+\delta^2(m^2+n^2))]^{J+1}} \left(D_0^{k+1}\epsilon, A_{m,n}\right).$$

Proof. Expand the expression for E^2_ϵ and use the symmetric property of the inner product to obtain

$$E^2_\epsilon = ((I - D_J G)u_N - D_J\epsilon, (I - D_J G)u_N - D_J\epsilon)$$

$$= E_0^2 - 2\left((I - D_J G)u_N, D_J\epsilon\right) + \left(D_J\epsilon, D_J\epsilon\right).$$

Equation (2.12) gives

$$(D_J\epsilon, D_J\epsilon) = \left(\sum_{j=1}^{J} \alpha^j D_0^{j+1}\epsilon, \sum_{k=1}^{J} \alpha^k D_0^{k+1}\epsilon\right).$$

Applying (2.12) and Lemma 2.4.1, the mixed terms expand to

$$\begin{aligned}
&((I - D_J G)u_N, D_J\epsilon) \\
&\quad = \left(\sum_{m,n=1}^{N} (1 - \widehat{D_J}(m,n)\widehat{G}(m,n))(m^2+n^2)^{-7/6} A_{m,n}, \sum_{k=1}^{J} \alpha^k D_0^{k+1}\epsilon \right) \\
&\quad = \sum_{m,n=1}^{N} \sum_{k=1}^{J} \alpha^{J+1+k} \left(\frac{\left[1+\delta^2(m^2+n^2)\right]^{J+1} (m^2+n^2)^{-7/6}}{\left[1+\alpha(1+\delta^2(m^2+n^2))\right]^{J+1}} A_{m,n}, D_0^{k+1}\epsilon \right).
\end{aligned}$$

Combining these together yields the result. □

In each of Figures 1, 2, 3 and 4, we plot E_ε using Matlab for the projections into the spaces where $n \leq N$ and $m \leq N$ for $N = 4$, 8, 16, and 32. The true solution was filtered using a filter radius $\delta = 0.25$ and then noise of $10^{-5} A_{8,8}$ was added. The error was calculated between the true solution and the deconvolution of the noisy and filtered data. Figures 1, 2, 3 and 4 show for $J = 0, 1, 2,$ and 3 respectively the slope of $J+1$ in the error when the noise is not in the projection space as Theorem 2.3.12 predicts. When the noise is in the projection space, we see the predicted error slope until the error reaches the level of the noise and then we see no further improvement.

2.4.2 Sensitivity calculation

The sensitivity calculations are demonstrated by applying iterated Tikhonov regularization to the Fredholm integral equation of the first kind discussed by Shaw [89] and given by

$$\int_{-\pi/2}^{\pi/2} \kappa(s,t)x(s)ds = b(t), \quad -\pi/2 \leq t \leq \pi/2, \tag{2.44}$$

where

$$\begin{aligned}
\kappa(s,t) &= (\cos(s) + \cos(t))\left(\frac{\sin(u(s,t))}{u(s,t)}\right)^2, \\
u(s,t) &= \pi(\sin(s) + \sin(t)), \text{ and} \\
b(t) &= 2e^{-6(t-0.8)^2} + e^{-2(t+0.5)^2}.
\end{aligned}$$

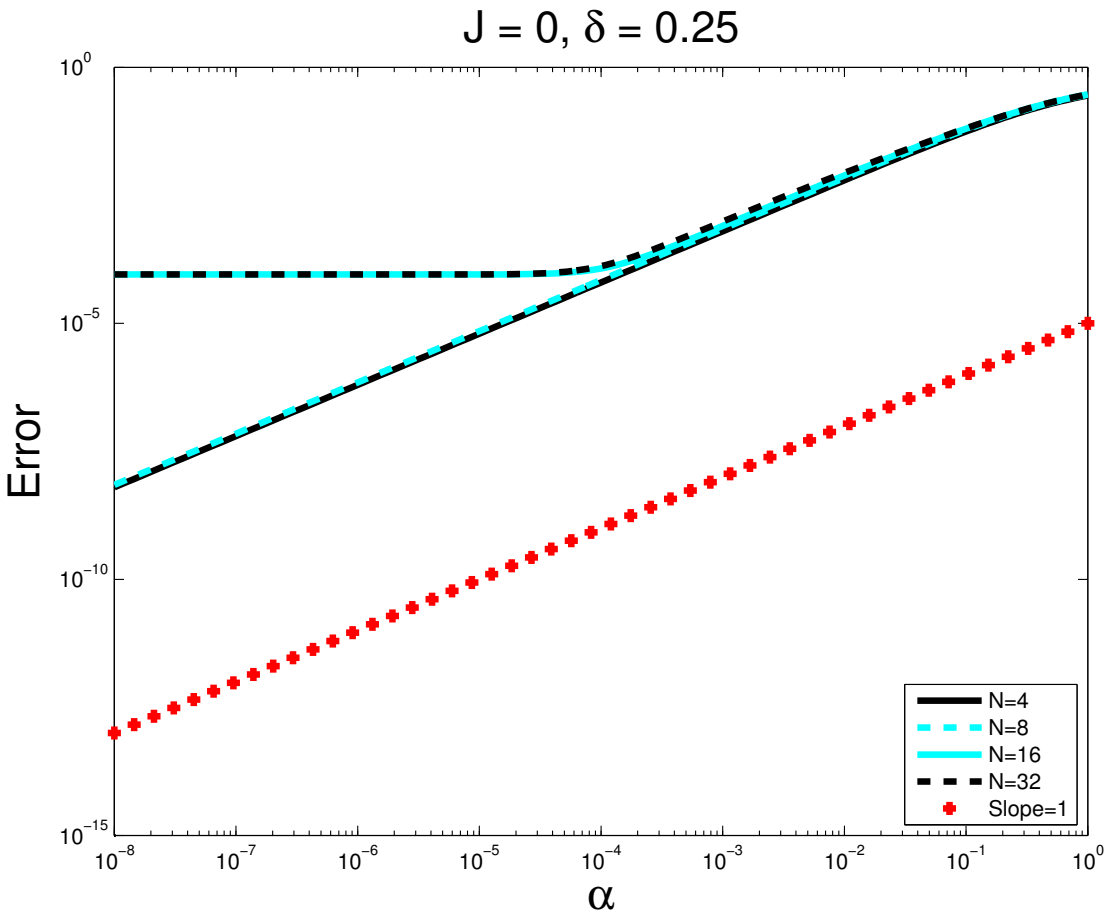

Figure 1: Norm of the projection of the error as a function of α for the $J = 0$ regularization method. Observe that when the noise=$10^{-5}A_{8,8}$ is in the projection space (when N=16 and 32), the error is bounded by the size of the noise. However, when the noise is not in the projection space (when N=4 and 8), we observe the predicted O(α^1) error.

The discretization of the operator A was calculated with 200 equally spaced quadrature points in t using the Matlab regularization toolbox by Hansen [41]. We approximate the continuous solution $x(t)$ of the continuous Shaw problem (2.44) by solving

$$Ax = b,$$

where $b_k = b(t_k)$.

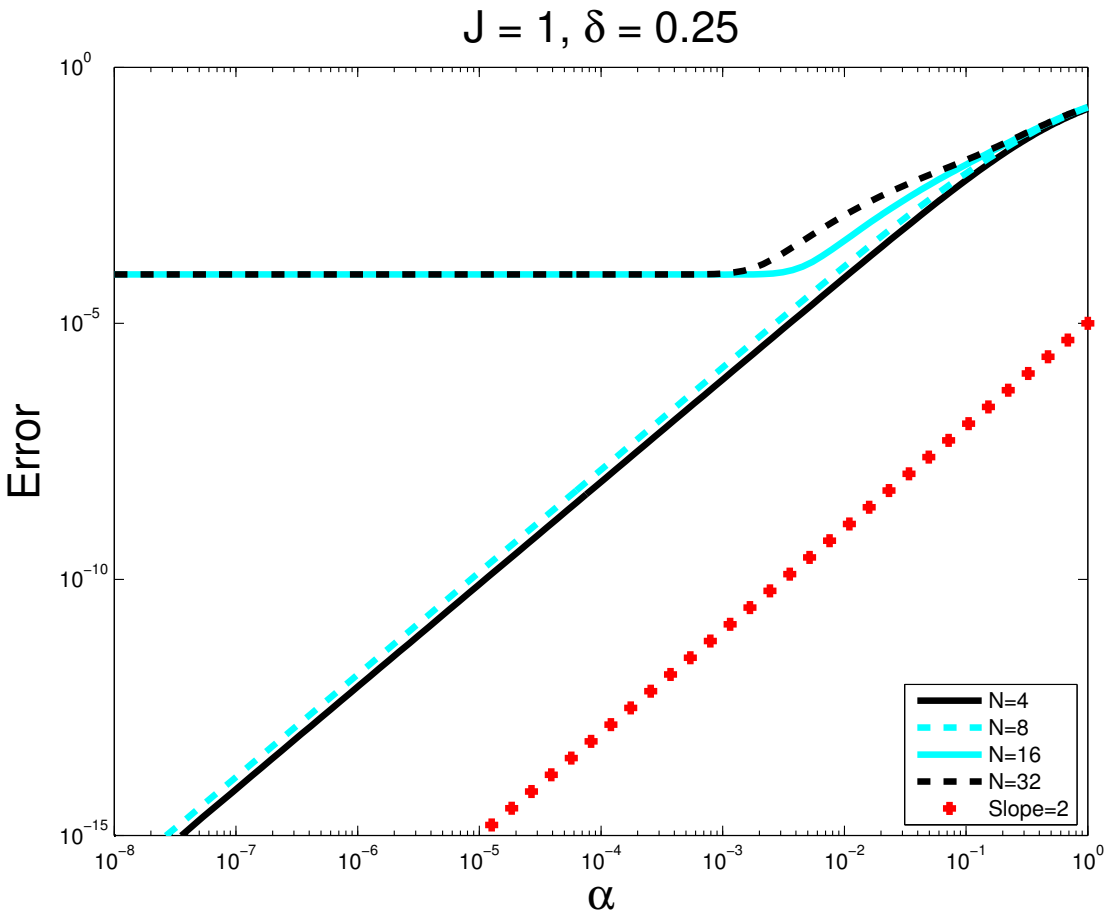

Figure 2: Norm of the projection of the error as a function of α for the $J = 1$ regularization method. Observe that when the noise=$10^{-5}A_{8,8}$ is in the projection space (when N=16 and 32), the error is bounded by the size of the noise. However, when the noise is not in the projection space (when N=4 and 8), we observe the predicted $O(\alpha^2)$ error.

This is known to be an extremely ill-conditioned system with condition number 5.5×10^{19}. We add noise to the right-hand side b_k using uniformly distributed noise $\epsilon \in \mathbb{R}^{200}$, where $\|\epsilon\| = 10^{-3}\|b\|$.

We use the L-curve method (via the regulation toolbox) [23, 40–42] to obtain regularization parameter $\alpha = 0.00180$. We use this value of α to show the benefit of applying iterated Tikhonov regularization to an initially α-optimized procedure. Moreover, since this

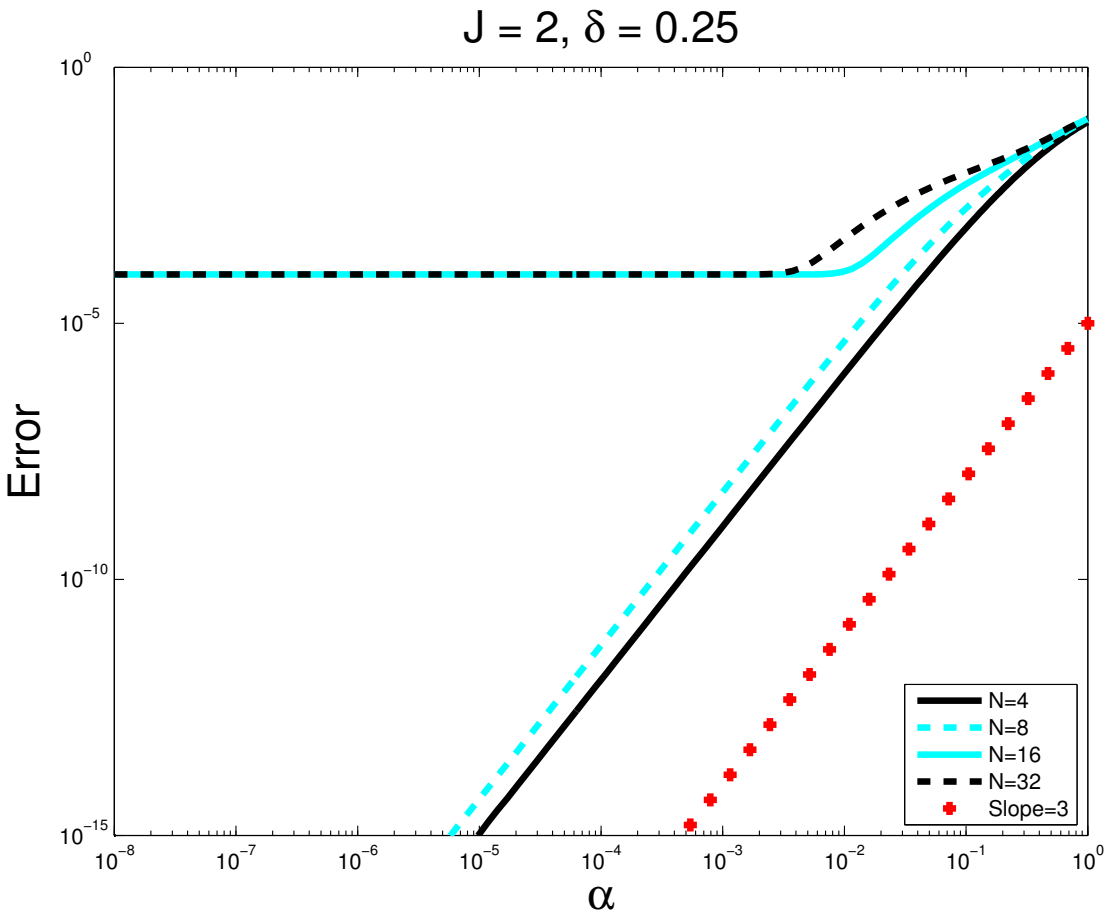

Figure 3: Norm of the projection of the error as a function of α for the $J = 2$ regularization method. Observe that when the noise=$10^{-5}A_{8,8}$ is in the projection space (when N=16 and 32), the error is bounded by the size of the noise. However, when the noise is not in the projection space (when N=4 and 8), we observe the predicted O(α^3) error.

is a synthetic test with a known noise, we can use the noise-free energy functional,

$$E(v) = \frac{1}{2}(Av, v) - (b, v),$$

to determine when our noisy solution is no longer converging to the true solution. For this example, 31 iterates were taken before $E(x_j) > E(x_{j-1})$.

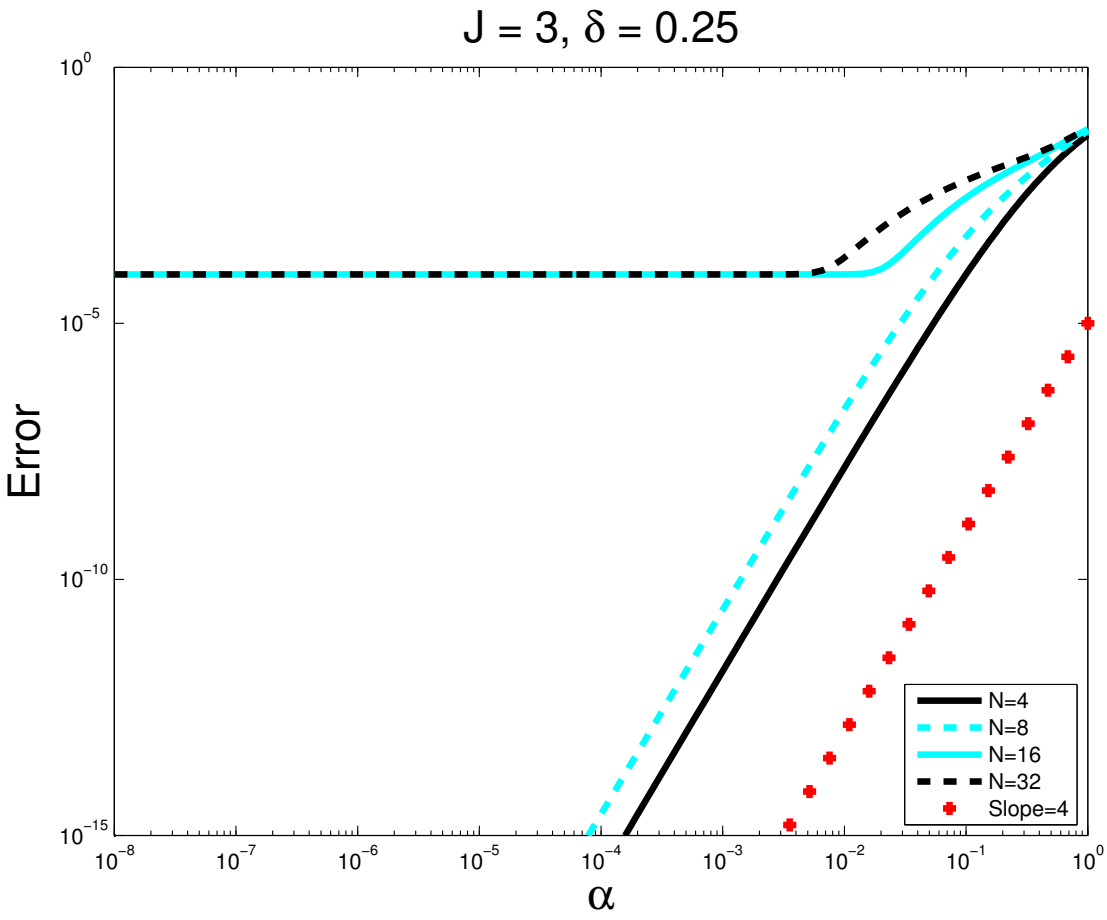

Figure 4: Norm of the projection of the error as a function of α for the $J = 3$ regularization method. Observe that when the noise=$10^{-5}A_{8,8}$ is in the projection space (when N=16 and 32), the error is bounded by the size of the noise. However, when the noise is not in the projection space (when N=4 and 8), we observe the predicted O(α^4) error.

The results of our experiment are summarized in Figure 5 and Table 1. Figure 5 shows the clear improvement of the solution $x_3 1$ compared to x_0. Also, the band of sensitivity values decreases from the Tikhonov approximation to the iterated-Tikhonov approximation, supporting our theory in Section 2.3.1 that suggests updating with iterated Tikhonov acts to further stabilize the regularization scheme. Table 1 shows the more accurate solutions correspond to a smaller sensitivity. We note that the errors do not approach zero due to the

noise added to the problem.

2.5 CONCLUSIONS

Iterated regularization provides a much higher attainable accuracy that is uniform in the problem parameters on the largest scale of the deconvolved approximation in Theorem 2.3.12, and a much smaller error in the deconvolved approximation in interpolation spaces in Theorem 2.2.8, and loss of uniformity in the deconvolved approximations accuracy on the small scales and a bound on the attainable global accuracy consistent with the less regularity of the turbulent velocity data in Theorem 2.2.11.

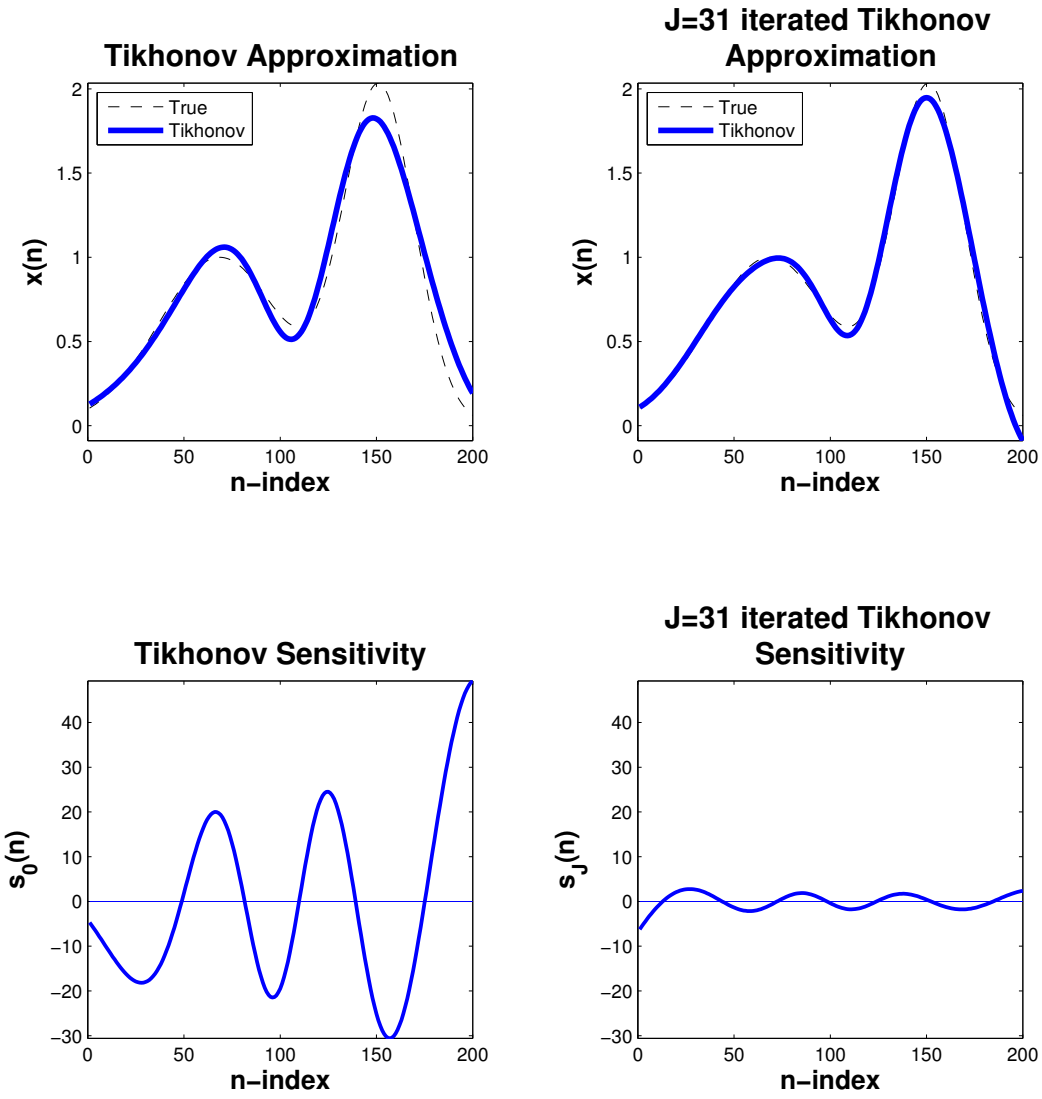

Figure 5: Sensitivity comparison between the Tikhonov and iterated Tikhonov solutions for an optimally chosen regularization parameter. Notice the band of sensitivity values decreases for the more accurate solution.

Table 1: Convergence statistics for the Shaw problem. Note the decrease in error and sensitivities as the number of iteration steps increases.

J	$\frac{\|x_J - x_{true}\|}{\|x_{true}\|}$	$\frac{\|G^{1/2}(x_J - x_{true})\|}{\|x_{true}\|}$	$E(x_{j-1}) - E(x_j)$	$\|s_J\|$
0	0.1108	0.003494	8.288e-4	1.380
1	0.08401	0.001972	1.990e-4	1.590
6	0.05226	0.0006155	6.929e-6	0.8773
11	0.04922	0.0004500	9.725e-7	0.3405
16	0.04868	0.0004173	2.016e-7	0.1338
21	0.04853	0.0004100	4.457e-8	0.09605
26	0.04847	0.0004084	8.444e-9	0.1053
31	0.04843	0.0004082	-8.934e-11	0.1185

3.0 MODIFIED ITERATED TIKHONOV-LAVRENTIEV

"A very small cause which escapes our notice determines a considerable effect that we cannot fail to see, and then we say that the effect is due to chance." (Henri Poincaré)

3.1 INTRODUCTION

Problem 3.1.1 (Noise Free Model Problem)**.** *Let X and Y be Hilbert spaces. Given a linear filter operator $G : X \to Y$ and a filtered signal $\bar{u} \in Range(G)$. The noise free model problem is to find $u \in X$ which satisfies*

$$Gu = \bar{u}. \tag{3.1}$$

Problem 3.1.2 (Noisy Model Problem)**.** *Let X and Y be Hilbert spaces. Given a linear filter operator $G : X \to Y$ and a filtered signal $\bar{u} \in Range(G)$ and noise $\epsilon \in Y$. The noisy model problem is to find $u \in X$ satisfying*

$$Gu = \bar{u} + \epsilon. \tag{3.2}$$

If the filter G is a convolution operator, then the deconvolution problem is to solve either Problem 3.1.1 or Problem 3.1.2. The deconvolution problem is an important inverse problem [26, 56, 66, 67, 98]. This problem occurs in many applications including parameter identification [22, 23], the deconvolution problem of image processing [11], and the closure problem in turbulence modeling [10, 28, 59, 67]. The deconvolution problem gets more complicated when noise is added to the signal.

It is known that if G is compact and $Range(G)$ is infinite dimensional, then Problems 3.1.1 and 3.1.2 are ill-posed [1, 4, 41, 70, 86, 106, 109]. Tikhonov-Lavrentiev regularization, a regularization method described further in Algorithm 3.2.8 that introduces a regularization parameter α, is one method that can be used to solve Problem 3.1.2. Tikhonov-Lavrentiev is a robust method that does not exploit the properties of the filter (with filtering radius δ). Theorem 3.3.8 shows that a small modification to the Tikhonov-Lavrentiev algorithm that exploits the properties of this filter and improves the error bounds from $\mathcal{O}(\alpha^{J+1})$ to $\mathcal{O}((\alpha\delta^2)^{J+1})$ in the noise free model problem. That is, a small algorithmic modification leads to a large improvement in the error bounds.

3.2 PRELIMINARIES AND NOTATION

Throughout this chapter, we use the standard notation for Lebesgue and Sobolev spaces and their norms. Also, Ω will be a regular, bounded, polyhedral domain in $\mathbb{R}^n$. We define the following space

$$X = H_0^1(\Omega)^d = \left\{ v \in L^2(\Omega)^d : \nabla v \in L^2(\Omega)^{dxd} \text{ and } v = 0 \text{ on } \partial\Omega \right\}. \tag{3.3}$$

The norm $\|\cdot\|$ will denote the $L^2(\Omega)$ norm unless otherwise specified in a proof. Similarly the inner product $(\cdot,\cdot)$ will denote the $L^2(\Omega)$ inner product.

We will use the notation $X^h \subset X$ to denote a finite dimensional subset of X. An example of X^h is the set of continuous polynomials of degree k. We also assume that we have homogenous boundary data throughout.

We use the following approximation inequalities, see [13],

$$\begin{aligned} \inf_{v\in X^h} \|u - v\|_{L^2(\Omega)} &\leq Ch^{k+1}\|u\|_{H^{k+1}(\Omega)}, \quad u \in H^{k+1}(\Omega)^n, \\ \inf_{v\in X^h} \|u - v\|_{H^1(\Omega)} &\leq Ch^{k}\|u\|_{H^{k}(\Omega)}, \quad u \in H^{k+1}(\Omega)^n. \end{aligned} \tag{3.4}$$

Other well known inequalities used herein include:

- Cauchy-Schwartz inequality: $|(f,g)| \leq \|f\|\|g\|, \quad \forall f, g \in L^2(\Omega)$.

- Young's inequality: $ab \leq \frac{\epsilon}{p}a^p + \frac{\epsilon^{-q/p}}{q}b^q$, where $1 < p, q < \infty$, $\frac{1}{p} + \frac{1}{q} = 1$, $\epsilon > 0$, and $a, b \geq 0$.
- Poincare-Friedrich's inequality: $\|v\| \leq C_{PF}\|\nabla v\|, \quad \forall v \in X.$
- Triangle inequality: $\|a + b\| \leq \|a\| + \|b\|$.

3.2.1 The differential filter

The differential filter (also called the Helmholz filter) is used in multiple large eddy simulation models [10,26,28,59,66,67]. This filter is equivalent to the Pao filter used in image processing [59].

Definition 3.2.1 (Differential filter)**.** *The differential filter G is defined as $Gu = \bar{u}$ where u and $\bar{u}$ satisfy*

$$-\delta^2 \Delta \bar{u} + \bar{u} = u \quad \text{in } \Omega. \tag{3.5}$$

Remark 3.2.2 (Variational differential filter)**.** *The differential filter is equivalent (see [66, 67]) to the following variational formulation. Find $\overline{u} \in H_0^1(\Omega)$ satisfying*

$$\delta^2(\nabla \overline{u}, \nabla v) + (\overline{u}, v) = (u_{true}, v), \quad \forall v \in X. \tag{3.6}$$

Definition 3.2.3 (Discrete differential filter)**.** *Let X^h be a finite dimensional subspace of X. We define $G^h : L^2(\Omega)^d \to X^h$ where $\overline{u}^h = G^h u$ which is the unique solution in X^h to*

$$\delta^2 \left(\nabla \overline{u}^h, \nabla v^h\right) + \left(\overline{u}^h, v^h\right) = \left(u, v^h\right), \quad \forall v^h \in X^h. \tag{3.7}$$

Lemmas 3.2.4, 3.2.5, 3.2.6 and 3.2.7 are quoted from [66] for completeness.

Lemma 3.2.4. *If $u \in L^2(\Omega)^d$, the following stability estimate for problem (3.6) holds:*

$$\delta^2 \|\nabla \overline{u}\|^2 + \frac{1}{2}\|\overline{u}\|^2 \leq \frac{1}{2}\|u\|^2. \tag{3.8}$$

Lemma 3.2.5. *The operator $G : L^2(\Omega)^d \to X$ is self-adjoint.*

Lemma 3.2.6. *If $\nabla u \in L^2(\Omega)^d$ and $\overline{u}$ satisfies (3.6), then*

$$\frac{\delta^2}{2}\|\nabla(u-\overline{u})\|^2 + \|u-\overline{u}\|^2 \leq \frac{\delta^2}{2}\|\nabla u\|^2. \tag{3.9}$$

If, additionally $\Delta u \in L^2(\Omega)^d$, then

$$\delta^2\|\nabla(u-\overline{u})\|^2 + \frac{1}{2}\|u-\overline{u}\|^2 \leq \delta^4\|\Delta u\|^2. \tag{3.10}$$

Lemma 3.2.7. *The operator $G^h : L^2(\Omega)^d \to X^h$ is self-adjoint and positive semi-definite on $L^2(\Omega)$ and positive definite on X^h.*

3.2.2 Tikhonov regularization

A workhorse to solve inverse problems is Tikhonov regularization [23,103,104]. If the operator G is symmetric and positive definite, then instead of passing to the normal equations as is the case in Tikhonov regularization, Tikhonov-Lavrentiev regularization can be applied.

Definition 3.2.8 (Tikhonov-Lavrentiev regularization)**.** *Choose a regularization parameter $\alpha > 0$. Solve for u_0 satisfying*

$$(G+\alpha I)u_0 = \overline{u}, \quad \text{in } \Omega.$$

This idea can be extended by an iteration method.

Definition 3.2.9 (Iterated Tikhonov-Lavrentiev regularization)**.** *Choose a regularization parameter $\alpha > 0$ and fix the number of updates $J \geq 1$. The iterated Tikhonov-Lavrentiev approximations u_j $(0 \leq j \leq J)$ are found by solving*

$$\begin{aligned}(G+\alpha I)u_0 &= \overline{u}, \quad \text{in } \Omega,\\ (G+\alpha I)(u_j - u_{j-1}) &= \overline{u} - Gu_{j-1}, \quad \text{in } \Omega.\end{aligned}$$

Given a source condition, it is known [23,51] Tikhonov-Lavrentiev and iterated Tikhonov-Lavrentiev regularization converge to u_{true} as $\epsilon \to 0$ and $\alpha \to 0$.

Theorem 3.2.10 (Error bound of Tikhonov-Lavrentiev regularization)**.** *Suppose that G is non-negative definite. Fix $\alpha > 0$. Let $e_j = u_{true} - u_j$ for all $j = 0, \ldots, J$. Suppose, for some $\beta \geq 0$ that $u_{true} \in Range(G^\beta)$ and the noise is bounded $\|\epsilon\| \leq \epsilon_0 < \infty$. Then, there exists a constant $C(J) < \infty$ such that, for any $0 \leq J \leq \beta$,*

$$\|e_J\| \leq \frac{(J+1)\epsilon_0}{\alpha} + \alpha^{J+1} C(J). \tag{3.11}$$

Moreover, if $\alpha = \alpha(\epsilon_0) = C\epsilon_0^{1/(J+2)}$ we have that $\|e_J\| \leq C\epsilon_0^{1-1/(J+2)}$.

This error result for iterated Tikhonov-Lavrentiev regularization is similar to that of iterated Tikhonov regularization, see [23, 51, 107].

3.3 MODIFICATION TO TIKHONOV REGULARIZATION

Algorithm 3.3.1 defines a modification to the iterated Tikhonov-Lavrentiev regularization (MITLAR) for the differential filter. We analyze the error in the continuous case by separating it into the following components: the regularization error in the MITLAR algorithm and the amount of noise amplification due to our regularization. We then discretize MITLAR in Algorithm 3.3.9. We analyze the error in the discretized case by separating it into the following components: the regularization error in the continuous MITLAR algorithm, the discretization error in the solution, and the discretized noise amplification due to the discrete MITLAR algorithm.

Algorithm 3.3.1. *(Modified Iterated Tikhonov-Lavrentiev Regularization [MITLAR]) Given convolved data $\overline{u}$ satisfying $Gu_{true} = \overline{u}$, fix the maximum number of iterations $J \geq 1$ and regularization parameter $\alpha > 0$. Solve for u_0 satisfying*

$$[(1-\alpha)G + \alpha I]u_0 = \bar{u}. \tag{3.12}$$

Then for $j = 1, ..., J$ solve for u_j satisfying

$$[(1-\alpha)G + \alpha I](u_j - u_{j-1}) = \bar{u} - Gu_{j-1}. \tag{3.13}$$

Define the following regularization operators D_α and $D_{\alpha,j}$ for convenience of notation.

Definition 3.3.2. *For $\alpha > 0$ define the modified Tikhonov-Lavrentiev operator D_α to be*

$$D_\alpha = [(1-\alpha)G + \alpha I]^{-1}. \tag{3.14}$$

For $j > 0$, define the j^{th} modified iterated Tikhonov-Lavrentiev operator $D_{\alpha,j}$ by

$$D_{\alpha,j}\overline{u} = u_j, \tag{3.15}$$

where u_j is obtained via Algorithm 3.3.1.

Remark 3.3.3 (Variational formulation of MITLAR)**.** *Assume G is the differential filter defined in (3.6). Algorithm 3.3.1 is equivalent to the following variational formulation. Given $u \in L^2(\Omega)$, then $u_J = D_J\overline{u}$ is the unique solution to the following equations*

$$\begin{aligned} &\alpha\delta^2\left(\nabla u_0, \nabla v\right) + \left(u_0, v\right) = \left(u, v\right), \quad \forall v \in X, \text{ and} \\ &\alpha\delta^2\left(\nabla u_j, \nabla v\right) + \left(u_j, v\right) = \left(u, v\right) + \alpha\delta^2\left(\nabla u_{j-1}, \nabla v\right), \quad \forall v \in X. \end{aligned} \tag{3.16}$$

Theorem 3.3.8 shows that this modification to Tikhonov-Lavrentiev regularization provides a higher order deconvolution error compared to iterated Tikhonov-Lavrentiev regularization. The following lemmas and propositions are needed for the proof of Theorem 3.3.8.

Lemma 3.3.4. *For $0 \leq \alpha \leq 1$, the function $f(x) = ((1-\alpha)x+\alpha)^{-1}$ maps the interval $(0,1]$ to $[1, \frac{1}{\alpha})$, and the function $g(x) = x((1-\alpha)x+\alpha)^{-1}$ maps the interval $(0,1]$ to $(0,1]$.*

Proof. The term $(1-\alpha)x + \alpha$ is a convex combination of x and 1, so

$$\begin{aligned} &\alpha < (1-\alpha)x + \alpha \leq 1, \text{ and} \\ &1 \leq \frac{1}{(1-\alpha)x+\alpha} < \frac{1}{\alpha}. \end{aligned}$$

For the bounds on $g(x)$, consider

$$g'(x) = x((1-\alpha)x+\alpha)^{-2}.$$

So $g'(x)$ has no critical points in the interval $(0,1)$. Therefore $g(x)$ attains its extrema on the boundary of $[0,1]$. Note that $g(1) = 1$, and $g(x) = 0$ if and only if $x = 0$. Therefore $g : (0,1] \to (0,1]$. □

Lemma 3.3.5. *For $0 \leq \alpha \leq 1$, the operators D_α, $D_\alpha G$, and $I - D_\alpha G$ are bounded. In particular, they satisfy*

$$\|D_\alpha\| \leq \frac{1}{\alpha}, \quad \|D_\alpha G\| \leq 1, \text{ and } \|I - D_\alpha G\| \leq 1. \tag{3.17}$$

Proof. The method of proof is similar to that employed in [67]. The differential filter operator G has a spectrum that lies in $(0, 1]$. Therefore by Lemma 3.3.4, the spectrum of $D_\alpha = ((1-\alpha)G + \alpha I)^{-1}$ lies between $[1, \frac{1}{\alpha})$. Also by Lemma 3.3.4, the spectrum of $D_\alpha G = ((1-\alpha)G + \alpha I)^{-1}G$ lies between (0,1]. Similarly, the spectrum of $I - D_\alpha G$ lies between [0,1). □

Proposition 3.3.6. *The error equation $e_J = u_{true} - u_J$ is given by*

$$e_J = (-\alpha\delta^2)^{J+1}(D_\alpha G)^{J+1}(\Delta^{J+1}u), \tag{3.18}$$

and the error is bounded

$$\|e_J\| \leq (\alpha\delta^2)^{J+1}\|\Delta^{J+1}u\|. \tag{3.19}$$

Proof. For $0 < j \leq J$, we start with (3.13) and an identity for u_{true},

$$[(1-\alpha)G + \alpha I](u_j - u_{j-1}) = \bar{u} - Gu_{j-1} \text{ and}$$
$$[(1-\alpha)G + \alpha I](u_{true} - u_{true}) = \bar{u} - Gu_{true}.$$

Subtracting these equations and rearranging gives

$$e_j = \alpha D_\alpha(I - G)e_{j-1} = \alpha D_\alpha G(G^{-1} - I)e_{j-1}. \tag{3.20}$$

For $j = 0$, we use (3.12) and the true solution

$$[(1-\alpha)G + \alpha I]u_0 = \bar{u} \text{ and}$$
$$[(1-\alpha)G + \alpha I]u_{true} = (1-\alpha)\overline{u} + \alpha u_{true}.$$

Subtraction gives

$$e_0 = \alpha D_\alpha(I - G)u_{true} = \alpha D_\alpha G(G^{-1} - I)u_{true}. \tag{3.21}$$

The norm of the error is bounded by taking the norm of the error equation (3.18) and using the bound on $\|D_\alpha G\|$ in (3.17) to obtain

$$\begin{aligned}\|e_J\| &= \|(-\alpha\delta^2)^{J+1}(D_\alpha G)^{J+1}(\Delta^{J+1}u)\| \\ &\leq (\alpha\delta^2)^{J+1}\|(D_\alpha G)^{J+1}\|\|\Delta^{J+1}u\| \\ &\leq (\alpha\delta^2)^{J+1}\|\Delta^{J+1}u\|.\end{aligned}$$

□

Proposition 3.3.7. *The j^{th} step of the MITLAR algorithm, u_j, is given by*

$$u_j := D_{\alpha,j}\overline{u} = D_\alpha \sum_{i=0}^{j}(\alpha D_\alpha(I-G))^i\overline{u}. \tag{3.22}$$

Proof. Starting with (3.13), solve for u_j and use the equations

$$I - D_\alpha G = \alpha D_\alpha(I-G) \text{ and } u_0 = D_\alpha\overline{u}.$$

$$\begin{aligned}u_j &= u_{j-1} + D_\alpha(\overline{u} - Gu_{j-1}) \\ &= D_\alpha\overline{u} + (I - D_\alpha G)u_{j-1} \\ &= D_\alpha\overline{u} + \alpha D_\alpha(I-G)u_{j-1} \\ &= D_\alpha \sum_{i=0}^{j}(\alpha D_\alpha(I-G))^i\overline{u}.\end{aligned}$$

as claimed. □

Noise amplification is one of the fundamental difficulties of ill-posed inverse problems [23]. The noise amplification is studied in Problem 3.1.2 where $\bar{u}$ has additive noise ϵ. The MITLAR algorithm applied to this problem gives an improvement over iterated Tikhonov regularization in the noise free portion of the error as shown in Proposition 3.3.6. The bound on the error in the noisy data is no worse as shown in Theorem 3.3.8.

Theorem 3.3.8. *Under the conditions of Algorithm 3.3.1 and (3.5) and if there exists some ϵ_0 such that $\|\epsilon\| < \epsilon_0$, then the error in the j^{th} step of the MITLAR algorithm is*

$$e_J = (-\alpha\delta^2)^{J+1}(D_\alpha G)^{J+1}(\Delta^{J+1}u) + D_\alpha \sum_{i=0}^{J}(I - D_\alpha G)^i \epsilon. \tag{3.23}$$

The error is bounded,

$$\|e_J\| \leq (\alpha\delta^2)^{J+1}\|\Delta^{J+1}u\| + \frac{(J+1)\epsilon_0}{\alpha}. \tag{3.24}$$

Proof. Using Proposition 3.3.6 and Proposition 3.3.7, we have

$$\begin{aligned} u_J &= D_{\alpha,J}(\overline{u} + \epsilon) \\ &= D_{\alpha,J}\overline{u} + D_{\alpha,J}\epsilon \\ &= (-\alpha\delta^2)^{J+1}(D_\alpha G)^{J+1}(\Delta^{J+1}u) + D_\alpha \sum_{i=0}^{J}(I - D_\alpha G)^i \epsilon, \end{aligned}$$

as claimed. To get a bound on the norm of the error, start with the error equation and take the norm and use the inequalities in (3.17).

$$\begin{aligned} \|e_J\| &= \left\| (-\alpha\delta^2)^{J+1}(D_\alpha G)^{J+1}(\Delta^{J+1}u) + D_\alpha \sum_{i=0}^{J}(I - D_\alpha G)^i \epsilon \right\| \\ &\leq (\alpha\delta^2)^{J+1}\|\Delta^{J+1}u\| + \|D_\alpha\| \sum_{i=0}^{J} \|(I - D_\alpha G)^i\| \|\epsilon\| \\ &\leq (\alpha\delta^2)^{J+1}\|\Delta^{J+1}u\| + \frac{1}{\alpha}\sum_{i=0}^{J}\epsilon_0 \\ &\leq (\alpha\delta^2)^{J+1}\|\Delta^{J+1}u\| + \frac{(J+1)\epsilon_0}{\alpha}. \end{aligned}$$

□

We see that this is an improvement over modified Tikhonov-Lavrentiev regularization because of its double asymptotic behavior in α and δ. Each update step in the method adds an extra factor of $\alpha\delta^2$, whereas each update step of Tikhonov-Lavrentiev adds an extra factor of α.

3.3.1 Discrete MITLAR applied to the differential operator

The results of the previous section are now extended to the discrete form of the MITLAR algorithm. The modified iterated Tikhonov-Lavrentiev regularization operator applied to the differential filter is defined in Definition 3.2.3 variationally on a finite dimensional space.

Algorithm 3.3.9 (Discrete modified iterated Tikhonov-Lavrentiev regularization)**.** *Let X^h be a finite dimensional subspace of X. Let $u \in X$ and $G^h u = \overline{u}^h \in X^h$ satisfy Definition 3.2.3. Choose $\alpha > 0$ and filter radius $\delta > 0$ and define $u_j^h = D_{\alpha,j}^h \overline{u}$ recursively by finding the unique solution in X^h to the problems*

$$\begin{aligned} &\alpha\delta^2 \left(\nabla u_0^h, \nabla v^h\right) + \left(u_0^h, v^h\right) = \left(u, v^h\right), \quad \forall v^h \in X^h \text{ and} \\ &\alpha\delta^2 \left(\nabla u_j^h, \nabla v^h\right) + \left(u_j^h, v^h\right) = \left(u, v^h\right) + \alpha\delta^2 \left(\nabla u_{j-1}^h, \nabla v^h\right) \quad \forall v^h \in X^h. \end{aligned} \tag{3.25}$$

Theorem 3.3.10. *Given a filter radius $\delta > 0$ of the differential filter operator G, and fix a regularization parameter $0 \le \alpha \le 1$ and stopping number $J \ge 0$. If $\|\Delta^j u\|_{L^2(\Omega)}$ is bounded for all $j \le J+1$, then the error to the problem in (3.1) using the discrete MITLAR algorithm is bounded. In particular,*

$$\begin{aligned} \|u - D_{\alpha,J}^h G^h u\|_{L^2(\Omega)} \le (\alpha\delta^2)^{J+1} \|\Delta^{J+1} u\|_{L^2(\Omega)} \\ + C(\sqrt{\alpha}\delta h^k + h^{k+1}) \max_{0 \le j \le J} \|D_{\alpha,j} G u\|_{k+1}. \end{aligned} \tag{3.26}$$

Proof. Denote $\|\cdot\|_{L^2(\Omega)}$ by $\|\cdot\|$. Add and subtract the exact deconvolution term, and then use the triangle inequality,

$$\|u - D_{\alpha,J}^h G^h u\| \le \|u - D_{\alpha,J} G u\| + \|D_{\alpha,J} G u - D_{\alpha,J}^h G^h u\|. \tag{3.27}$$

The first term of (3.27) is bounded by (3.19)

$$\|u - D_{\alpha,J} G u\| \le (\alpha\delta^2)^{J+1} \|\Delta^{J+1} u\|.$$

For the second term of (3.27), start with (3.16) and take $v = v^h$, then subtract equation (3.25). For $j = 1, \ldots, J$, we have

$$\alpha\delta^2 \left(\nabla(u_j - u_j^h), \nabla v^h\right) + \left(u_j - u_j^h, v^h\right) = \alpha\delta^2 \left(\nabla(u_{j-1} - u_{j-1}^h), \nabla v^h\right). \tag{3.28}$$

The case when $j = 0$ follows similarly or see [67]. We define $\eta_j = u_j - w_j^h$ and $\phi_j^h = u_j^h - w_j^h$ for some $w_j^h \in X^h$ to be chosen later for each $j = 1, \dots, J$. Using these definitions, we write (3.28) as

$$\alpha\delta^2 \left(\nabla(\eta_j - \phi_j^h), \nabla v^h\right) + \left(\eta_j - \phi_j^h, v^h\right) = \alpha\delta^2 \left(\nabla(\eta_{j-1} - \phi_{j-1}^h), \nabla v^h\right). \tag{3.29}$$

Take $v^h = \phi_j^h$, denote $e_j = u_j - u_j^h = \eta_j - \phi_j^h$, and separate the terms to get

$$\begin{aligned}
\alpha\delta^2\|\nabla\phi_j^h\|^2 + \|\phi_j^h\|^2 &= \alpha\delta^2 \left(\nabla\eta_j, \nabla\phi_j^h\right) + \left(\eta_j, \phi_j^h\right) + \alpha\delta^2 \left(\nabla e_{j-1}\nabla\phi_j^h\right) \\
&\leq \alpha\delta^2\|\nabla\eta_j\|^2 + \frac{\alpha\delta^2}{4}\|\nabla\phi_j^h\|^2 + \frac{1}{2}\|\eta_j\|^2 + \frac{1}{2}\|\phi_j^h\|^2 \\
&\quad + \alpha\delta^2\|\nabla e_{j-1}\|^2 + \frac{\alpha\delta^2}{4}\|\nabla\phi_j^h\|^2.
\end{aligned}$$

Subtract the $\|\nabla\phi_j^h\|^2$ term to the left hand side and multiply by 2 to get

$$\alpha\delta^2\|\nabla\phi_j^h\|^2 + \|\phi_j^h\|^2 \leq 2\alpha\delta^2\|\nabla\eta_j\|^2 + \|\eta_j\|^2 + 2\alpha\delta^2\|\nabla e_{j-1}\|^2.$$

Use $\|e_j\| \leq \|\eta_j\| + \|\phi_j^h\|$ and $\|\nabla e_j\| \leq \|\nabla\eta_j\| + \|\nabla\phi_j^h\|$ to obtain the recursion

$$\alpha\delta^2\|\nabla e_j\|^2 + \|e_j\|^2 \leq 3\alpha\delta^2\|\nabla\eta_j\|^2 + 2\|\eta_j\|^2 + 2\alpha\delta^2\|\nabla e_{j-1}\|^2. \tag{3.30}$$

Thus

$$\|e_J\| \leq C(J) \max_{0\leq j\leq J} \left(\sqrt{\alpha\delta^2}\|\nabla\eta_j\| + \|\eta_j\|\right) \tag{3.31}$$

This inequality holds for all $w_j^h \in X^h$, so take the infimum over X^h and apply the approximation inequalities (3.4) to obtain

$$\|D_{\alpha,J}Gu - D_{\alpha,J}^h G^h u\| \leq C(\sqrt{\alpha}\delta h^k + h^{k+1}) \max_{0\leq j\leq J} \|D_{\alpha,j}Gu\|_{k+1}. \tag{3.32}$$

Combining equations (3.19) and (3.32) proves the claim. □

Problem 3.1.2 still needs to be addressed. If our data consists of discrete measurements that contain noise $\overline{u}^h + \varepsilon$, then approximations of the error from that noise are needed. This problem is addressed by applying the discretized modified iterated Tikhonov-Lavrentiev algorithm to the discretized data $\overline{u}^h + \varepsilon$.

First, we prove the boundedness of operators G^h, D^h, and D_J^h.

Lemma 3.3.11. *The operators $G^h : X^h \to X^h$, $D^h : X^h \to X^h$, and $D_J^h : X^h \to X^h$ are bounded and furthermore they satisfy*

$$\|G^h\| \leq 1, \tag{3.33}$$

$$\|D^h\| \leq \frac{1}{\alpha}, \tag{3.34}$$

$$\|D_J^h\| \leq \frac{J+1}{\alpha}, \tag{3.35}$$

$$\|D^h G^h\| \leq 1, \text{ and} \tag{3.36}$$

$$\|I - D^h G^h\| \leq 1. \tag{3.37}$$

Proof. For the first, take $u \in X^h$ then $\|G^h u\| \leq \|u^h\|$ by Cauchy-Schwartz and Young inequalities to equation (3.6). For the second, note that $D^h = [(1-\alpha)G^h + \alpha I]^{-1}$ is the convex combination of positive operators, so its spectrum is bounded by $\frac{1}{\alpha}$. For the third, we write out $D_J^h = D^h \sum_{i=0}^{J} (\alpha D^h (I - G^h))^i$. Then taking $u \in X^h$ we obtain,

$$\|D_J^h u\| = \|D^h \sum_{i=0}^{J} (\alpha D^h (I - G^h))^i u\| \tag{3.38}$$

$$\leq \|D^h\| \sum_{i=0}^{J} \|(\alpha D^h (I - G^h))^i\| \|u\| \tag{3.39}$$

$$\leq \frac{1}{\alpha} \sum_{i=0}^{J} \|u\| \tag{3.40}$$

$$\leq \frac{J+1}{\alpha} \|u\|. \tag{3.41}$$

The spectrum of $D^h G^h$ lies in between (0,1] and the spectrum of $I - D^h G^h$ lies in between [0,1) proving the result. □

Theorem 3.3.12. *If the noise $\varepsilon \in X^h$ is bounded $\|\varepsilon\| \leq \epsilon_0$, then the error e_j between the noise free solution and the discretized MITLAR solution applied to noisy data $\overline{u}^h + \varepsilon$ is bounded, and*

$$\begin{aligned} \|e_j\| &:= \|u_{true} - D_J^h(\overline{u}^h + \varepsilon)\| \\ &\leq \frac{J+1}{\alpha}\epsilon_0 + (\alpha\delta^2)^{J+1} \|\Delta^{J+1} u\| \\ &\quad + C(\sqrt{\alpha}\delta h^k + h^{k+1}) \max_{0 \leq j \leq J} \|D_{\alpha,j} G u\|_{k+1}. \end{aligned} \tag{3.42}$$

Proof. Use the triangle inequality to separate the error into two pieces, the true discretization error and the error associated with noise

$$\|u_{true} - D_J^h(\overline{u}^h + \varepsilon)\| \leq \|D_J^h \varepsilon\| + \|u_{true} - D_J^h(\overline{u}^h)\|. \tag{3.43}$$

Use Lemma 3.3.11to bound the first term,

$$\|D_J^h \varepsilon\| \leq \frac{J+1}{\alpha}\|\varepsilon\|. \tag{3.44}$$

Theorem 3.3.10 gives a bound on the second term,

$$\begin{aligned}\|u_{true} - D_J^h(\overline{u}^h)\| \leq (\alpha\delta^2)^{J+1}\|\Delta^{J+1}u\| \\ + C(\sqrt{\alpha}\delta h^k + h^{k+1}) \max_{0\leq j\leq J}\|D_{\alpha,j}Gu\|_{k+1}.\end{aligned} \tag{3.45}$$

Combine these results to prove the claim. □

3.4 DESCENT PROPERTIES OF MODIFIED ITERATED TIKHONOV-LAVRENTIEV APPROXIMATIONS

Problem 3.1.2 for self-adjoint and positive definite G is equivalent to the minimization problem

$$v = \arg\min_{v\in X} E_\epsilon(v), \text{ where } E_\epsilon(v) := \frac{1}{2}(Gv, v)_X - (\bar{u} + \epsilon, v)_X$$

We analyze when the MITLAR approximations u_0, u_1, ... form a minimizing sequence for $E_\epsilon(\cdot)$ and the noise-free functional $E_0(\cdot) := E_\epsilon(\cdot)|_{\epsilon=0}$.

Proposition 3.4.1. *Let G be self-adjoint and positive definite and $0 < \alpha \leq \frac{1}{2}$. Then the Modified Iterative Tikhonov-Lavrentiev iterates are a minimizing sequence for E_ϵ. In particular,*

$$E_\epsilon(u_j) - E_\epsilon(u_{j+1}) = ([(\frac{1}{2} - \alpha)G + \alpha I](u_{j+1} - u_j), u_{j+1} - u_j) \geq 0. \tag{3.46}$$

Thus

$$E_\epsilon(u_{j+1}) < E_\epsilon(u_j), \text{ unless } u_{j+1} = u_j.$$

Proof. Expand the definitions of $E_\epsilon(\cdot)$ and cancel terms to prove the identity.

$$\begin{aligned}
E_\epsilon(u_j) - E_\epsilon(u_{j+1}) &= \frac{1}{2}(Gu_j, u_j) - (\bar{u}+\epsilon, u_j) - \frac{1}{2}(Gu_{j+1}, u_{j+1}) + (\bar{u}+\epsilon, u_{j+1}) \\
&= \frac{1}{2}(Gu_j, u_j - u_{j+1}) + \frac{1}{2}(G(u_j - u_{j+1}), u_j) - (\bar{u}+\epsilon, u_j - u_{j+1}) \\
&= \frac{1}{2}(G(u_j - u_{j+1}), u_j + u_{j+1}) \\
&\quad - ([(1-\alpha)G + \alpha I](u_{j+1} - u_j) + Gu_j, u_j - u_{j+1}) \\
&= \frac{1}{2}(G(u_j - u_{j+1}), u_j + u_{j+1}) - (G(u_j - u_{j+1}), u_{j+1}) \\
&\quad + \alpha([I - G](u_j - u_{j+1}), u_j - u_{j+1}) \\
&= ([(\frac{1}{2} - \alpha)G + \alpha I](u_{j+1} - u_j), u_{j+1} - u_j).
\end{aligned}$$

Equation (3.46) defines a norm as long as $0 < \alpha \leq \frac{1}{2}$, so $E_\epsilon(u_{j+1}) < E_\epsilon(u_j)$ unless $u_{j+1} = u_j$ as claimed. □

Equation (3.13) implies that if $u_j = u_{j+1}$, then $Gu_j = \bar{u} + \epsilon$. Thus, as $j \to \infty$, u_j converges to the undesired solution of the noisy data problem. This implies that it is critical to stop after a finite number of update steps.

Problem 3.1.1 desires the solution to the noise-free equation

$$Gu_{true} = \bar{u},$$

from noisy data, we analyze the sequence of noisy MITLAR approximations u_j in the noise-free functional

$$E_0(v) := \frac{1}{2}(Gv, v)_X - (\bar{u}, v)_X.$$

First, note that $E_0(v) = E_\epsilon(v) + (\epsilon, v)$, and then by Proposition 3.4.1,

$$E_0(u_j) - E_0(u_{j+1}) = (\epsilon, u_{j+1} - u_j) + ([(\frac{1}{2} - \alpha)G + \alpha I](u_{j+1} - u_j), u_{j+1} - u_j).$$

Theorem 3.4.2. *Let G be self-adjoint and positive definite. Suppose an estimate on the noise $||\epsilon||_X \leq \epsilon_0$ is known. Then the Modified Iterative Tikhonov-Lavrentiev approximations are a minimizing sequence for the noise-free functional E_0 as long as*

$$\frac{\epsilon_0}{||u_{j+1} - u_j||_X} \leq \alpha \leq \frac{1}{2}. \tag{3.47}$$

Proof. First, the Cauchy-Schwartz inequality implies

$$|(\epsilon, u_{j+1} - u_j)| \leq \|\epsilon\| \|u_{j+1} - u_j\|$$

Then, if (3.47) holds, then

$$\begin{aligned}
0 &\leq \|\epsilon\| \|u_{j+1} - u_j\| - |(\epsilon, u_{j+1} - u_j)| \\
&\leq \alpha \|u_{j+1} - u_j\|^2 - |(\epsilon, u_{j+1} - u_j)| \\
&\leq \left([(\frac{1}{2} - \alpha)G + \alpha I](u_{j+1} - u_j), u_{j+1} - u_j \right) - |(\epsilon, u_{j+1} - u_j)| \\
&\leq \left([(\frac{1}{2} - \alpha)G + \alpha I](u_{j+1} - u_j), u_{j+1} - u_j \right) + (\epsilon, u_{j+1} - u_j) \\
&= E_0(u_j) - E_0(u_{j+1}).
\end{aligned}$$

□

Theorem 3.4.2 implies that when the size of the updates is larger than twice the noise, the updates move the approximate solution closer to the noise free solution. As the updates become smaller, u_j begins to deviate from an approximation of the noise free solution unless α is increased.

This result can be extended if more is known about the noise or its statistical distribution. In particular if there a projection operator P where $P\epsilon \perp (u_{j+1} - u_j)$, then

$$(\epsilon, u_{j+1} - u_j)_X = (\epsilon, (I - P)[u_{j+1} - u_j])_X.$$

In other words, if a component of the MITLAR update is in the range of the projection, then that updated component will reduce the error to the noise free problem. This suggests the following small algorithmic modification.

Algorithm 3.4.3. *Given data $\bar{u}+\epsilon$, suppose $\|\epsilon\|_X \leq \epsilon_0$ and given a projection operator P satisfying $\bar{P}\epsilon = 0$. Fix $J \geq 0$. Solve for u_0 in*

$$((1-\alpha)G + \alpha I)u_0 = \bar{u} + \epsilon.$$

Then for $j = 1, \ldots, J$ and while $\frac{\epsilon_0}{||u_j - u_{j-1}||_X} \leq \alpha \leq \frac{1}{2}$, solve for u_j in

$$((1-\alpha)G + \alpha I)(u_j - u_{j-1}) = \bar{u} + \epsilon - Gu_{j-1}$$

If $\alpha < \frac{\epsilon_0}{||u_j - u_{j-1}||_X}$, then either increase α so that the hypothesis for Theorem 3.4.2 applies and recompute or compute as above $u_j - u_{j-1}$ and calculate

$$\tilde{u}_j = u_{j-1} + P(u_j - u_{j-1}). \tag{3.48}$$

Then set $D_j\bar{u} := \tilde{u}_j$.

3.5 NUMERICAL ILLUSTRATIONS

We investigate several applications. In section 3.5.1, we verify the use of our stopping criterion. In section 3.5.2, we compare the four methods of Tikhonov, iterated Tikhonov, modified Tikhonov, and modified iterated Tikhonov in the application of deconvolution of the differential filter. Section 3.5.3 verifies the convergence rates of the MITLAR algorithm applied to a test problem.

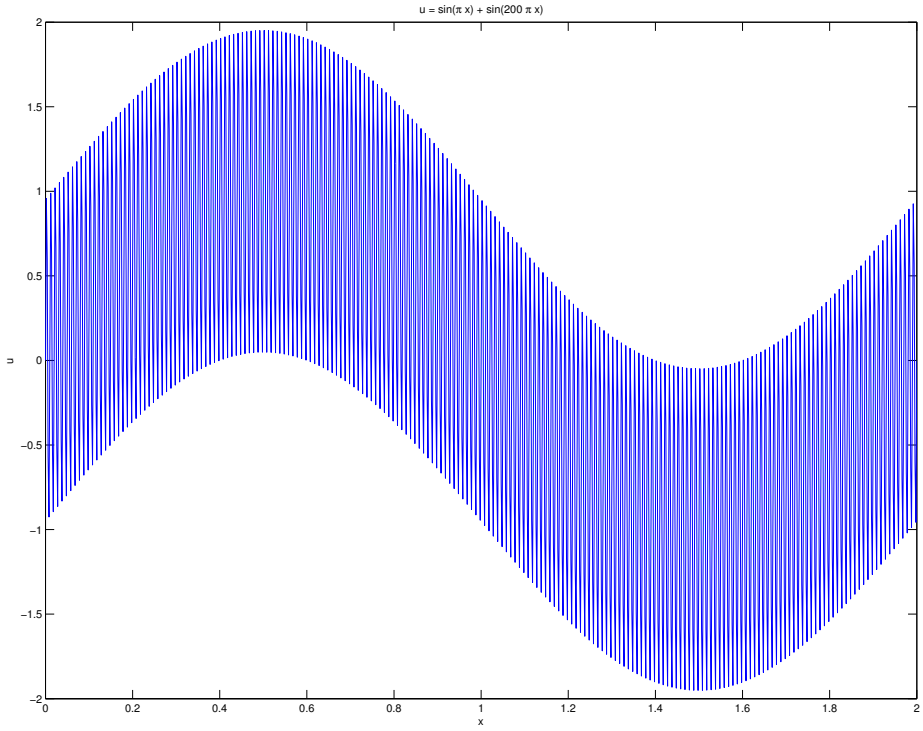

Figure 6: True solution, with high and low frequencies, that is filtered to obtain the data in the stopping criterion problem.

3.5.1 Stopping Criterion

We verify our stopping criterion (Theorem 3.4.2) by choosing a true solution to be $u = \sin(\pi x) + \sin(200\pi x)$, plotted in Figure 6, over the interval $[0, 2]$.

We discretize the interval with a step size of $h = \frac{2}{1001}$ and choosing the filtering radius for the differential filter to be $\delta = 6h$. Our simulated data was obtained by filtering the true solution and adding 1% random noise to the filtered data. We select initial regularization parameter $\alpha = 0.1$.

Figure 7 shows the noise-free functional calculated with the noisy MITLAR approximation u_j. The calculated optimal stopping point (via Theorem 3.4.2) occurs after $J = 4$ steps

and is shown as a green dot. Theorem The figure demonstrates the how the algorithm stops before the noise-free energy functional increases and converges to the noisy solution.

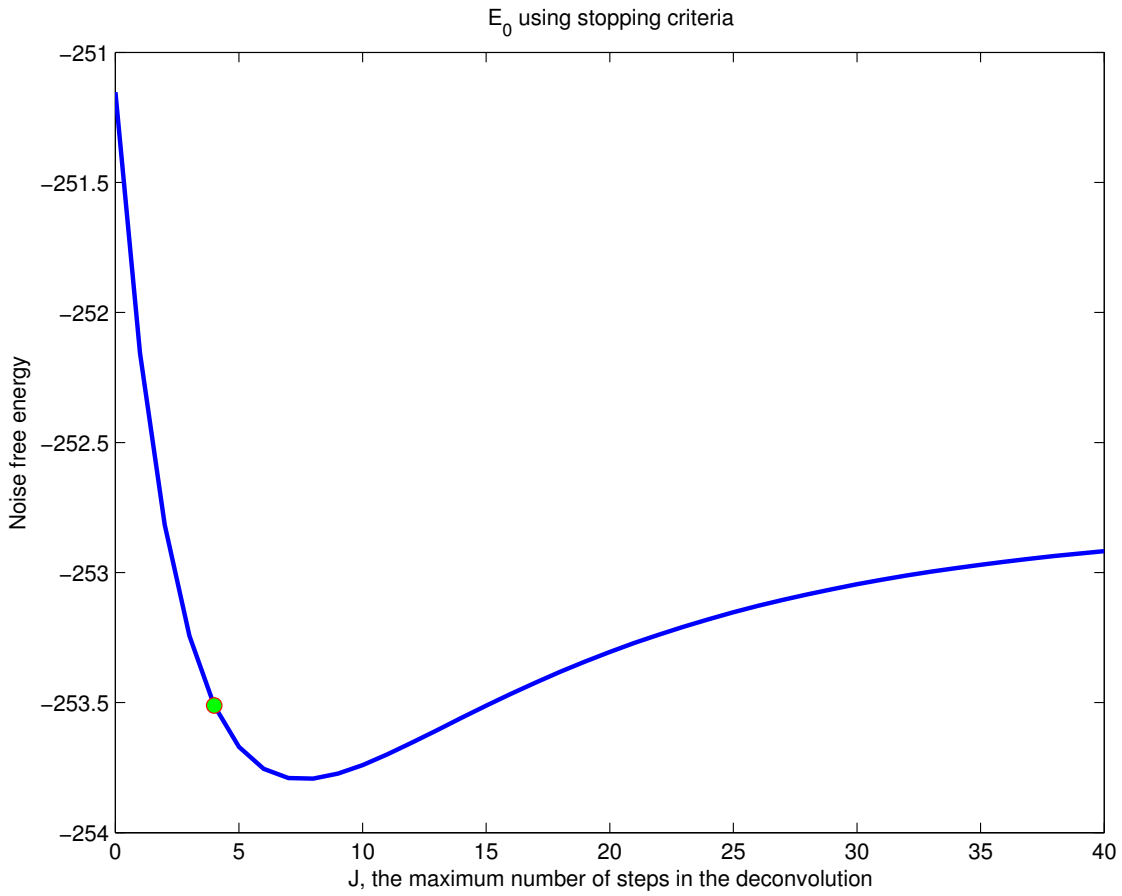

Figure 7: Noise-free energy functional calculated for values of J between 0 and 40. The stopping criterion forces us to stop after 4 iteration steps (as shown with the green dot). Notice the stopping criterion stopped the algorithm before the iterations converge to the noisy solution.

3.5.2 Comparison of Four Deconvolution Algorithms

We check the efficiency of Algorithm 3.3.1 by comparing the relative error of a solution for a given parameter α to the relative errors found with Tikhonov-Lavrentiev, Iterative Tikhonov-Lavrentiev, and Modified Tikhonov-Lavrentiev using the same α. We start out

with the original data as $\mathbf{u} = sin(\pi x) + 0.1sin(100\pi x)$, with 1000 sample points taken over the interval $[0, 2]$; hence the step size is $h = 2/1001$. We set our filtering radius at $\delta = 0.01$. We let the α vary from 1 to 10^{-3} and calculate 1, 2, and 3 steps for the iterative methods. The results are shown in Figures 8, 9, and 10 respectively.

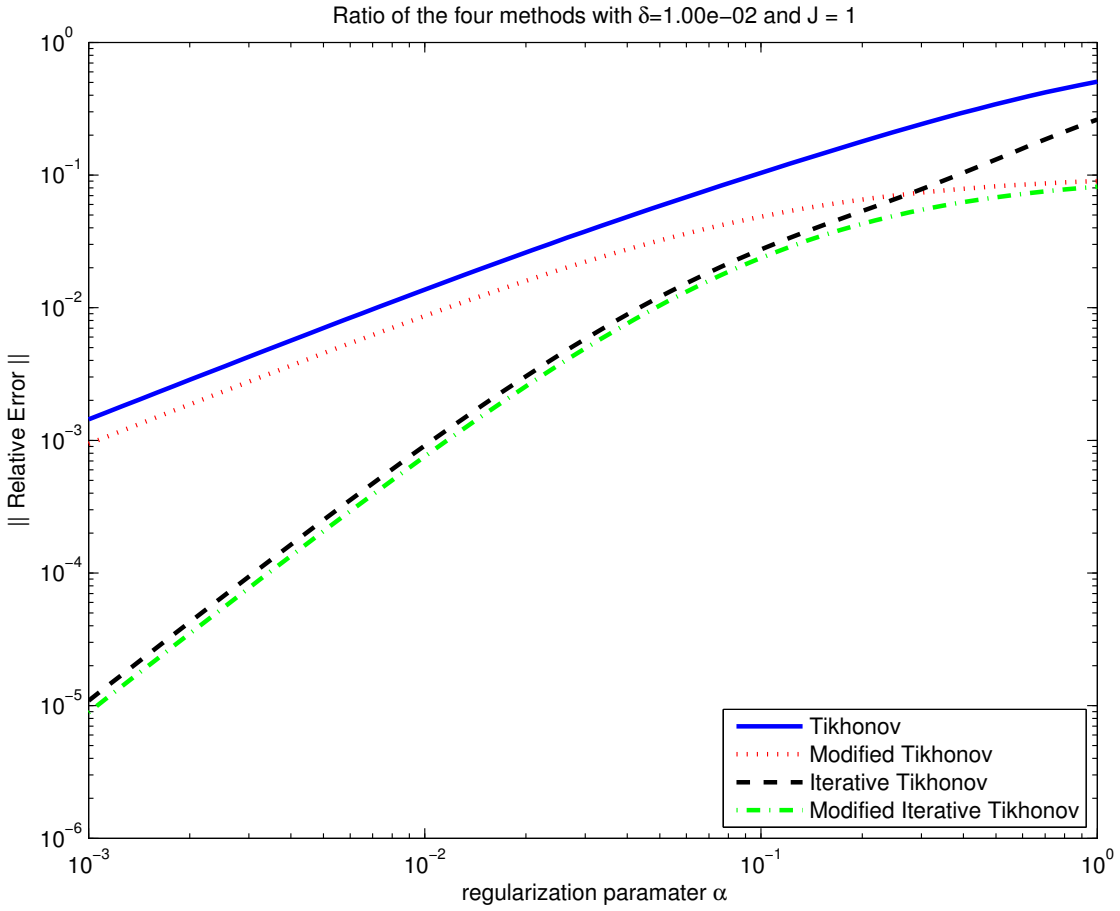

Figure 8: Relative errors for the four algorithms with 1 iterative step over $\alpha = 10^{-3}$ to $\alpha = 1$. Notice that the modified iterated Tikhonov-Lavrentiev plot has the lowest error over the entire range of regularization parameters.

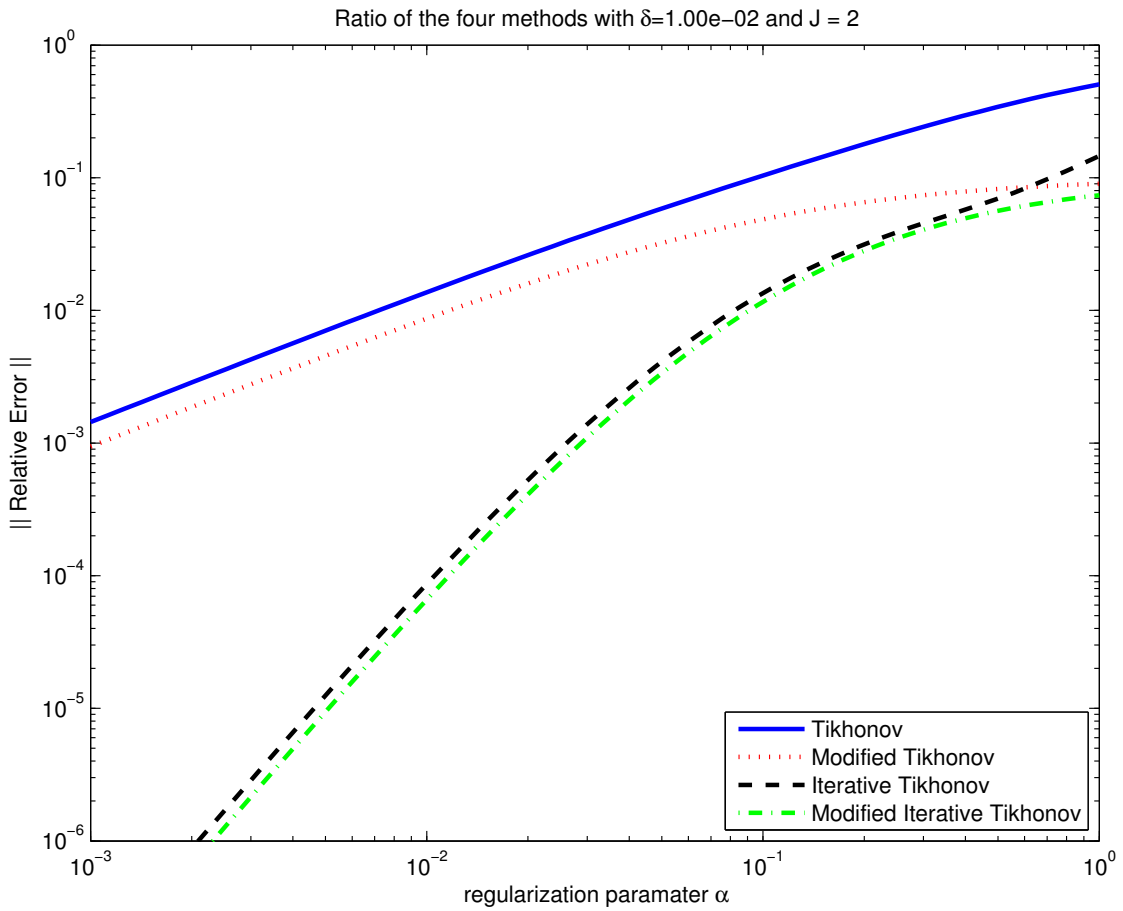

Figure 9: Relative errors for the four algorithms with 2 iterative step over $\alpha = 10^{-3}$ to $\alpha = 1$. Notice that the modified iterated Tikhonov-Lavrentiev plot has the lowest error over the entire range of regularization parameters.

3.5.3 Verification of Convergence Rates

We calculate the convergence rates of three different problems to verify the convergence rates predicted in Theorem 3.3.10. We take a true solution over the domain $[0,1] \times [0,1]$ of

$$u = \sin(\pi x)\sin(\pi y).$$

We discretize using the square command in FreeFEM++ [72] with $n \times n$ intervals and use piecewise continuous linear polynomials. We use a filter radius of $\delta = 0.1(\frac{2\pi}{n})^{1/4}$ and

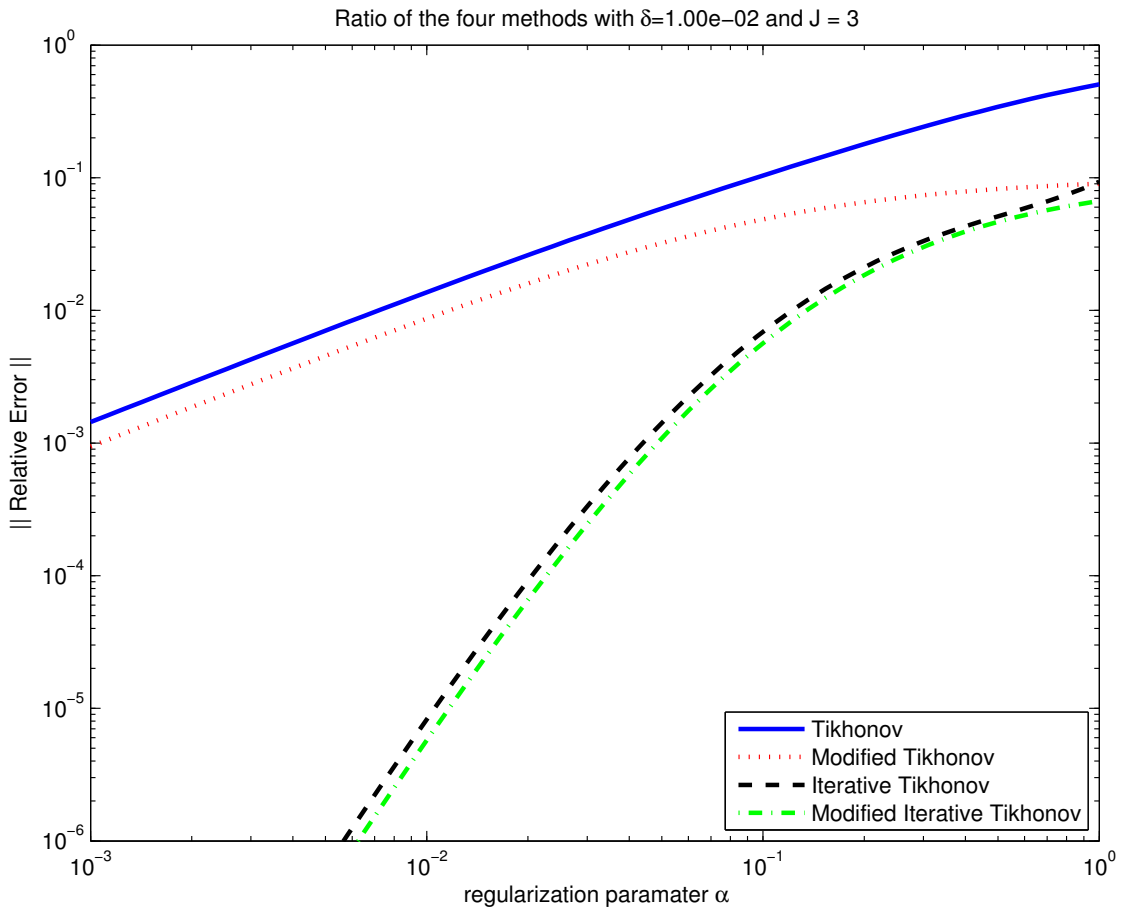

Figure 10: Relative errors for the four algorithms with 3 iterative step over $\alpha = 10^{-3}$ to $\alpha = 1$. Notice that the modified iterated Tikhonov-Lavrentiev plot has the lowest error over the entire range of regularization parameters.

regularization parameter $\alpha = 0.1(\frac{2\pi}{n})^{1/2}$.

The theoretical convergence rate predicted by Theorem 3.3.10 for $J = 0$ is $\mathcal{O}(h)$. Table 2

Table 2: Convergence rates for MITLAR $J = 0$. The convergence rates are approximating the theoretical value of 1 (error $= \mathcal{O}(\alpha\delta^2) = \mathcal{O}(h)$).

n	L_2 error	rate	H_1 error	rate
20	0.00308162		0.0136919	
40	0.00154557	0.995547	0.00686712	0.995547
60	0.00103144	0.997457	0.0045828	0.997457
80	0.000773982	0.998207	0.00343888	0.998207
100	0.000619377	0.998612	0.00275195	0.998612
120	0.000516254	0.998867	0.00229377	0.998867
140	0.000442569	0.999043	0.00196638	0.999043

Table 3: Convergence rates for MITLAR $J = 1$. The convergence rates are approximating the theoretical value of 2 (error $= \mathcal{O}((\alpha\delta^2)^2) = \mathcal{O}(h^2)$).

n	L_2 error	rate	H_1 error	rate
20	1.89939e-05		8.43985e-05	
40	4.77789e-06	1.99109	2.12376e-05	1.9906
60	2.12789e-06	1.99491	9.46506e-06	1.99318
80	1.19818e-06	1.99641	5.33555e-06	1.99253
100	7.6731e-07	1.99722	3.42222e-06	1.99021
120	5.33075e-07	1.99773	2.38236e-06	1.98658
140	3.91763e-07	1.99807	1.75523e-06	1.98179

Table 4: Convergence rates for Tikhonov $J = 0$. The convergence rates are approximating the theoretical value of 1/2 (error $= \mathcal{O}(\alpha) = \mathcal{O}(h^{1/2})$).

n	L_2 error	rate	H_1 error	rate
20	1.89939e-05		8.43985e-05	
40	4.77789e-06	1.99109	2.12376e-05	1.9906
60	2.12789e-06	1.99491	9.46506e-06	1.99318
80	1.19818e-06	1.99641	5.33555e-06	1.99253
100	7.6731e-07	1.99722	3.42222e-06	1.99021
120	5.33075e-07	1.99773	2.38236e-06	1.98658
140	3.91763e-07	1.99807	1.75523e-06	1.98179

Table 5: Convergence rates for Tikhonov $J = 1$. The convergence rates are approximating the theoretical value of 1 (error $= \mathcal{O}(\alpha^2) = \mathcal{O}(h)$).

n	L_2 error	rate	H_1 error	rate
20	0.00171708		0.00762915	
40	0.000839742	1.03194	0.00373106	1.03194
60	0.000553807	1.02667	0.00246062	1.02667
80	0.00041256	1.02347	0.00183305	1.02347
100	0.000328488	1.02124	0.0014595	1.02124
120	0.000272764	1.01957	0.00121192	1.01957
140	0.000233141	1.01826	0.00103587	1.01826

3.6 CONCLUSION

We introduced a novel tool for solving inverse problems, that is the modified iterated Tikhonov-Lavrentiev regularization algorithm. We show that the noise free errors in using this method are doubly asymptotic in α and δ, that is $\mathcal{O}((\alpha\delta^2)^{J+1})$, when applied to the deconvolution of the differential filter. However, using Tikhonov-Lavrentiev regularization or iterated Tikhonov-Lavrentiev regularization only results in noise free errors depending on α, $\mathcal{O}(\alpha)$ and $\mathcal{O}(\alpha^{J+1})$ respectively.

We also introduce a tool for calculating when to stop the iteration steps for our iterated algorithm. We show that continuing to iterate until the solution converges gives the unwanted, noisy solution. However, our stopping criterion guarantees that the iteration steps are getting closer to the noise free solution.

The example chosen to illustrate the stopping criterion did not show optimal stopping. This is due to the restriction on regularization parameter that $\alpha \leq \frac{1}{2}$. If we incorporated more knowledge about the noise added into the model, then we would be able to get a more accurate bound on the maximum number of iteration steps. As it is, the method will always stop us before the minimum energy.

4.0 APPLICATION OF MITLAR TO FLOW MODELING

"A cloud is made of billows upon billows upon billows that look like clouds. As you come closer to a cloud you don't get something smooth, but irregularities at a smaller scale." (Benoit Mandelbrot)

4.1 CONTINUOUS APPROXIMATION OF NSE

The Navier-Stokes equations (NSE) constitute a well-accepted continuum model for incompressible, viscous, Newtonian fluids with a wide range of applications in climate modeling, energy sciences, and bio-engineering. We consider flow in a sufficiently smooth domain $\Omega \subset \mathbb{R}^3$, with velocity field $\mathbf{u}$, pressure p, and body force $\mathbf{f}$. Let $Re = LU/\nu$ be the Reynold's number, $\nu > 0$ the kinematic viscosity, L and U the problem's characteristic length and velocity respectively.

Problem 4.1.1 (Navier-Stokes equation)**.** *Find* $\mathbf{u} : \Omega \times (0,T) \to \mathbb{R}^3$ *and* $p : \Omega \times (0,T) \to \mathbb{R}$ *satisfying*

$$\mathbf{u}_t + \mathbf{u} \cdot \nabla \mathbf{u} - Re^{-1} \Delta \mathbf{u} + \nabla p = \mathbf{f}, \qquad \nabla \cdot \mathbf{u} = 0. \tag{4.1}$$

For turbulent flows (characterized by $Re >> 1$) in complex domains, it is infeasible to properly resolve all persistent and energetically significant scales down to the Kolmogorov length scale of $O(Re^{-3/4})$ with a direct numerical simulation in a given time constraint. Various methods have been employed to approximate NSE-solutions. Regularization methods are particularly enticing because they are *simple* and *efficient* to implement. Although many regularization methods have been analyzed for this problem, there are still many open

considerations. Among regularization methods, ones currently studied include

$$\begin{aligned}
&\text{(Leray)} && \mathbf{u}_t + \overline{\mathbf{u}} \cdot \nabla \mathbf{u} - Re^{-1}\Delta \mathbf{u} + \nabla p = \mathbf{f} \text{ and } \nabla \cdot \mathbf{u} = 0,\\
&\text{(NS-}\alpha\text{)} && \mathbf{u}_t + \overline{\mathbf{u}} \times (\nabla \times \mathbf{u}) - Re^{-1}\Delta \mathbf{u} + \nabla P = \mathbf{f} \text{ and } \nabla \cdot \mathbf{u} = 0,\\
&\text{(NS-}\overline{\omega}\text{)} && \mathbf{u}_t + \mathbf{u} \times (\nabla \times \overline{\mathbf{u}}) - Re^{-1}\Delta \mathbf{u} + \nabla P = \mathbf{f} \text{ and } \nabla \cdot \mathbf{u} = 0,\\
&\text{(time relaxation)} && \mathbf{u}_t + \mathbf{u} \cdot \nabla \mathbf{u} - Re^{-1}\Delta \mathbf{u} + \nabla p + \chi(\mathbf{u} - \overline{\mathbf{u}}) = \mathbf{f} \text{ and } \nabla \cdot \mathbf{u} = 0.
\end{aligned}$$

where $\overline{\mathbf{u}}$ is an averaged velocity field $\mathbf{u}$, p is pressure, and P, Bernoulli pressure. All are simple to approximate with known methods but are not accurate. Moreover, only time relaxation regularization truncates scales sufficiently for practical computations: the time relaxation term $\chi(\mathbf{u} - \overline{\mathbf{u}})$ for $\chi > 0$ damps unresolved fluctuations over time [60, 98]. Significant improvements based on using deconvolution operators, i.e. replacing $\overline{\mathbf{u}}$ by $D(\overline{\mathbf{u}})$, to all four have been studied.

The general Leray-deconvolution problem ($D\overline{\mathbf{u}}$ instead of $\overline{\mathbf{u}}$) was proposed by Dunca in [19] as a more accurate extension to Leray's model [63]. Leray took G (also frequently denoted by *overbar*), the smoothing operator, to be the Gaussian filter. Germano proposed the differential filter $G = (-\delta^2\Delta + I)^{-1}$ for some filter length $\delta > 0$ which is an approximation of the Gaussian and fits nicely in the variational framework of the finite element method [27].

Previous analysis of the time-relaxation model used the van Cittert deconvolution operators which are very easy to program but somewhat expensive [60]. Another popular example for stable deconvolution is Tikhonov-Lavrentiev regularization $D = (G + \alpha I)^{-1}$, for some $0 < \alpha \leq 1$. Previous analysis of the Leray-deconvolution model used Tikhonv-Lavrentiev regularization [67]. Determining the appropriate value of α to ensure stability while preserving accuracy of the approximation is a challenging problem, see e.g. [14, 29, 36, 38, 39, 62]. Alternatively, *iterated* Tikhonov regularization is well-known to decouple stability and accuracy from the selection of regularization parameter α, see e.g. [21, 23, 51, 107]. It is a special case of the general deconvolution operator we propose herein, which attains high accuracy at reduced computational cost.

We study a synthesis of the Leray deconvolution and time relaxation models with this general deconvolution operator.

Problem 4.1.2 (Leray-deconvolution, time relaxation)**.** *Find velocity* $\mathbf{u} : \Omega \times (0,T) \to \mathbb{R}^3$ *and pressure* $\pi : \Omega \times (0,T) \to \mathbb{R}$ *approximations satisfying*

$$\mathbf{u}_t + D(\overline{\mathbf{u}}) \cdot \nabla \mathbf{u} - Re^{-1}\Delta \mathbf{u} + \nabla \pi + \chi(\mathbf{u} - D(\overline{\mathbf{u}})) = \mathbf{f}, \qquad \nabla \cdot \mathbf{u} = 0. \tag{4.2}$$

The fundamental issues associated with regularization methods include ensuring that

- scales are truncated (i.e. model microscale = filter radius = mesh width)
- smooth parts of the solution are accurately approximated, i.e. $D(\overline{\mathbf{u}})$ approaches $\mathbf{u}$ for smooth $\mathbf{u}$, and
- physical fidelity of flow is preserved.

Due to the nonlinearity in (4.2), differences choices of D yield significant changes in the solution of the induced model. We propose and provide analysis herein for a general family of regularization operators (Section 4.2.2). In particular, we consider a base deconvolution operator D satisfying minimal conditions described in Assumption 4.2.4. From these conditions and motivated by the improvement in accuracy suggested by (4.4), we study a sequence of associated updates: for $j = 1, 2, \ldots$, define D_j by $\boldsymbol{\omega}_j := D_j \overline{\mathbf{u}}$ through

$$\boldsymbol{\omega}_0 := D\overline{\mathbf{u}}, \qquad \boldsymbol{\omega}_j - \boldsymbol{\omega}_{j-1} := D\overline{(\mathbf{u} - \boldsymbol{\omega}_{j-1})}. \tag{4.3}$$

These iterates represent defect correction generalization of iterated Tikhonov regularization operator [51]. The idea is to choose α small but conservatively large and then update to recover high accuracy. For example,

$$\begin{array}{ll} \text{Modified Tikhonov } (j = 0) & \text{error}(\mathbf{u} - DG\mathbf{u}) \leq \mathcal{O}(\alpha\delta^2) \\ \text{Iterated Modified Tikhonov } (j > 0) & \text{error}(\mathbf{u} - DG\mathbf{u}) \leq \mathcal{O}((\alpha\delta^2)^j) \end{array} \tag{4.4}$$

In Section 4.2 we provide notation and definitions necessary for the scheme and for the numerical analysis. We provide a brief overview of differential filters (continuous and discrete) in Section 4.2.1. We propose a general family of regularization operators D (continuous and discrete) in Section 4.2.2. In Section 4.2.3 we show that the updated approximations

D_j derived from base deconvolution operator D inherit all of the properties of D (Assumption 4.2.5) in Proposition 4.2.9. We present a specific example of the iterated modified Tikhonov-Lavrentiev regularization operator in Section 4.2.4 based on

$$D = ((1-\alpha)G + \alpha I)^{-1}$$

that satisfies the proposed conditions.

In Section 4.3, we propose and analyze a finite element spatial and Crank-Nicolson temporal discretization of (4.2) based on the family of deconvolution operators D, D_j satisfying Assumption 4.2.5. In Section 4.4, we show that the proposed family of Leray-deconvolution problems with time relaxation is well-posed and stable (Theorem 4.4.5). In Section 4.5, a convergence theory is presented in the form of Theorem 4.5.1, for $\alpha, \delta, h, \Delta t \to 0$, where $h > 0$ is a characteristic spatial discretization parameter, and $\Delta t > 0$ is the time-step size. Numerical experiments are presented in Section 4.6.

4.2 PRELIMINARIES AND MODEL FORMULATION

We use standard notation for Lebesgue and Sobolev spaces and their norms. Let $||\cdot||$ and $(\cdot,\cdot)$ be the L^2-norm and inner product respectively. Let $||\cdot||_{p,k} := ||\cdot||_{W_p^k(\Omega)}$ represent the $W_p^k(\Omega)$-norm. We write $H^k(\Omega) := W_2^k(\Omega)$ and $||\cdot||_k$ for the corresponding norm. Let the context determine whether $W_p^k(\Omega)$ denotes a scalar, vector, or tensor function space. For example let $\mathbf{v} : \Omega \to \mathbb{R}^d$. Then, $\mathbf{v} \in H^1(\Omega)$ implies that $\mathbf{v} \in H^1(\Omega)^d$ and $\nabla \mathbf{v} \in H^1(\Omega)$ implies that $\nabla \mathbf{v} \in H^1(\Omega)^{d\times d}$. Write $W_q^m(0,T;W_p^k(\Omega)) = W_q^m(W_p^k)$ equipped with the standard norm. For example,

$$||\mathbf{v}||_{L^q(W_p^k)} := \begin{cases} \left(\int_0^T ||\mathbf{v}(\cdot,t)||_{p,k}^q dt\right)^{1/q}, & \text{if } 1 \le q < \infty \\ \text{ess sup}_{0<t<T} ||\mathbf{v}(\cdot,t)||_{p,k}, & \text{if } q = \infty. \end{cases}$$

Let the flow domain $\Omega \in \mathbb{R}^d$, $d = 2, 3$, be a regular, bounded, polyhedral. Denote the pressure and velocity spaces by $Q := L_0^2(\Omega) = \left\{q \in L^2(\Omega) : \int_\Omega q = 0\right\}$ and $X := H_0^1(\Omega) =$

$\{\mathbf{v} \in H^1(\Omega) : \mathbf{v}|_{\partial\Omega} = 0\}$ respectively. A weak formulation of (4.1) with homogeneous Dirichlet boundary data is: Find $\mathbf{u} : [0,T] \to X$ and $p : [0,T] \to Q$ for a.e. $t \in (0,T]$ satisfying

$$(\mathbf{u}_t, \mathbf{v}) + (\mathbf{u} \cdot \nabla \mathbf{u}, \mathbf{v}) + Re^{-1}(\nabla \mathbf{u}, \nabla \mathbf{v}) - (p, \nabla \cdot \mathbf{v}) = (\mathbf{f}, \mathbf{v}), \quad \forall \mathbf{v} \in X \tag{4.5}$$

$$(q, \nabla \cdot \mathbf{u}) = 0, \quad \forall q \in Q \tag{4.6}$$

$$\mathbf{u}(\mathbf{x}, 0) = \mathbf{u}_0(\mathbf{x}), \quad \text{a.e. } \mathbf{x} \in \Omega. \tag{4.7}$$

Let $V := \{\mathbf{v} \in H_0^1(\Omega) : \nabla \cdot \mathbf{v} = 0\}$. We say that $\mathbf{u}$ is a *strong solution* of the NSE if it satisfies (4.5), (4.6), (4.7), $\mathbf{u} \in L^2(0,T;X) \cap L^\infty(0,T;L^2(\Omega)) \cap L^4(0,T;X)$, $p \in L^2(0,T;Q)$, and $\mathbf{u}_t \in L^2(0,T;X^*)$, and $\mathbf{u}(x,t) \to \mathbf{u}_0(x) \in V$ a.e. as $t \to 0$.

Restricting test functions $\mathbf{v} \in V$ reduces (4.5), (4.6), (4.7) to: find $\mathbf{u} : [0,T] \to V$ satisfying

$$(\mathbf{u}_t, \mathbf{v}) + (\mathbf{u} \cdot \nabla \mathbf{u}, \mathbf{v}) + Re^{-1}(\nabla \mathbf{u}, \nabla \mathbf{v}) = (\mathbf{f}, \mathbf{v}), \quad \forall \mathbf{v} \in V. \tag{4.8}$$

and (4.7). Solving the problem associated with (4.8), (4.7) is equivalent to (4.5), (4.6), (4.7).

Let τ_h be a uniformly regular triangulation (see [30] for a precise definition) of Ω with $E \in \tau_h$ (e.g. triangles for $d = 2$ or tetrahedra for $d = 3$). Set $h = \sup_{E \in \tau_h} \{\text{diameter}(E)\}$. Let $X_h \subset X$ and $Q_h \subset Q$ be a conforming velocity-pressure mixed finite element space. We provide a more precise setting for the problem discretization in Section 4.3.

4.2.1 Differential filters

Definition 4.2.1. *Let Y be a Hilbert space and $T : Y \to Y$. Write $T \geq 0$ if T is self-adjoint $T = T^*$ and $(T\mathbf{v}, \mathbf{v})_Y \geq 0$ for all $\mathbf{v} \in Y$ and call T symmetric non-negative (snn). Write $T > 0$ if T is self-adjoint $T = T^*$ and $(T\mathbf{v}, \mathbf{v})_Y > 0$ for all $0 \neq \mathbf{v} \in Y$ and call T symmetric positive-definite (spd).*

Let $G = G(\delta) > 0$ be a linear, bounded, compact operator on X representing a generic *smoothing filter* with filter radius $\delta > 0$:

$$G : L^2(\Omega) \to L^2(\Omega), \qquad G\boldsymbol{\phi} = \overline{\boldsymbol{\phi}}$$

One example of this operator is the continuous differential filter $G = A^{-1}$ (Definition 4.2.2), which is used, together with its discrete counterpart A_h^{-1} (Definition 4.2.3), for both implementation and analysis of our numerical scheme.

Definition 4.2.2 (Continuous differential filter)**.** *Fix $\boldsymbol{\phi} \in L^2(\Omega)$. Then $\overline{\boldsymbol{\phi}} \in X$ is the unique solution of $-\delta^2 \Delta \overline{\boldsymbol{\phi}} + \overline{\boldsymbol{\phi}} = \boldsymbol{\phi}$ with corresponding weak formulation*

$$\delta^2 (\nabla \overline{\boldsymbol{\phi}}, \nabla \mathbf{v}) + (\overline{\boldsymbol{\phi}}, \mathbf{v}) = (\boldsymbol{\phi}, \mathbf{v}), \qquad \forall \mathbf{v} \in X. \tag{4.9}$$

Set $A = -\delta^2 \Delta + I$ so that $A^{-1} : L^2(\Omega) \to X$ defined by $\overline{\boldsymbol{\phi}} = A^{-1} \boldsymbol{\phi}$ is well-defined.

Definition 4.2.3 (Discrete differential filter)**.** *Fix $\boldsymbol{\phi} \in L^2(\Omega)$. Then $\overline{\boldsymbol{\phi}}^h \in X_h$ is the unique solution of*

$$\delta^2 (\nabla \overline{\boldsymbol{\phi}}^h, \nabla \mathbf{v}^h) + (\overline{\boldsymbol{\phi}}^h, \mathbf{v}^h) = (\boldsymbol{\phi}, \mathbf{v}^h), \qquad \forall \mathbf{v}^h \in X_h. \tag{4.10}$$

Set $A_h = -\delta^2 \Delta_h + \Pi_h$ so that $A_h^{-1} : L^2(\Omega) \to X_h$ defined by $\overline{\boldsymbol{\phi}}^h = A_h^{-1} \boldsymbol{\phi}$ is well-defined. Here, $\Pi_h : L^2(\Omega) \to X_h$ is the L^2 projection and $\Delta_h : X \to X_h$ the discrete Laplace operator satisfying

$$(\Pi_h \boldsymbol{\phi} - \boldsymbol{\phi}, \mathbf{v}^h) = 0, \quad (\Delta_h \boldsymbol{\phi}, \mathbf{v}^h) = -(\nabla \boldsymbol{\phi}, \nabla \mathbf{v}^h) \quad \forall \mathbf{v}^h \in X_h. \tag{4.11}$$

It is well-known that A^{-1}, A_h^{-1} are each linear and bounded, A^{-1} is compact, and the spectrum of A, A_h (on X, X_h respectively) is contained in $[1, \infty)$ and spectrum of A^{-1}, A_h^{-1} (on X, X_h respectively) is contained in $(0, 1]$ so that

$$A^{-1} > 0 \quad \text{on } X, \qquad A_h^{-1} > 0 \quad \text{on } X_h. \tag{4.12}$$

For more detailed exposition on these operators, see [67].

4.2.2 A family of deconvolution operators

We analyze (4.2) for stable, accurate deconvolutions D of the smoothing filter G introduced in Section 4.2.1 so that $DG(\mathbf{u})$ accurately approximates $\mathbf{u}$. Due to the nonlinearity in (4.2) small perturbations in D yield significant changes in the solution of the induced model. We propose herein minimal conditions on D (Assumption 4.2.4) to ensure (4.2) results in a stable and accurate regularized discretization of (4.1).

Assumption 4.2.4 (Continuous deconvolution operator)**.** *Suppose that $D : X \to X$ is linear, bounded, spd, and commutes with G such that*

$$||DG|| \leq 1, \qquad ||\nabla(DG\mathbf{v})|| \leq d_1||\nabla\mathbf{v}|| \quad \forall\ \mathbf{v} \in X, \tag{4.13}$$

for some constant $d_1 > 0$. Moreover, suppose that D is parametrized by $\alpha > 0$, $\delta > 0$ such that $D = D(\delta, \alpha)$ and

$$||(I - DG)\mathbf{v}|| \leq c_1(\delta, \alpha; \mathbf{v}) \to 0, \qquad \text{as } \delta, \alpha \to 0 \tag{4.14}$$

for any $\mathbf{v} \in X \cap H^k(\Omega)$ for some $k \in \mathbb{N}$ and $c_1 = c_1(\delta, \alpha; \mathbf{v}) > 0$.

Note that the first estimate in (4.13) is required so that the spectral radius satisfies $\rho(DG) \leq 1$. The second estimate in (4.13) (which controls the H^1-semi-norm of DG) and the approximation (4.14) are both required for the convergence analysis in Section 4.5.

We require a discrete analogue $D^h : X_h \to X_h$ of the continuous deconvolution operator $D : X \to X$.

Assumption 4.2.5 (Discrete deconvolution operator)**.** *Let D satisfy Assumption 4.2.4. Let $G^h : X_h \to X_h$ be a discrete analogue of G that is linear, bounded, spd. Suppose that $D^h : X_h \to X_h$ is linear, bounded, spd, and commutes with G^h such that*

$$||D^hG^h|| \leq 1, \qquad ||\nabla D^hG^h\mathbf{v}|| \leq d_1||\nabla\mathbf{v}|| \quad \forall\ \mathbf{v} \in X \tag{4.15}$$

for some constant $d_1 > 0$. Moreover, suppose that D^h is parametrized by $\alpha > 0$, $\delta > 0$, h such that $D = D(h, \delta, \alpha)$ and

$$||(DG - D^hG^h)\mathbf{v}|| \leq c_2(h, \delta, \alpha; \mathbf{v}) \to 0, \qquad \text{as } h, \delta, \alpha \to 0 \tag{4.16}$$

for all $\mathbf{v} \in X \cap H^k(\Omega)$ for some fixed $k \in \mathbb{N}$ and $c_2 = c_2(h, \delta, \alpha; \mathbf{v}) > 0$.

The estimates in (4.15) are motivated by the continuous case of (4.13). The approximation (4.16) is required for the convergence analysis in Section 4.5 (see Theorem 4.5.1, Corollary 4.5.2).

Remark 4.2.6. *If $D = f(G)$ for some continuous map $f : \mathbb{R} \to \mathbb{R}$, then commutativity is satisfied $DG = GD$. Tikhonov-Lavrentiev (modified) regularization with $G = A^{-1}$, $G^h = A_h^{-1}$ given by $D = ((1-\alpha)A^{-1} + \alpha I)^{-1}$, $D^h = ((1-\alpha)A_h^{-1} + \alpha\Pi_h)^{-1}$ is one such example with $f(x) = ((1-\alpha)x + \alpha)^{-1}$ and $d_1 = 1$, $c_1 = \alpha\delta^2||\Delta\mathbf{v}||$, $c_2 = (\delta h^k + h^{k+1})||\mathbf{v}||_{k+1}$, see [67].*

Moreover, letting $\lambda_k(\cdot)$ denote the k-th (ordered) eigenvalue of a given operator, commutativity of D and G provides $\lambda_k(DG) = \lambda_k(D)\lambda_k(G)$ and similarly for the discrete operator D^hG^h.

We next derive several important consequences of D, D^h under Assumptions 4.2.4, 4.2.5 required in the forthcoming analysis.

Lemma 4.2.7. *Suppose that G, G^h, D, D^h satisfy Assumptions 4.2.4 and 4.2.5. Then,*

$$||DG\mathbf{v}|| \leq ||\mathbf{v}|| \quad \text{and} \quad \left|\left|D^hG^h\mathbf{v}\right|\right| \leq ||\mathbf{v}|| \qquad \forall \mathbf{v} \in L^2(\Omega). \tag{4.17}$$

Proof. For the continuous operator,

$$||DG\mathbf{v}|| \leq ||DG||\ ||\mathbf{v}||.$$

Then, the first equation in (4.17) follows from Assumption 4.2.4, and the second is derived similarly applying Assumption 4.2.5 instead. □

Lemma 4.2.8. *Suppose that G, G^h, D, D^h satisfy Assumptions 4.2.4 and 4.2.5. Then, the spectrum of both DG and D^hG^h are contained in $[0,1]$ so that*

$$||I - DG|| \leq 1, \qquad ||I - D^hG^h|| \leq 1. \tag{4.18}$$

As a consequence,

$$\left.\begin{aligned} ||\mathbf{v}||_\star^2 &:= (\mathbf{v} - DG\mathbf{v}, \mathbf{v}) \\ ||\mathbf{v}||_{\star h}^2 &:= (\mathbf{v} - D^hG^h\mathbf{v}, \mathbf{v}) \end{aligned}\right\} \geq 0, \qquad \forall \mathbf{v} \in L^2(\Omega). \tag{4.19}$$

Proof. Assumptions 4.2.4 and 4.2.5 guarantee that the spectral radius $\rho(DG) \leq 1$ and $\rho(D^h G^h) \leq 1$. Also, $D > 0$, $G > 0$ and commute so that $DG \geq 0$. Similarly, $D^h G^h \geq 0$. Therefore, the spectrum of DG, $D^h G^h \geq 0$ are each contained in $[0, 1]$. So, $I - DG$, $I - D^h G_h \geq 0$ have spectrum contained in $[0, 1]$ which ensures the non-negativity of both $||\cdot||_\star$ and $||\cdot||_{\star h}$. □

4.2.3 Iterated deconvolution

One can show, by eliminating intermediate steps in the definition of the iterated regularization operator D_j in (4.3) with base operator D satisfying Assumption 4.2.4, that

$$D_j = D \sum_{i=0}^{j} (FD)^i, \qquad F := D^{-1} - G \tag{4.20}$$

Similarly, the discrete iterated regularization operator D_j^h with discrete base operator D^h satisfying Assumption 4.2.5, is given by

$$D_j^h = D^h \sum_{i=0}^{j} (F^h D^h)^i, \qquad F^h := (D^h)^{-1} - G^h \tag{4.21}$$

We next show that D_j, D_j^h for $j > 0$ inherit several important properties from D, D^h via Assumption 4.2.5.

Proposition 4.2.9. *Fix $j \in \mathbb{N}$. Then $D_j : X \to X$ defined by (4.20) satisfies Assumption 4.2.5. In particular, $D_j > 0$ is linear, bounded, commutes with G and satisfies (4.13)(a). Estimate (4.13)(b) is replaced by*

$$||\nabla(D_j G\mathbf{v})|| \ \leq d_{1,j}||\nabla \mathbf{v}|| \quad \forall\ \mathbf{v} \in X, \tag{4.22}$$

for some constant $d_{1,j} > 0$. Estimate (4.14) is replaced by

$$||(I - D_j G)\mathbf{v}|| \ \leq c_{1,j}(\delta, \alpha; \mathbf{v}) \ \to 0, \quad \text{as } \delta, \alpha \to 0 \tag{4.23}$$

for any $\mathbf{v} \in X \cap H^k(\Omega)$ for some $k \in \mathbb{N}$ where $c_{1,j} = c_{1,j}(\delta, \alpha; \mathbf{v}) > 0$. Moreover,

$$d_{1,j} \leq \sum_{i=0}^{j} d_1^i, \qquad c_{1,j} \leq \sum_{i=0}^{j} c_1^i.$$

Proof. First notice that D_j is linear and bounded since it is a linear combination of linear and bounded operators $D(FD)^i = D(I - DG)^i$, for $i = 0, 1, \ldots, j$. Moreover, since G commutes with D, it follows that G commutes with $D(I - DG)^i$ and hence with D_j. Next, D_j is a sum of spd and snn operators $D > 0$, $D(I - DG)^i \geq 0$. Hence, $D_j > 0$.

Next, notice that

$$D_j G = \left(\sum_{i=0}^{j} (I - DG)^i \right) DG = \left(I + (I - DG) + \ldots + (I - DG)^j \right) DG. \tag{4.24}$$

Letting $\lambda_k(\cdot)$ denote the k-th (ordered) eigenvalue of a given operator, we can characterize the spectrum of D_j by summing the resulting finite geometric series (4.24) to get

$$\lambda_k(D_j G) = \lambda_k(D)\lambda_k(G) \sum_{i=0}^{j} (1 - \lambda_k(DG))^i = \left(1 - (1 - \lambda_k(DG))^{j+1} \right). \tag{4.25}$$

Then under Assumption 4.2.4, Lemma 4.2.8 with (4.25) implies that $0 \leq \lambda_k(D_j G) \leq ||D_j G|| \leq 1$. Hence, D_j satisfies (4.13)(a). Expanding out the terms in (4.24) as powers of DG, we see that (4.24) can be written as a polynomial (with coefficients a_i) in DG, so that

$$\nabla D_j G\mathbf{v} = \sum_{i=0}^{j} a_i \nabla (DG)^i \mathbf{v} \qquad \text{and} \qquad ||\nabla D_j G\mathbf{v}|| \leq C \sum_{i=0}^{j} d_1^i ||\nabla \mathbf{v}||, \tag{4.26}$$

since $||\nabla DG\mathbf{v}|| \leq d_1 ||\nabla \mathbf{v}||$ can be applied successfully. Therefore (4.22) follows with $d_{1,j} = \sum_{i=0}^{j} d_1^i$. Next, start with (4.24) to get

$$\begin{aligned} ||(I - D_j G)\mathbf{v}|| &= || \left((I - DG)\mathbf{v} + DG(I - DG)\mathbf{v} + \ldots + DG(I - DG)^j \mathbf{v} \right) || \\ &\leq ||(I - DG)\mathbf{v}|| + ||DG||||(I - DG)\mathbf{v}|| + \ldots + ||DG||||I - DG||^{j-1}||(I - DG)\mathbf{v}|| \end{aligned}$$

Estimate (4.23) follows by noting $||DG|| \leq 1$, $||I - DG|| \leq 1$, and by Assumption 4.2.5, $||(I - DG)\mathbf{v}|| \leq c_1$. □

Proposition 4.2.10. *Fix $j \in \mathbb{N}$. Then $D_j^h : X_h \to X_h$ defined by (4.21) satisfies Assumption 4.2.5. In particular, $D_j^h > 0$ is linear, bounded, commutes with G^h and satisfies (4.15)(a). Estimate (4.15)(b) is replaced by*

$$||\nabla(D_j^h G^h \mathbf{v})|| \ \leq d_{1,j}||\nabla \mathbf{v}^h|| \quad \forall\ \mathbf{v}^h \in X_h \tag{4.27}$$

for some constant $d_{1,j} > 0$. Estimate (4.16) is replaced by

$$||(D_j G - D_j^h G^h)\mathbf{v}|| \ \leq c_{2,j}(h, \delta, \alpha; \mathbf{v}) \ \to 0, \quad \text{as } h, \delta, \alpha \to 0 \tag{4.28}$$

for any $\mathbf{v} \in X \cap H^k(\Omega)$ for some $k \in \mathbb{N}$ where $c_{2,j} = c_{2,j}(h, \delta, \alpha; \mathbf{v}) > 0$. Moreover,

$$c_{2,j} \leq \alpha(j) c_2$$

for some constant $\alpha = \alpha(j) > 0$.

Proof. The first two assertions follow similarly as in the previous proof of Proposition 4.2.9. To prove (4.28), we start by writing

$$D_j^h G^h = \left(\sum_{i=0}^{j} (I - D^h G^h)^i \right) D^h G^h \tag{4.29}$$

and then subtract (4.29) from (4.24) to get

$$D_j G - D_j^h G^h = \Lambda_j (DG - D^h G^h) + (\Lambda_j - \Lambda_j^h) D^h G^h, \tag{4.30}$$

where

$$\Lambda_j = \sum_{i=0}^{j} (I - DG)^i, \qquad \Lambda_j^h = \sum_{i=0}^{j} (I - D^h G^h)^i.$$

Then taking norms across (4.30), we get

$$||(D_j G - D_j^h G^h)\mathbf{v}|| = ||\Lambda_j||||(DG - D^h G^h)\mathbf{v}|| + ||D^h G^h||||(\Lambda_j - \Lambda_j^h)\mathbf{v}||. \tag{4.31}$$

Notice that $||I - DG|| \leq 1$ so that $||\Lambda_j|| \leq j+1$. Moreover, $||(DG - D^hG^h)\mathbf{v}|| \leq c_2$ via Assumption 4.2.5. Next, using the binomial theorem and factoring, we get

$$\begin{aligned} ||(\Lambda_j - \Lambda_j^h)\mathbf{v}|| &= \left\| \sum_{i=0}^{j} \frac{j!}{i!(j-i)!}(-1)^i \left[(DG)^i - (D^hG^h)^i \mathbf{v} \right] \right\| \\ &= \left\| \sum_{i=0}^{j} \frac{j!}{i!(j-i)!}(-1)^i \left[\sum_{n=0}^{i} (DG)^n (D^hG^h)^{n-i} \right] (DG - D^hG^h)\mathbf{v} \right\|. \end{aligned} \tag{4.32}$$

Then, applying $||DG|| \leq 1$, $||D^hG^h|| \leq 1$ to (4.32) provides

$$||(\Lambda_j - \Lambda_j^h)\mathbf{v}|| = \left(\sum_{i=0}^{j} \frac{j!i}{(i)!(j-i)!} \right) ||(DG - D^hG^h)\mathbf{v}||.$$

Again, $||(DG - D^hG^h)\mathbf{v}|| \leq c_2$ via Assumption 4.2.5. So, we combine these above results to conclude (4.28) with $\alpha(j) = \sum_{i=0}^{j} \frac{j!i}{(i)!(j-i)!}$. □

4.2.4 Tikhonov-Lavrentiev regularization

We provide two examples of discrete deconvolution operators D^h to make the abstract formulation in the previous section more concrete. The Tikhonov-Lavrentiev and modified Tikhonov-Lavrentiev operator (for linear, compact $G > 0$) is given by

$$\begin{aligned} &\text{Tikhonov-Lavrentiev} && \Rightarrow && D_{\alpha,0} = (G + \alpha I)^{-1} \\ &\text{modified Tikhonov-Lavrentiev} && \Rightarrow && D_{\alpha,0} = ((1-\alpha)G + \alpha I)^{-1} \end{aligned} \tag{4.33}$$

Definition 4.2.11 (Modified Tikhonov-Lavrentiev deconvolution (weak))**.** *Fix $\alpha > 0$. Let $G = A^{-1}$. For any $\mathbf{w} \in X$, let $\boldsymbol{\omega}_0 := D_{\alpha,0}\overline{\mathbf{w}} \in X$ be the unique solution of*

$$\alpha\delta^2 (\nabla\boldsymbol{\omega}_0, \nabla\mathbf{v}) + (\boldsymbol{\omega}_0, \mathbf{v}) = (\mathbf{w}, \mathbf{v}), \qquad \forall \mathbf{v} \in X. \tag{4.34}$$

Definition 4.2.12 (Modified Tikhonov-Lavrentiev deconvolution (discrete))**.** *Fix $\alpha > 0$. Let $G^h = A_h^{-1}$ and $D_{\alpha,0}^h = \left((1-\alpha)A_h^{-1} + \alpha\Pi_h\right)^{-1}$. For any $\mathbf{w} \in X$, let $\boldsymbol{\omega}_0^h := D_{\alpha,0}^h\overline{\mathbf{w}}^h \in X_h$ be the unique solution of*

$$\alpha\delta^2 \left(\nabla\boldsymbol{\omega}_0^h, \nabla\mathbf{v}^h\right) + \left(\boldsymbol{\omega}_0^h, \mathbf{v}^h\right) = \left(\mathbf{w}, \mathbf{v}^h\right), \qquad \forall \mathbf{v}^h \in X_h. \tag{4.35}$$

The iterated modified Tikhonov-Lavrentiev operator (for linear, compact $G > 0$) is obtained from the Tikhonov-Lavrentiev operator with updates via (4.3):

$$\begin{aligned} &\text{Iterated Tikhonov-Lavrentiev} && \Rightarrow && D_{\alpha,j} = D_{\alpha,0} \sum_{i=0}^{j} (\alpha D_{\alpha,0})^i \\ &\text{Iterated modified Tikhonov-Lavrentiev} && \Rightarrow && D_{\alpha,j} = D_{\alpha,0} \sum_{i=0}^{j} (\alpha (I - G) D_{\alpha,0})^i \end{aligned} \tag{4.36}$$

Definition 4.2.13 (Iterated modified Tikhonov-Lavrentiev deconvolution (weak))**.** *Fix $\alpha > 0$ and $J \in \mathbb{N}$. Let $G = A^{-1}$. Define $\boldsymbol{\omega}_{-1} = 0$, then for any $\mathbf{w} \in X$ and $j = 1, 2, \ldots, J$, let $\boldsymbol{\omega}_j := D_{\alpha,j}\overline{\mathbf{w}} \in X$ be the unique solution of*

$$\alpha\delta^2 \left(\nabla \boldsymbol{\omega}_j, \nabla \mathbf{v}\right) + \left(\boldsymbol{\omega}_j, \mathbf{v}\right) = \left(\mathbf{w}, \mathbf{v}\right) + \alpha\delta^2 \left(\nabla \boldsymbol{\omega}_{j-1}, \nabla \mathbf{v}\right), \qquad \forall \mathbf{v} \in X. \tag{4.37}$$

Definition 4.2.14 (Iterated modified Tikhonov-Lavrentiev deconvolution (discrete))**.** *Fix $\alpha > 0$ and $J \in \mathbb{N}$. Let $G^h = A_h^{-1}$, and $D_{\alpha,j}^h = D_{\alpha,0}^h \sum_{i=0}^{j} \left(\alpha(\Pi_h - A_h^{-1}) D_{\alpha,0}^h\right)^i$. Define $\boldsymbol{\omega}_{-1}^h = 0$, then for any $\mathbf{w} \in X$ and $j = 1, 2, \ldots, J$, let $\boldsymbol{\omega}_j^h := D_{\alpha,j}^h \overline{\mathbf{w}}^h \in X_h$ be the unique solution of*

$$\alpha\delta^2 \left(\nabla \boldsymbol{\omega}_j^h, \nabla \mathbf{v}^h\right) + \left(\boldsymbol{\omega}_j^h, \mathbf{v}^h\right) = \left(\mathbf{w}, \mathbf{v}^h\right) + \alpha\delta^2 \left(\nabla \boldsymbol{\omega}_{j-1}^h, \nabla \mathbf{v}^h\right), \qquad \forall \mathbf{v}^h \in X_h. \tag{4.38}$$

4.3 FULLY DISCRETE APPROXIMATION

We require a more precise setting and approximating properties of the finite element space $X_h \times Q_h$. Assume that $X_h \times Q_h$ satisfy an inf-sup condition of the form

$$\inf_{q\in Q_h} \sup_{\mathbf{v}\in X_h} \frac{(q, \nabla\cdot\mathbf{v})}{||\nabla\mathbf{v}||||q||} \geq C > 0. \tag{4.39}$$

and that $\mathbf{u} \in L^2(H^{k+1})$, and $p \in L^2(H^{s+1})$ for some $k \geq 0$, $s \geq 0$. Then there exists $C > 0$ such that

$$\begin{aligned} \inf_{\mathbf{v}_h\in X_h} ||\mathbf{u} - \mathbf{v}_h|| + h \inf_{\mathbf{v}_h\in X_h} ||\mathbf{u} - \mathbf{v}_h||_1 \leq \;& Ch^{k+1}||\mathbf{u}||_{k+1} \\ \inf_{q_h\in Q_h} ||p - q_h|| \leq \;& Ch^{s+1}||p||_{s+1}. \end{aligned} \tag{4.40}$$

We also need an inverse triangle inequality as follows

$$||\nabla\mathbf{v}_h|| \leq Ch^{-1}||\mathbf{v}_h||, \qquad \forall\mathbf{v}_h \in X_h. \tag{4.41}$$

Let $V^h = \{\mathbf{v} \in X_h : (q, \nabla\cdot\mathbf{v}) = 0 \quad \forall q \in Q_h\}$. Note that in general $V^h \not\subset V$. For the time-discretization, let $0 = t_0 < t_1 < \ldots < t_{M-1} = T < \infty$ be a discretization of the time interval $[0, T]$ for a constant time step $\Delta t = t_{n+1} - t_n$. If $\boldsymbol{\xi}$ is a continuous variable, we write $\boldsymbol{\xi}(t_{n+1/2}) = \boldsymbol{\xi}((t_{n+1} + t_n)/2)$ and if $\boldsymbol{\xi}$ is either continuous or discrete, $\boldsymbol{\xi}^{n+1/2} = \frac{1}{2}(\boldsymbol{\xi}_{n+1} + \boldsymbol{\xi}_n)$. Lastly, we require a skew-symmetrization for the convective term:

$$b^*(\mathbf{u}, \mathbf{v}, \mathbf{w}) := \frac{1}{2}(\mathbf{u}\cdot\nabla\mathbf{v}, \mathbf{w}) - \frac{1}{2}(\mathbf{u}\cdot\nabla\mathbf{w}, \mathbf{v}). \tag{4.42}$$

The trilinear from $b^*(\cdot,\cdot,\cdot)$ is continuous and skew-symmetric on $X \times X \times X$.

Problem 4.3.1 (CNFE for Leray-Deconvolution)**.** *Let* $(\mathbf{w}_0, \pi_0) \in (X_h, Q_h)$*. Then, for each* $n = 0, 1, \ldots, M-1$*, find* $(\mathbf{w}^h_{n+1}, \pi^h_{n+1}) \in (X_h, Q_h)$ *satisfying*

$$\begin{aligned} &\frac{1}{\Delta t}(\mathbf{w}^h_{n+1} - \mathbf{w}^h_n, \mathbf{v}^h) + b^*(\mathbf{z}_h(\mathbf{w}^h_{n+1/2}), \mathbf{w}^h_{n+1/2}, \mathbf{v}^h) - (\pi^h_{n+1/2}, \nabla\cdot\mathbf{v}^h) + Re^{-1}(\nabla\mathbf{w}^h_{n+1/2}, \nabla\mathbf{v}^h) \\ &\quad + \chi(\mathbf{w}^h_{n+1/2} - z_h(\mathbf{w}^h_{n+1/2}), \mathbf{v}^h) = (\mathbf{f}_{n+1/2}, \mathbf{v}^h), \qquad \forall\mathbf{v}^h \in X_h \end{aligned} \tag{4.43}$$

$$(\nabla\cdot\mathbf{w}^h_{n+1}, q^h) = 0, \qquad \forall q^h \in Q_h \tag{4.44}$$

where $z_h(\mathbf{w}^h_{n+1/2}) = D^h\overline{\mathbf{w}^h_{n+1/2}}^h$.

Notice that $(q^h_{n+1/2}, \nabla \cdot \mathbf{v}^h) = 0$ when $\mathbf{v}^h \in V_h$ so that the problem of finding $\mathbf{w}^h_{n+1} \in V_h$ satisfying

$$\frac{1}{\Delta t}(\mathbf{w}^h_{n+1} - \mathbf{w}^h_n, \mathbf{v}^h) + b^*(z_h(\mathbf{w}^h_{n+1/2}), \mathbf{w}^h_{n+1/2}, \mathbf{v}^h) + Re^{-1}(\nabla \mathbf{w}^h_{n+1/2}, \nabla \mathbf{v}^h) + \chi(\mathbf{w}^h_{n+1/2} - z_h(\mathbf{w}^h_{n+1/2}), \mathbf{v}^h) = (\mathbf{f}_{n+1/2}, \mathbf{v}^h), \qquad \forall \mathbf{v}^h \in V_h \tag{4.45}$$

is an equivalent formulation of Problem 4.3.1.

Lemma 4.3.2. *If* $\mathbf{u}, \mathbf{v}, \mathbf{w} \in X$,

$$b^*(\mathbf{u}, \mathbf{v}, \mathbf{w}) \le C\sqrt{||\mathbf{u}||||\nabla \mathbf{u}||}||\nabla \mathbf{v}||||\nabla \mathbf{w}||,$$
$$b^*(\mathbf{u}, \mathbf{v}, \mathbf{w}) \le C||\nabla \mathbf{u}||||\nabla \mathbf{v}||\sqrt{||\mathbf{w}||||\nabla \mathbf{w}||}. \tag{4.46}$$

Moreover, if $\mathbf{v} \in H^2(\Omega)$, *then*

$$b^*(\mathbf{u}, \mathbf{v}, \mathbf{w}) \le C||\mathbf{u}||||\mathbf{v}||_2||\nabla \mathbf{w}||, \quad b^*(\mathbf{u}, \mathbf{v}, \mathbf{w}) \le C||\nabla \mathbf{u}||||\mathbf{v}||_2||\mathbf{w}||. \tag{4.47}$$

Proof. The following estimates are derived e.g. in [61]. □

The discrete Gronwall inequality is essential to the analysis in Section 4.5.

Lemma 4.3.3. *Let* $D \ge 0$ *and* κ_n, A_n, B_n, $C_n \ge 0$ *for any integer* $n \ge 0$ *and satisfy*

$$A_N + \Delta t \sum_{n=0}^{N} B_n \le \Delta t \sum_{n=0}^{N} \kappa_n A_n + \Delta t \sum_{n=0}^{N} C_n + D, \quad \forall N \ge 0.$$

Suppose that for all n, $\Delta t \kappa_n < 1$ *and set* $g_n = (1 - \Delta t \kappa_n)^{-1}$. *Then,*

$$A_N + \Delta t \sum_{n=0}^{N} B_n \le \exp\left(\Delta t \sum_{n=0}^{N} g_n \kappa_n\right)\left[\Delta t \sum_{n=0}^{N} C_n + D\right], \quad \forall N \ge 0.$$

For any $n = 0, 1, \ldots, M-1$,

$$||\frac{\boldsymbol{\theta}_{n+1} - \boldsymbol{\theta}(t_n)}{\Delta t}||^2 \le C\Delta t^{-1} \int_{t_n}^{t_{n+1}} ||\boldsymbol{\theta}_t(t)||^2 dt \tag{4.48}$$

$$||\boldsymbol{\theta}_{n+1/2} - \boldsymbol{\theta}(t_{n+1/2})||_k^2 \le C\Delta t^3 \int_{t_n}^{t_{n+1}} ||\boldsymbol{\theta}_{tt}(t)||_k^2 dt \tag{4.49}$$

$$||\frac{1}{\Delta t}(\boldsymbol{\theta}_{n+1} - \boldsymbol{\theta}_n) - \boldsymbol{\theta}_t(t_{n+1/2})||^2 \le C\Delta t^3 \int_{t_n}^{t_{n+1}} ||\boldsymbol{\theta}_{ttt}(t)||^2 dt. \tag{4.50}$$

where $\boldsymbol{\theta} \in H^1(L^2)$, $\boldsymbol{\theta} \in H^2(H^k)$, and $\boldsymbol{\theta} \in H^3(L^2)$ is required respectively. Each estimate (4.48), (4.49), (4.50) is a result of a Taylor expansion with integral remainder.

4.4 EXISTENCE THEORY

We now proceed to establish well-posedness of Problem 4.3.1. Existence at each time step is established via Leray-Schauder's fixed point theorem.

Lemma 4.4.1. *Let*

$$\begin{aligned} a(\boldsymbol{\theta}^h, \mathbf{v}^h) &= \frac{\Delta t}{2Re}\left(\nabla\boldsymbol{\theta}^h, \nabla\mathbf{v}^h\right) + \frac{\chi\Delta t}{2}\left(\boldsymbol{\theta}^h - z_h(\boldsymbol{\theta}^h), \mathbf{v}^h\right) \\ l_y(\mathbf{v}^h) &= (\mathbf{y}, \mathbf{v}^h). \end{aligned}$$

for any $\mathbf{y} \in X^*$ *and* $\boldsymbol{\theta}^h$, $\mathbf{v}^h \in V_h$. *Suppose that* D^h *satisfies Assumption 4.2.5. Then* $a(\cdot,\cdot) : V_h \times V_h \to \mathbb{R}$ *is a continuous and coercive bilinear form and* $l_y(\cdot) : V_h \to \mathbb{R}$ *is a linear, continuous functional.*

Proof. Linearity for $l_y(\cdot)$ is obvious, and continuity follows from an application of Hölder's inequality. Continuity for $a(\cdot,\cdot)$ also follows from Hölder's inequality and Assumption 4.2.5. Coercivity is proven by application of (4.19). □

Lemma 4.4.2. *Let* $T : X^* \to V_h$ *be such that, for any* $\mathbf{y} \in X^*$, $\boldsymbol{\theta}^h := T(\mathbf{y})$ *solves*

$$a\left(\boldsymbol{\theta}^h, \mathbf{v}^h\right) = l_y(\mathbf{v}^h), \qquad \forall \mathbf{v}^h \in V_h.$$

Then T *is a well-defined, linear, bounded operator.*

Proof. Linearity is clear. The results of Lemma 4.4.1, and the Lax-Milgram theorem prove the rest. □

Lemma 4.4.3. *Fix* $n = 0, 1, \ldots, M-1$. *Let* $\mathbf{w}_n^h$ *be a solution of Problem 4.3.1 and let* $N : V_h \to X^*$ *satisfy, for any* $\boldsymbol{\theta}^h \in V_h$,

$$\begin{aligned} (N(\boldsymbol{\theta}^h), \mathbf{v}^h) = -(\boldsymbol{\theta}^h - 2\mathbf{w}_n^h, \mathbf{v}^h) - \frac{\Delta t}{4} b^*(z_h(\boldsymbol{\theta}^h), \boldsymbol{\theta}^h, \mathbf{v}^h) \\ + \Delta t(\mathbf{f}_{n+1/2}, \mathbf{v}^h) =: c(\boldsymbol{\theta}^h, \mathbf{v}^h), \qquad \forall \mathbf{v}^h \in V_h \end{aligned}$$

Then $N(\boldsymbol{\theta}^h)$ *is well-defined, bounded, and continuous.*

Proof. For each $\boldsymbol{\theta}^h \in V_h$, the map $\mathbf{v}^h \in V_h \mapsto c(\boldsymbol{\theta}^h, \mathbf{v}^h)$ is a bounded, linear functional (apply Hölder's inequality and (4.46)). Since V_h is a Hilbert space, we conclude that $N(\boldsymbol{\theta}^h)$ is well defined, by the Riesz-Representation theorem. Moreover, $N(\boldsymbol{\theta}^h)$ is bounded on V_h and since the underlying function space is finite dimensional, continuity follows. □

Lemma 4.4.4. *Fix $n \in \mathbb{N}$. Let $F : V_h \to V_h$ be defined such that $F(\boldsymbol{\theta}^h) = (T \circ N)(\boldsymbol{\theta}^h)$. Then, F is a compact operator.*

Proof. $N(\cdot)$ is a compact operator (continuous on a finite dimensional function space). Thus, F is a continuous composition of a compact operator and hence compact itself. □

Theorem 4.4.5 (Well-posedness)**.** *Fix $n = 0, 1, 2, \ldots, M-1 < \infty$. There exists $(\mathbf{w}_n^h, \pi_n^h) \in X_h \times Q_h$ satisfying Problem 4.3.1. Moreover,*

$$||\mathbf{w}_m^h||^2 + \frac{1}{2Re}\Delta t \sum_{n=0}^{m-1} ||\nabla \mathbf{w}_{n+1/2}^h||^2 + \chi \Delta t \sum_{n=0}^{m-1} ||\mathbf{w}_{n+1/2}^h||_{\star h}^2 \leq ||\mathbf{w}_0^h||^2 + \frac{\Delta t Re}{2} \sum_{n=0}^{m-1} ||\mathbf{f}_{n+1/2}||_{-1}^2 \tag{4.51}$$

for all integers $1 \leq m \leq M$, independent of $\Delta t > 0$.

Proof. First, assume that $(\mathbf{w}_{n+1}^h, q_{n+1}^h)$ is a solution to (4.43), (4.44). Set $\mathbf{v}^h = \mathbf{w}_{n+1/2}^h$ in (4.43) so that skew-symmetry of the nonlinear term provides

$$\begin{aligned} &\frac{1}{2\Delta t}\left(||\mathbf{w}_{n+1}^h||^2 - ||\mathbf{w}_n^h||^2\right) + Re^{-1}||\nabla \mathbf{w}_{n+1/2}^h||^2 \\ &\qquad + \chi(\mathbf{w}_{n+1/2}^h - z_h(\mathbf{w}_{n+1/2}^h), \mathbf{w}_{n+1/2}^h) = (\mathbf{f}_{n+1/2}, \mathbf{w}_{n+1/2}^h) \end{aligned} \tag{4.52}$$

Duality of $H^{-1}(\Omega)$, $H_0^1(\Omega)$ with Young's inequality implies

$$(\mathbf{f}_{n+1/2}, \mathbf{w}_{n+1/2}^h) \leq \frac{Re}{2}||\mathbf{f}_{n+1/2}||_{-1}^2 + \frac{Re}{2}||\nabla \mathbf{w}_{n+1/2}^h||^2 \tag{4.53}$$

From (4.19), we have

$$||\mathbf{w}_{n+1/2}^h||_{\star h}^2 = (\mathbf{w}_{n+1/2}^h - z_h(\mathbf{w}_{n+1/2}^h), \mathbf{w}_{n+1/2}^h) \geq 0 \tag{4.54}$$

Then applying (4.53), (4.54) to (4.52), combining like-terms and simplifying provides

$$\frac{1}{2\Delta t}\left(||\mathbf{w}_{n+1}^h||^2 - ||\mathbf{w}_n^h||^2\right) + \frac{Re}{2}||\nabla \mathbf{w}_{n+1/2}^h||^2 + \chi||\mathbf{w}_{n+1/2}^h||_{\star h}^2 \leq \frac{Re}{2}||\mathbf{f}_{n+1/2}||_{-1}^2$$

Summing from $n = 0$ to $m - 1$, we get the desired bound.

Next, let $\mathbf{W}_n^h = \mathbf{w}_{n+1}^h + \mathbf{w}_n^h$. Showing that $\mathbf{W}_n^h = F(\mathbf{W}_n^h)$ has a fixed point will ensure existence of solutions to (4.45). Indeed, if we can show that $\mathbf{W}_0^h = F(\mathbf{W}_0^h)$, then since $\mathbf{w}_0^h$ is given initial data, existence of $\mathbf{w}_1^h$ is immediate. Induction can be applied to prove existence of $(\mathbf{w}_n^h)_{1\leq n\leq M}$. To this end, since F is compact, it is enough to show (via Leray Schauder) that any solution $\mathbf{W}_{n,\lambda}^h$ of the fixed point problem $\mathbf{W}_{n,\lambda}^h = \lambda F(\mathbf{W}_{n,\lambda}^h)$ is uniformly bounded with respect to $0 \leq \lambda \leq 1$. Hence, we consider

$$a(\mathbf{W}_{n,\lambda}^h, \mathbf{v}^h) = \lambda(N(\mathbf{W}_{n,\lambda}^h), \mathbf{v}^h).$$

Test with $\mathbf{v}^h = \mathbf{W}_{n,\lambda}^h$, use skew-symmetry of the trilinear form and properties of D^h given in Assumption 4.2.5 and (4.19) to get

$$\lambda||\mathbf{W}_{n,\lambda}^h||^2 + \frac{\Delta t}{2Re}||\nabla\mathbf{W}_{n,\lambda}^h||^2 + \frac{\chi\Delta t}{2}||\mathbf{W}_{n,\lambda}^h||_{\star h}^2 \leq 2\lambda(\mathbf{w}_n^h, \mathbf{W}_{n,\lambda}^h) + \lambda\Delta t(\mathbf{f}_{n+1/2}, \mathbf{W}_{n,\lambda}^h) \quad (4.55)$$

Duality of $H^{-1}(\Omega)$, $H_0^1(\Omega)$ followed by Young's inequality implies

$$\lambda\Delta t(\mathbf{f}_{n+1/2}, \mathbf{W}_{n,\lambda}^h) \leq \Delta t Re||\mathbf{f}_{n+1/2}||_{-1}^2 + \frac{\Delta t}{4Re}||\nabla\mathbf{W}_{n,\lambda}^h||^2. \quad (4.56)$$

Since $\mathbf{w}_n^h \in L^2(\Omega)$ from the a priori estimate (4.51), we apply Hölder's and Young's inequalities to get

$$2\lambda(\mathbf{w}_n^h, \mathbf{W}_{n,\lambda}^h) \leq 2||\mathbf{w}_n^h||^2 + \frac{\lambda}{2}||\mathbf{W}_{n,\lambda}^h||^2 \quad (4.57)$$

Applying estimates (4.56), (4.57) to (4.55) we get that $||\nabla\mathbf{W}_{n,\lambda}^h|| \leq C < \infty$ independent of λ. By the Leray-Schauder fixed point theorem, given $\mathbf{w}_n^h$, there exists a solution to the fixed point theorem $\mathbf{W}_n^h = F(\mathbf{W}_n^h)$. By the induction argument noted above, there exists a solution $\mathbf{w}_n^h$ for each $n = 0, 1, 2, \ldots, M - 1$ to (4.45).

Existence of an associated discrete pressure follows by a classical argument, since the pair (X_h, Q_h) satisfies the discrete inf-sup condition (4.39). □

4.5 CONVERGENCE THEORY

For the convergence estimate, we state the main results in Theorem 4.5.1.

Theorem 4.5.1 (Convergence estimate)**.** *Suppose that* $(\mathbf{u}, p)$ *are strong solutions to (4.5), (4.6), (4.7) and that* G, G^h, D, D^h *satisfy Assumption 4.2.5. Let* $E_* = E^{(1)} + E^{(2)}$ *given in (4.81) and (4.87), respectively. Suppose further that* $\mathbf{u} \in C^0([0,T]; H^2)$, $p \in C^0([0,T]; L^2)$, *and* $\mathbf{f} \in C^0([0,T]; H^{-1})$. *If*

$$CRe\Delta t||\mathbf{u}_n||_2^2 < 1, \qquad \forall n = 0, 1, \ldots, M \tag{4.58}$$

then,

$$\begin{aligned} &||\mathbf{u}_M - \mathbf{w}_M^h||^2 + Re^{-1}\Delta t \sum_{n=0}^{M-1} ||\nabla(\mathbf{u}_{n+1/2} - \mathbf{w}_{n+1/2}^h)||^2 + \chi\Delta t \sum_{n=0}^{M-1} ||\mathbf{u}_{n+1/2} - \mathbf{w}_{n+1/2}^h||_{\star h}^2 \\ &\quad \le C(||\mathbf{u}_0 - \mathbf{w}_0^h||^2 + E_* + ||p||_{L^2(L^2)}^2 + (||\mathbf{u}||_{L^\infty(H^1)}^2 + 1)||\mathbf{u}||_{L^2(H^1)}^2 \\ &\qquad + ||\mathbf{u}||_{L^\infty(L^2)}^2 + ||\mathbf{u}||_{L^2(L^2)}^2) \end{aligned} \tag{4.59}$$

Corollary 4.5.2 (Convergence estimate)**.** *Under the assumptions of Theorem 4.5.1, suppose further that* $(\mathbf{u}, p)$ *satisfy the assumptions for (4.40) for some* $k \ge 1$ *and* $s \ge 0$, *and* $\mathbf{u}_{tt} \in L^2(H^1)$, $\mathbf{u}_{ttt} \in L^2(H^{-1})$, $p_{tt} \in L^2(L^2)$, $\mathbf{f}_{tt} \in L^2(H^{-1})$. *Then,*

$$\begin{aligned} &\{||\mathbf{u}_M - \mathbf{w}_M^h||^2 + Re^{-1}\Delta t \sum_{n=0}^{M-1} ||\nabla(\mathbf{u}_{n+1/2} - \mathbf{w}_{n+1/2}^h)||^2\}^{1/2} \\ &\qquad \le C(Re, \chi, C_*, d_1)(h^k + h^{s+1} + \Delta t^2 + c_1(\delta, \alpha) + c_2(h, \delta, \alpha)). \end{aligned} \tag{4.60}$$

Proof of Theorem 4.5.1, Corollary 4.5.2

Recall that $z_h(\mathbf{v}) = D^h\overline{\mathbf{v}}^h$. The consistency error for the time-discretization and deconvolution, time-relaxation modeling error are given by, for $n = 0, 1, \ldots,$

$$\begin{aligned}\tau_n^{(1)}(\mathbf{u}, p; \mathbf{v}^h) := &(\frac{\mathbf{u}_{n+1} - \mathbf{u}_n}{\Delta t} - \mathbf{u}_t(t_{n+1/2}), \mathbf{v}^h) + Re^{-1}(\nabla\left(\mathbf{u}_{n+1/2} - \mathbf{u}(t_{n+1/2})\right), \nabla\mathbf{v}^h)\\ &+ b^*(\mathbf{u}_{n+1/2}, \mathbf{u}_{n+1/2}, \mathbf{v}^h) - b^*(\mathbf{u}(t_{n+1/2}), \mathbf{u}(t_{n+1/2}), \mathbf{v}^h)\\ &- (p_{n+1/2} - p(t_{n+1/2}), \nabla\cdot\mathbf{v}^h) - (\mathbf{f}_{n+1/2} - \mathbf{f}(t_{n+1/2}), \mathbf{v}^h) \qquad (4.61)\\ \tau_n^{(2)}(\mathbf{u}, p; \mathbf{v}^h) := &-b^*(\mathbf{u}_{n+1/2} - z_h(\mathbf{u}_{n+1/2}), \mathbf{u}_{n+1/2}, \mathbf{v}^h) + \chi(\mathbf{u}_{n+1/2} - z_h(\mathbf{u}_{n+1/2}), \mathbf{v}^h) \qquad (4.62)\end{aligned}$$

where $\mathbf{v}^h \in X^h$. Write $\tau_n := \tau_n^{(1)} + \tau_n^{(2)}$. Using (4.61), (4.62), rewrite (4.8) in a form conducive to analyzing the error between the continuous and discrete models:

$$\begin{aligned}&(\frac{\mathbf{u}_{n+1} - \mathbf{u}_n}{\Delta t}, \mathbf{v}^h) + b^*(z_h(\mathbf{u}_{n+1/2}), \mathbf{u}_{n+1/2}, \mathbf{v}^h) + Re^{-1}(\nabla\mathbf{u}_{n+1/2}, \nabla\mathbf{v}^h)\\ &\quad - (p_{n+1/2}, \nabla\cdot\mathbf{v}^h) + \chi(\mathbf{u}_{n+1/2} - z_h(\mathbf{u}_{n+1/2}), \mathbf{v}^h) = (\mathbf{f}_{n+1/2}, \mathbf{v}^h) + \tau_n(\mathbf{u}, p; \mathbf{v}^h) \qquad (4.63)\end{aligned}$$

Decompose the velocity error

$$\mathbf{e}_n = \mathbf{w}_n^h - \mathbf{u}_n = \boldsymbol{\phi}_n^h - \boldsymbol{\eta}_n, \qquad \boldsymbol{\phi}_n^h = \mathbf{w}_n^h - \mathbf{U}_n^h, \qquad \boldsymbol{\eta}_n = \mathbf{u}_n - \mathbf{U}_n^h,$$

where $\mathbf{U}_n^h \in V_h$. Fix $\tilde{q}_h^{n+1/2} \in Q_h$. Note that $(\tilde{q}_h^{n+1/2}, \nabla\cdot\mathbf{v}^h) = 0$ for any $\mathbf{v}^h \in V_h$. Subtract (4.63) from (4.45) and test with $\mathbf{v}^h = \boldsymbol{\phi}_{n+1/2}^h$ to get the error equation

$$\begin{aligned}&\frac{1}{2\Delta t}\left(||\boldsymbol{\phi}_{n+1}^h||^2 - ||\boldsymbol{\phi}_n^h||^2\right) + Re^{-1}||\nabla\boldsymbol{\phi}_{n+1/2}^h||^2 + \chi(\boldsymbol{\phi}_{n+1/2}^h - z_h(\boldsymbol{\phi}_{n+1/2}^h), \boldsymbol{\phi}_{n+1/2}^h)\\ &= -(\tilde{q}_h^{n+1/2} - p_{n+1/2}, \nabla\cdot\boldsymbol{\phi}_{n+1/2}^h) + \frac{1}{\Delta t}(\boldsymbol{\eta}_{n+1} - \boldsymbol{\eta}_n, \boldsymbol{\phi}_{n+1/2}^h) - b^*(z_h(\boldsymbol{\phi}_{n+1/2}^h), \mathbf{u}_{n+1/2}, \boldsymbol{\phi}_{n+1/2}^h)\\ &\quad + b^*(z_h(\boldsymbol{\eta}_{n+1/2}), \mathbf{u}_{n+1/2}, \boldsymbol{\phi}_{n+1/2}^h) + b^*(z_h(\mathbf{w}_{n+1/2}^h), \boldsymbol{\eta}_{n+1/2}, \boldsymbol{\phi}_{n+1/2}^h)\\ &\quad + Re^{-1}(\nabla\boldsymbol{\eta}_{n+1/2}, \nabla\boldsymbol{\phi}_{n+1/2}^h) + \chi(\boldsymbol{\eta}_{n+1/2} - z_h(\boldsymbol{\eta}_{n+1/2}), \boldsymbol{\phi}_{n+1/2}^h) - \tau_n(\mathbf{u}, p; \boldsymbol{\phi}_{n+1/2}^h) \qquad (4.64)\end{aligned}$$

Let $\mathbf{U}_n^h = \tilde{\mathbf{v}}^h$ be the L^2-projection of $\mathbf{u}(\cdot, t_n)$ so that $(\boldsymbol{\eta}_{n+1} - \boldsymbol{\eta}_n, \boldsymbol{\phi}_{n+1/2}^h) = 0$. Using (4.19), the error equation (4.64) simplifies to

$$\begin{aligned}
&\frac{1}{2\Delta t}\left(||\boldsymbol{\phi}_{n+1}^h||^2 - ||\boldsymbol{\phi}_n^h||^2\right) + Re^{-1}||\nabla\boldsymbol{\phi}_{n+1/2}^h||^2 + \chi||\boldsymbol{\phi}_{n+1/2}^h||_{\star h}^2 \\
&= -(\tilde{q}_h^{n+1/2} - p_{n+1/2}, \nabla\cdot\boldsymbol{\phi}_{n+1/2}^h) - b^*(z_h(\boldsymbol{\phi}_{n+1/2}^h), \mathbf{u}_{n+1/2}, \boldsymbol{\phi}_{n+1/2}^h) \\
&\quad + b^*(z_h(\boldsymbol{\eta}_{n+1/2}), \mathbf{u}_{n+1/2}, \boldsymbol{\phi}_{n+1/2}^h) + b^*(z_h(\mathbf{w}_{n+1/2}^h), \boldsymbol{\eta}_{n+1/2}, \boldsymbol{\phi}_{n+1/2}^h) \\
&\quad + Re^{-1}(\nabla\boldsymbol{\eta}_{n+1/2}, \nabla\boldsymbol{\phi}_{n+1/2}^h) + \chi(\boldsymbol{\eta}_{n+1/2} - z_h(\boldsymbol{\eta}_{n+1/2}), \boldsymbol{\phi}_{n+1/2}^h) - \tau_n(\mathbf{u}, p; \boldsymbol{\phi}_{n+1/2}^h) \quad (4.65)
\end{aligned}$$

Let $\varepsilon > 0$ be an arbitrary (Young's inequality) constant to be fixed after all majorizations to allow absorption of appropriate terms into the left-hand-side of (4.65). We apply standard estimates and those of Lemma 4.3.2 without explicit reference in the following.

First, $\mathbf{u} \in H^1(\Omega)$ and $p \in L^2(\Omega)$ implies

$$Re^{-1}(\nabla\boldsymbol{\eta}_{n+1/2}, \nabla\boldsymbol{\phi}_{n+1/2}^h) \le CRe^{-1}||\nabla\boldsymbol{\eta}_{n+1/2}||^2 + \frac{1}{\varepsilon Re}||\nabla\boldsymbol{\phi}_{n+1/2}^h||^2 \quad (4.66)$$

$$(p^{n+1/2} - \tilde{q}_h^{n+1/2}, \nabla\cdot\boldsymbol{\phi}_{n+1/2}^h) \le CRe||p^{n+1/2} - \tilde{q}_h^{n+1/2}||^2 + \frac{1}{\varepsilon Re}||\nabla\boldsymbol{\phi}_{n+1/2}^h||^2. \quad (4.67)$$

Also, from Lemma 4.2.8, $||I - D^h G_h|| \le 1$, so that

$$\chi(\boldsymbol{\eta}_{n+1/2} - z_h(\boldsymbol{\eta}_{n+1/2}), \boldsymbol{\phi}_{n+1/2}^h) \le C\chi^2 Re||\boldsymbol{\eta}_{n+1/2}||^2 + \frac{1}{\varepsilon Re}||\nabla\boldsymbol{\phi}_{n+1/2}^h||. \quad (4.68)$$

We bound the convective terms next. First, $\mathbf{u} \in H^2(\Omega)$ implies

$$b^*(z_h(\boldsymbol{\phi}_{n+1/2}^h), \mathbf{u}^{n+1/2}, \boldsymbol{\phi}_{n+1/2}^h) \le CRe||z_h(\boldsymbol{\phi}_{n+1/2}^h)||^2||\mathbf{u}^{n+1/2}||_2^2 + \frac{1}{\varepsilon Re}||\nabla\boldsymbol{\phi}_{n+1/2}^h||^2 \quad (4.69)$$

and $\mathbf{u} \in L^\infty(H^1(\Omega))$ implies

$$\begin{aligned}
&b^*(z_h(\boldsymbol{\eta}_{n+1/2}), \mathbf{u}^{n+1/2}, \boldsymbol{\phi}_{n+1/2}^h) \\
&\quad \le CRe||\mathbf{u}||_{L^\infty(H^1)}^2||\nabla z_h(\boldsymbol{\eta}_{n+1/2})||^2 + \frac{1}{\varepsilon Re}||\nabla\boldsymbol{\phi}_{n+1/2}^h||^2. \quad (4.70)
\end{aligned}$$

Next, rewrite the remaining nonlinear term

$$\begin{aligned}
b^*(z_h(\mathbf{w}_{n+1/2}^h), \boldsymbol{\eta}_{n+1/2}, \boldsymbol{\phi}_{n+1/2}^h) &= b^*(z_h(\mathbf{u}_{n+1/2}), \boldsymbol{\eta}_{n+1/2}, \boldsymbol{\phi}_{n+1/2}^h) \\
&\quad - b^*(z_h(\boldsymbol{\eta}_{n+1/2}), \boldsymbol{\eta}_{n+1/2}, \boldsymbol{\phi}_{n+1/2}^h) + b^*(z_h(\boldsymbol{\phi}_{n+1/2}^h), \boldsymbol{\eta}_{n+1/2}, \boldsymbol{\phi}_{n+1/2}^h).
\end{aligned}$$

Once again, $\mathbf{u} \in L^\infty(H^1(\Omega))$ implies

$$b^*(z_h(\mathbf{u}_{n+1/2}), \boldsymbol{\eta}_{n+1/2}, \boldsymbol{\phi}^h_{n+1/2}) \leq CRe||z_h(\mathbf{u})||^2_{L^\infty(H^1)}||\nabla\boldsymbol{\eta}_{n+1/2}||^2 + \frac{1}{\varepsilon Re}||\nabla\boldsymbol{\phi}^h_{n+1/2}||^2 \quad (4.71)$$

and similarly for $b^*(z_h(\boldsymbol{\eta}_{n+1/2}), \boldsymbol{\eta}_{n+1/2}, \boldsymbol{\phi}^h_{n+1/2})$. Lastly, Lemma 4.3.2 and inverse inequality (4.41) give

$$\begin{aligned} &b^*(z_h(\boldsymbol{\phi}^h_{n+1/2}), \boldsymbol{\eta}_{n+1/2}, \boldsymbol{\phi}^h_{n+1/2}) \\ &\quad \leq C\sqrt{||z_h(\boldsymbol{\phi}^h_{n+1/2})||||\nabla z_h(\boldsymbol{\phi}^h_{n+1/2})||}||\nabla\boldsymbol{\eta}_{n+1/2}||||\nabla\boldsymbol{\phi}^h_{n+1/2}|| \\ &\quad \leq CRe h^{-1}||z_h(\boldsymbol{\phi}^h_{n+1/2})||^2||\nabla\boldsymbol{\eta}_{n+1/2}||^2 + \frac{1}{\varepsilon Re}||\nabla\boldsymbol{\phi}^h_{n+1/2}||^2. \end{aligned} \quad (4.72)$$

By noting that Assumption 4.2.5 provides $||z_h(\mathbf{v})|| \leq ||\mathbf{v}||$ and $||\nabla z_h(\mathbf{v})|| \leq d_1||\nabla\mathbf{v}||$, we have

$$\begin{aligned} &b^*(z_h(\boldsymbol{\phi}^h_{n+1/2}), \mathbf{u}_{n+1/2}, \boldsymbol{\phi}^h_{n+1/2}) \\ &\quad - b^*(z_h(\boldsymbol{\eta}_{n+1/2}), \mathbf{u}_{n+1/2}, \boldsymbol{\phi}^h_{n+1/2}) - b^*(z_h(\mathbf{w}^h_{n+1/2}), \boldsymbol{\eta}_{n+1/2}, \boldsymbol{\phi}^h_{n+1/2}) \\ &\leq \frac{5}{\varepsilon Re}||\nabla\boldsymbol{\phi}^h_{n+1/2}||^2 + CRe(||\mathbf{u}_{n+1/2}||^2_2 + h^{-1}||\nabla\boldsymbol{\eta}_{n+1/2}||^2)||\boldsymbol{\phi}^h_{n+1/2}||^2 \\ &\quad + Cd_1^2Re(||\mathbf{u}||^2_{L^\infty(H^1)} + ||\nabla\boldsymbol{\eta}_{n+1/2}||^2)||\nabla\boldsymbol{\eta}_{n+1/2}||^2. \end{aligned} \quad (4.73)$$

Bounding the time-consistency error remains. First, $\mathbf{u}_t \in H^{-1}(\Omega)$ implies

$$(\frac{\mathbf{u}_{n+1} - \mathbf{u}_n}{\Delta t} - \mathbf{u}_t(t_{n+1/2}), \boldsymbol{\phi}^h_{n+1/2}) \leq CRe||\frac{\mathbf{u}_{n+1} - \mathbf{u}_n}{\Delta t} - \mathbf{u}_t(t_{n+1/2})||^2_{-1} + \frac{1}{\varepsilon Re}||\nabla\boldsymbol{\phi}^h_{n+1/2}||^2 \quad (4.74)$$

and $\mathbf{u} \in H^1(\Omega)$ implies

$$\begin{aligned} &Re^{-1}(\nabla(\mathbf{u}_{n+1/2} - \mathbf{u}(t_{n+1/2})), \nabla\boldsymbol{\phi}^h_{n+1/2}) \\ &\quad \leq CRe^{-1}||\nabla(\mathbf{u}_{n+1/2} - \mathbf{u}(t_{n+1/2}))||^2 + \frac{1}{\varepsilon Re}||\nabla\boldsymbol{\phi}^h_{n+1/2}||^2. \end{aligned} \quad (4.75)$$

Similarly, $p \in L^2(\Omega)$ implies

$$\begin{aligned} &(p_{n+1/2} - p(t_{n+1/2}), \nabla\boldsymbol{\phi}^h_{n+1/2}) \\ &\quad \leq CRe||p_{n+1/2} - p(t_{n+1/2})||^2 + \frac{1}{\varepsilon Re}||\nabla\boldsymbol{\phi}^h_{n+1/2}||^2 \end{aligned} \quad (4.76)$$

and $\mathbf{f} \in H^{-1}(\Omega)$ implies

$$(\mathbf{f}(t_{n+1/2}) - \mathbf{f}_{n+1/2}, \boldsymbol{\phi}^h_{n+1/2}) \\ \leq CRe||\mathbf{f}(t_{n+1/2}) - \mathbf{f}_{n+1/2}||^2_{-1} + \frac{1}{\varepsilon Re}||\nabla \boldsymbol{\phi}^h_{n+1/2}||^2. \tag{4.77}$$

We decompose the nonlinear terms so that

$$b^*(\mathbf{u}_{n+1/2}, \mathbf{u}_{n+1/2}, \boldsymbol{\phi}^h_{n+1/2}) - b^*(\mathbf{u}(t_{n+1/2}), \mathbf{u}(t_{n+1/2}), \boldsymbol{\phi}^h_{n+1/2}) \\ = b^*(\mathbf{u}_{n+1/2} - \mathbf{u}(t_{n+1/2}), \mathbf{u}_{n+1/2}, \boldsymbol{\phi}^h_{n+1/2}) + b^*(\mathbf{u}(t_{n+1/2}), \mathbf{u}_{n+1/2} - \mathbf{u}(t_{n+1/2}), \boldsymbol{\phi}^h_{n+1/2}).$$

Then, $\mathbf{u} \in L^\infty(H^1(\Omega))$ implies

$$b^*(\mathbf{u}_{n+1/2} - \mathbf{u}(t_{n+1/2}), \mathbf{u}_{n+1/2}, \boldsymbol{\phi}^h_{n+1/2}) \\ \leq CRe||\mathbf{u}||^2_{L^\infty(H^1)}||\nabla(\mathbf{u}_{n+1/2} - \mathbf{u}(t_{n+1/2}))||^2 + \frac{1}{\varepsilon Re}||\nabla \boldsymbol{\phi}^h_{n+1/2}||^2 \tag{4.78}$$

and similarly for $b^*(\mathbf{u}(t_{n+1/2}, \mathbf{u}_{n+1/2} - \mathbf{u}(t_{n+1/2}), \boldsymbol{\phi}^h_{n+1/2})$. Then we have, for some $C > 0$,

$$\tau^{(1)}_n(\mathbf{u}, p; \boldsymbol{\phi}^h_{n+1/2}) \leq \frac{6}{\varepsilon Re}||\nabla \boldsymbol{\phi}^h_{n+1/2}||^2 + CReE^{(1)}_n \tag{4.79}$$

where

$$E^{(1)}_n := ||\frac{\mathbf{u}_{n+1} - \mathbf{u}_n}{\Delta t} - \mathbf{u}_t(t_{n+1/2})||^2_{-1} \\ + (Re^{-2} + ||\mathbf{u}||^2_{L^\infty(H^1)})||\nabla(\mathbf{u}_{n+1/2} - \mathbf{u}(t_{n+1/2}))||^2 \\ + ||p_{n+1/2} - p(t_{n+1/2})||^2 + ||\mathbf{f}(t_{n+1/2}) - \mathbf{f}_{n+1/2}||^2_{-1} \tag{4.80}$$

Moreover, $\Delta t \sum_{n=0}^{M-1} E^{(1)}_n \leq CE^{(1)}$ where $E^{(1)}$ is given by

$$E^{(1)} := \int_0^T \left\| \int_0^1 \left(\mathbf{u}_t(\cdot, t + s\Delta t) - \mathbf{u}_t(\cdot, t + \frac{\Delta t}{2}) \right) ds \right\|^2_{-1} dt \\ + \int_0^T ||\nabla(\frac{1}{2}(\mathbf{u}(\cdot, t + \Delta t) + \mathbf{u}(\cdot, t)) - \mathbf{u}(\cdot, t + \frac{\Delta t}{2}))||^2 dt \\ + \int_0^T ||\frac{1}{2}(p(\cdot, t + \Delta t) + p(\cdot, t)) - p(\cdot, t + \frac{\Delta t}{2})||^2 dt \\ + \int_0^T ||\frac{1}{2}(\mathbf{f}(\cdot, t + \Delta t) + \mathbf{f}(\cdot, t)) - \mathbf{f}(\cdot, t + \frac{\Delta t}{2})||^2_{-1} dt. \tag{4.81}$$

Notice that by introducing $\pm z(\mathbf{u}_{n+1/2})$ we can write

$$\begin{aligned}
&\tau_n^{(2)}(\mathbf{u}, p; \mathbf{v}^h) \\
&= -b^*(\mathbf{u}_{n+1/2} - z(\mathbf{u}_{n+1/2}), \mathbf{u}_{n+1/2}, \boldsymbol{\phi}^h_{n+1/2}) - b^*\left((z(\mathbf{u}_{n+1/2}) - z_h(\mathbf{u}_{n+1/2})), \mathbf{u}_{n+1/2}, \boldsymbol{\phi}^h_{n+1/2}\right) \\
&+ \chi(\mathbf{u}_{n+1/2} - z(\mathbf{u}_{n+1/2}), \boldsymbol{\phi}^h_{n+1/2}) + \chi(z(\mathbf{u}_{n+1/2}) - z_h(\mathbf{u}_{n+1/2}), \boldsymbol{\phi}^h_{n+1/2})
\end{aligned} \tag{4.82}$$

Then,

$$\begin{aligned}
&\chi(\mathbf{u}_{n+1/2} - z(\mathbf{u}_{n+1/2}), \boldsymbol{\phi}^h_{n+1/2}) + \chi(z(\mathbf{u}_{n+1/2}) - z_h(\mathbf{u}_{n+1/2}), \boldsymbol{\phi}^h_{n+1/2}) \\
&\quad \leq C\chi^2 Re||\mathbf{u}_{n+1/2} - z(\mathbf{u}_{n+1/2})||^2 + C\chi^2 Re||z(\mathbf{u}_{n+1/2}) - z^h(\mathbf{u}_{n+1/2})||^2 + \frac{2}{\varepsilon Re}||\nabla \boldsymbol{\phi}^h_{n+1/2}||^2
\end{aligned} \tag{4.83}$$

and $\mathbf{u} \in H^2(\Omega)$ implies

$$\begin{aligned}
&- b^*(\mathbf{u}_{n+1/2} - z(\mathbf{u}_{n+1/2}), \mathbf{u}_{n+1/2}, \boldsymbol{\phi}^h_{n+1/2}) - b^*(z(\mathbf{u}_{n+1/2}) - z_h(\mathbf{u}_{n+1/2}), \mathbf{u}_{n+1/2}, \boldsymbol{\phi}^h_{n+1/2}) \\
&\quad \leq CRe||\mathbf{u}_{n+1/2}||_2^2 \left(||\mathbf{u}_{n+1/2} - z(\mathbf{u}_{n+1/2})||^2 + ||z(\mathbf{u}_{n+1/2}) - z^h(\mathbf{u}_{n+1/2}||^2\right) \\
&\qquad + \frac{2}{\varepsilon Re}||\nabla \boldsymbol{\phi}^h_{n+1/2}||^2
\end{aligned} \tag{4.84}$$

These estimates combine to prove

$$\tau_n^{(2)}(\mathbf{u}, p; \boldsymbol{\phi}^h_{n+1/2}) \leq \frac{4}{\varepsilon Re}||\nabla \boldsymbol{\phi}^h_{n+1/2}||^2 + CReE_n^{(2)}. \tag{4.85}$$

where

$$E_n^{(2)} := (\chi^2 + ||\mathbf{u}_{n+1/2}||_2^2)\left[||\mathbf{u}_{n+1/2} - z(\mathbf{u}_{n+1/2})||^2 + ||z(\mathbf{u}_{n+1/2}) - z^h(\mathbf{u}_{n+1/2})||^2\right]. \tag{4.86}$$

Moreover, $\Delta t \sum_{n=0}^{M-1} E_n^{(2)} \leq CE^{(2)}$ where $E^{(2)}$ is given by

$$E^{(2)} := \int_0^T (\chi^2 + ||\mathbf{u}(\cdot,t)||_2^2)\left[||\mathbf{u}(\cdot,t) - D\overline{\mathbf{u}(\cdot,t)}||^2 + ||D\overline{\mathbf{u}(\cdot,t)} - D^h\overline{\mathbf{u}(\cdot,t)}^h||^2\right] dt. \tag{4.87}$$

Apply estimates from (4.66), (4.67), (4.68), (4.73), (4.79), and (4.85) to (4.65). Set $\varepsilon = 36$ and absorb all terms including $||\nabla \boldsymbol{\phi}^h_{n+1/2}||$ from the right into left-hand-side of (4.65). Sum

the resulting inequality on both sides from $n = 0$ to $n = M - 1$. Apply estimates (4.80), (4.86). The result is

$$
\begin{aligned}
&||\boldsymbol{\phi}_M^h||^2 + Re^{-1}\Delta t \sum_{n=0}^{M-1} ||\nabla \boldsymbol{\phi}_{n+1/2}^h||^2 + \chi \Delta t \sum_{n=0}^{M-1} ||\boldsymbol{\phi}_{n+1/2}^h||_{\star h}^2 \\
&\leq ||\boldsymbol{\phi}_0^h||^2 + CRe\Delta t \sum_{n=0}^{M-1} \left(E_n^{(1)} + E_n^{(2)}\right) + CRe\Delta t \sum_{n=0}^{M-1} ||p_{n+1/2} - \tilde{q}_{n+1/2}^h||^2 \\
&+ CRed_1^2 \Delta t \sum_{n=0}^{M-1} (||\mathbf{u}||_{L^\infty(H^1)}^2 + ||\nabla \boldsymbol{\eta}_{n+1/2}||^2)||\nabla \boldsymbol{\eta}_{n+1/2}||^2 \\
&+ CRe\Delta t \sum_{n=0}^{M-1} (||\mathbf{u}_{n+1/2}||_2^2 + h^{-1}||\nabla \boldsymbol{\eta}_{n+1/2}||^2)||\boldsymbol{\phi}_{n+1/2}^h||^2 \\
&+ C\chi^2 Re\Delta t \sum_{n=0}^{M-1} ||\boldsymbol{\eta}_{n+1/2}||^2 + CRe^{-1}\Delta t \sum_{n=0}^{M-1} ||\nabla \boldsymbol{\eta}_{n+1/2}||^2.
\end{aligned} \tag{4.88}
$$

The approximation (4.40) and $\mathbf{u} \in C^0([0,T], H^1) \cap L^2(H^2)$ imply

$$
\sup_n ||\nabla \boldsymbol{\eta}_n|| \leq C||\mathbf{u}||_{L^\infty(H^1)} < \infty, \qquad \frac{\Delta t}{h} \sum_{n=0}^{N-1} ||\nabla \boldsymbol{\eta}_n||^2 \leq C||\mathbf{u}||_{L^2(H^2)}^2 < \infty.
$$

Applying these results, (4.88) becomes

$$
\begin{aligned}
&||\boldsymbol{\phi}_M^h||^2 + Re^{-1}\Delta t \sum_{n=0}^{M-1} ||\nabla \boldsymbol{\phi}_{n+1/2}^h||^2 + \chi \Delta t \sum_{n=0}^{M-1} ||\boldsymbol{\phi}_{n+1/2}^h||_{\star h}^2 \\
&\leq ||\boldsymbol{\phi}_0^h||^2 + CRe\Delta t \sum_{n=0}^{M-1} \left(E_n^{(1)} + E_n^{(2)}\right) + CRe\Delta t \sum_{n=0}^{M-1} ||p_{n+1/2} - \tilde{q}_{n+1/2}^h||^2 \\
&+ CRe\Delta t \sum_{n=0}^{M-1} \left(((d_1^2+1)||\mathbf{u}||_{L^\infty(H^1)}^2 + Re^{-2})||\nabla \boldsymbol{\eta}^{n+1/2}||^2 + ||\mathbf{u}^{n+1/2}||_2^2 ||\boldsymbol{\phi}_{n+1/2}^h||^2\right) \\
&+ C\chi^2 Re\Delta t \sum_{n=0}^{M-1} ||\boldsymbol{\eta}_{n+1/2}||^2.
\end{aligned} \tag{4.89}
$$

Requiring $\mathbf{u} \in C^0([0,T];H^2)$ allows us to restrict the time-step by (4.58) so that the discrete Gronwall Lemma 4.3.3 applies to (4.89)

$$
\begin{aligned}
&||\boldsymbol{\phi}_M^h||^2 + Re^{-1}\Delta t \sum_{n=0}^{M-1} ||\nabla \boldsymbol{\phi}_{n+1/2}^h||^2 + \chi \Delta t \sum_{n=0}^{M-1} ||\boldsymbol{\phi}_{n+1/2}^h||_{\star h}^2 \\
&\quad \leq C_* ||\boldsymbol{\phi}_0^h||^2 + C_* Re \Delta t \sum_{n=0}^{M-1} \left(E_n^{(1)} + E_n^{(2)} \right) \\
&\quad + C_* Re \Delta t \sum_{n=0}^{M-1} \left(||p_{n+1/2} - \tilde{q}_{n+1/2}^h||^2 + ((d_1^2+1)||\mathbf{u}||_{L^\infty(H^1)}^2 + Re^{-2})||\nabla \boldsymbol{\eta}_{n+1/2}||^2 \right) \\
&\quad + C_* \chi^2 Re \Delta t \sum_{n=0}^{M-1} ||\boldsymbol{\eta}_{n+1/2}||^2.
\end{aligned} \tag{4.90}
$$

where

$$
C_* = C \exp\left(Re \Delta t \sum_{n=0}^{M-1} g_n ||\mathbf{u}_n||_2^2 \right), \qquad g_n = (1 - CRe\Delta t ||\mathbf{u}_n||_2^2)^{-1} \tag{4.91}
$$

Lastly, the triangle inequality applied to (4.90) implies

$$
\begin{aligned}
&||\mathbf{u}_M - \mathbf{w}_M^h||^2 + Re^{-1}\Delta t \sum_{n=0}^{M-1} ||\nabla(\mathbf{u}_{n+1/2} - \mathbf{w}_{n+1/2}^h)||^2 + \chi \Delta t \sum_{n=0}^{M-1} ||\mathbf{u}_{n+1/2} - \mathbf{w}_{n+1/2}^h||_{\star h}^2 \\
&\quad \leq C_* ||\boldsymbol{\phi}_0^h||^2 + C_* Re \Delta t \sum_{n=0}^{M-1} \left(E_n^{(1)} + E_n^{(2)} \right) \\
&\quad + C_* Re \Delta t \sum_{n=0}^{M-1} \left(||p_{n+1/2} - \tilde{q}_{n+1/2}^h||^2 + ((d_1^2+1)||\mathbf{u}||_{L^\infty(H^1)}^2 + Re^{-2})||\nabla \boldsymbol{\eta}_{n+1/2}||^2 \right) \\
&\quad + C_* \chi^2 Re \Delta t \sum_{n=0}^{M-1} ||\boldsymbol{\eta}_{n+1/2}||^2 \\
&\quad + ||\boldsymbol{\eta}_M||^2 + Re^{-1}\Delta t \sum_{n=0}^{M-1} ||\nabla \boldsymbol{\eta}_{n+1/2}||^2 + \chi \Delta t \sum_{n=0}^{M-1} ||\boldsymbol{\eta}_{n+1/2}||_{\star h}^2.
\end{aligned} \tag{4.92}
$$

Apply estimate (4.48) to (4.92). Then, after simplification, (4.92) results in (4.59) which proves Theorem 4.5.1.

Lastly, to prove Corollary 4.5.2, apply estimates (4.48), (4.49), (4.50) and (4.40) to the preliminary estimate (4.92).

4.6 APPLICATIONS

4.6.1 Iterated (modified) Tikhonov-Lavrentiev regularization

We now show that $D_{\alpha,J}$, $D^h_{\alpha,J}$ from Definitions 4.2.13, 4.2.14 with $G = A^{-1}$ satisfies Assumption 4.2.5. Proposition 4.2.9 implies that it is enough to show that $D_{\alpha,0}$ satisfies Assumption 4.2.5. In addition, we will provide sharpened estimates for $d_{1,j}$, $c_{1,j}$, and $c_{2,j}$. The key is that $A^{-1} > 0$ is a continuous function of the Laplace operator $-\Delta \geq 0$ and hence they commute (on X). Moreover, $D_{\alpha,0} > 0$ is a continuous function of A^{-1} so that $D_{\alpha,0}$ commutes with A^{-1} and Δ (on X).

Next, we characterize the spectrum of $D_{\alpha,0}$, $D^h_{\alpha,0}$.

Lemma 4.6.1. *Fix $0 < \alpha \leq 1$. Define $f : (0,1] \to \mathbb{R}$ and $g : (0,1] \to \mathbb{R}$ by*

$$f(x) := \frac{1}{(1-\alpha)x + \alpha}, \qquad g(x) := \frac{x}{(1-\alpha)x + \alpha}$$

The maps f, g are continuous such that $f((0,1]) = [1, \alpha^{-1})$ and $g((0,1]) = (0,1]$.

Proof. The functions f, g are clearly continuous with f *decreasing* and g increasing on $(0,1]$. Hence, the range of f is $[1, \alpha^{-1})$ and range of g is $(0,1]$. □

The next result shows that $D_{\alpha,0}$, $D^h_{\alpha,0}$ satisfy part of Assumption 4.2.5.

Proposition 4.6.2. *$D_{\alpha,0}$, $D^h_{\alpha,0}$ (on X, X_h respectively) are linear, bounded, spd, and commute with G, G^h (respectively). Moreover,*

$$\begin{aligned} &||D_{\alpha,0}A^{-1}|| \leq 1, \quad ||\nabla(D_{\alpha,0}A^{-1}\mathbf{u})|| \leq ||\nabla \mathbf{u}|| \quad \forall\ \mathbf{u} \in X \\ &||D^h_{\alpha,0}A_h^{-1}|| \leq 1, \quad ||\nabla(D^h_{\alpha,0}A_h^{-1}\mathbf{u}^h)|| \leq ||\nabla \mathbf{u}^h|| \quad \forall\ \mathbf{u}^h \in X_h \end{aligned} \tag{4.93}$$

Hence $d_1 = 1$ in Assumptions 4.2.4, 4.2.5.

Proof. It is immediately clear that $D_{\alpha,0}$, $D^h_{\alpha,0}$ are linear. As a consequence, since $A^{-1} > 0$ with spectrum in $(0,1]$, then $D_{\alpha,0} = f(A^{-1})$ with spectrum contained in $[1, \alpha^{-1})$ so that $D > 0$. Therefore, $D_{\alpha,0}A^{-1} = g(A^{-1})$ with spectrum contained in $(0,1]$. A similar argument shows that A_h^{-1} has spectrum in $(0,1]$, $D^h_{\alpha,0}$ has spectrum in $[1,\alpha^{-1})$, and $D^h_{\alpha,0}A_h^{-1}$ has spectrum in $(0,1]$. Thus $D_{\alpha,0} > 0$, $D^h_{\alpha,0} > 0$ and $||D_{\alpha,0}A^{-1}|| \leq 1$ and $||D^h_{\alpha,0}A_h^{-1}|| \leq 1$. Therefore, $D_{\alpha,0}$ and $D^h_{\alpha,0}$ are bounded and commute with $G = A^{-1}$, $G^h = A_h^{-1}$ respectively as discussed above.

The second set of inequalities on each line can be proved with an appropriate choice of $\mathbf{v}$ and $\mathbf{v}^h$ in Definitions 4.2.2 and 4.2.3. Starting with Definition 4.2.2, take $\boldsymbol{\phi} = \mathbf{u}$ and choose $\mathbf{v} = \Delta D_{\alpha,0}A^{-1}\mathbf{u}$. Then integration by parts and the Cauchy-Schwartz inequality give the result. The discrete form is proved using Definition4.2.3 and choosing $\boldsymbol{\phi} = \mathbf{u}^h$ and $\mathbf{v} = \Delta D^h_{\alpha,0}A_h^{-1}\mathbf{u}^h$ □

It remains to provide estimates on c_1, c_2, and sharpened estimates for $c_{1,j}$, $c_{2,j}$. Indeed, as a direct consequence of Propositions 4.6.3, 4.6.4, we have, for any $j = 0, 1, \ldots, J$,

$$\begin{aligned} c_{1,j} &= (\alpha\delta^2)^{j+1}||\Delta^{2j+2}\mathbf{v}||, && \forall \mathbf{v} \in H^{2j+2}(\Omega) \\ c_{2,j} &= C4^j(\alpha\delta^2 h^{2k} + h^{2k+2}) \max_{0\leq n\leq j} ||D_{\alpha,n}A^{-1}\mathbf{v}||^2_{k+1} && \forall \mathbf{v} \in H^{k+1}(\Omega). \end{aligned} \tag{4.94}$$

Proposition 4.6.3. *Let $j = 0, 1, \ldots, J$. Then*

$$||\mathbf{v} - D_{\alpha,j}A^{-1}\mathbf{v}|| \leq (\alpha\delta^2)^{j+1}||\mathbf{v}||_{2j+2}, \qquad \forall \mathbf{v} \in H^{2j+2}(\Omega). \tag{4.95}$$

Proof. Using (4.3), we have

$$D_{\alpha,0}^{-1}(D_{\alpha,J}A^{-1}\mathbf{v} - D_{\alpha,J-1}A^{-1}\mathbf{v}) = A^{-1}\mathbf{v} - A^{-1}D_{\alpha,J-1}A^{-1}\mathbf{v}. \tag{4.96}$$

Subtracting (4.96) from the identity

$$D_{\alpha,0}^{-1}(\mathbf{v} - \mathbf{v}) = A^{-1}\mathbf{v} - A^{-1}\mathbf{v}$$

gives us

$$D_{\alpha,0}^{-1}\left((I - D_{\alpha,J}A^{-1})\mathbf{v} - (I - D_{\alpha,J-1}A^{-1})\mathbf{v}\right) = -A^{-1}(I - D_{\alpha,J-1}A^{-1})\mathbf{v}. \tag{4.97}$$

Multiplying by $D_{\alpha,0}$, rearranging, simplifying, and using $A - I = -\delta^2\Delta$ from Definition 4.2.2 gives us

$$\begin{aligned}
(I - D_{\alpha,J}A^{-1})\mathbf{v} &= \left[-D_{\alpha,0}A^{-1}(I - D_{\alpha,J-1}A^{-1}) + (I - D_{\alpha,J-1}A^{-1})\right]\mathbf{v} \\
&= (I - D_{\alpha,J-1}A^{-1})(I - D_{\alpha,0}A^{-1})\mathbf{v} \\
&= (I - D_{\alpha,J-1}A^{-1})D_{\alpha,0}A^{-1}(D_{\alpha,0}^{-1}A - I)\mathbf{v} \\
&= (I - D_{\alpha,J-1}A^{-1})D_{\alpha,0}A^{-1}\left((1-\alpha)A^{-1} + \alpha I)A - I\right)\mathbf{v} \\
&= (I - D_{\alpha,J-1}A^{-1})D_{\alpha,0}A^{-1}\alpha(A - I)\mathbf{v} \\
&= -\alpha\delta^2\Delta D_{\alpha,0}A^{-1}[(I - D_{\alpha,J-1}A^{-1})\mathbf{v}].
\end{aligned}$$

Applying recursion, we obtain

$$(I - D_{\alpha,J}A^{-1})\mathbf{v} = (-\alpha\delta^2)^{J+1}(D_{\alpha,0}A^{-1})^{J+1}\Delta^{J+1}\mathbf{v}.$$

Thus, taking norms and applying $||D_{\alpha,0}A^{-1}|| \leq 1$, we get (4.95). □

Proposition 4.6.4. *Let $j = 0, 1, \ldots, J$. Then*

$$\begin{aligned}
&||D_{\alpha,j}A^{-1}\mathbf{w} - D_{\alpha,j}^{h}A_h^{-1}\mathbf{w}||^2 \\
&\quad \leq C4^j(\alpha\delta^2 h^{2k} + h^{2k+2}) \max_{0\leq n\leq j} ||D_{\alpha,n}A^{-1}\mathbf{w}||_{k+1}^2, \qquad \forall \mathbf{w} \in H^{k+1}(\Omega).
\end{aligned} \tag{4.98}$$

Proof. Take $\mathbf{v} = \mathbf{v}^h$ in (4.37). For $j = 1, \ldots, J$, let $\mathbf{e}_j = D_\alpha \overline{\mathbf{w}} - D_\alpha^h \overline{\mathbf{w}}^h := \boldsymbol{\eta}_j - \boldsymbol{\phi}_j^h$, where $\boldsymbol{\eta}_j := \boldsymbol{\omega}_j - \tilde{\mathbf{v}}_j^h$, and $\boldsymbol{\phi}_j^h := \boldsymbol{\omega}_j^h - \tilde{\mathbf{v}}_j^h$ ($\tilde{\mathbf{v}}_j^h \in X_h$ is the L^2-projection of $\boldsymbol{\omega}_j$). Then subtract (4.37) and (4.38) to get

$$\alpha\delta^2 \left(\nabla \boldsymbol{\phi}_j^h, \nabla \mathbf{v}^h\right) + \left(\boldsymbol{\phi}_j^h, \mathbf{v}^h\right) = \alpha\delta^2 \left(\nabla \boldsymbol{\eta}_j, \nabla \mathbf{v}^h\right) + \left(\boldsymbol{\eta}_j, \mathbf{v}^h\right) + \alpha\delta^2 \left(\nabla \mathbf{e}_{j-1}, \nabla \mathbf{v}^h\right). \tag{4.99}$$

Take $\mathbf{v}^h = \boldsymbol{\phi}_j^h$ in (4.99) to get

$$\alpha\delta^2 ||\nabla \boldsymbol{\phi}_j^h||^2 + ||\boldsymbol{\phi}_j^h||^2 = \alpha\delta^2 \left(\nabla \boldsymbol{\eta}_j, \nabla \boldsymbol{\phi}_j^h\right) + \left(\boldsymbol{\eta}_j, \boldsymbol{\phi}_j^h\right) + \alpha\delta^2 \left(\nabla \mathbf{e}_{j-1}, \nabla \boldsymbol{\phi}_j^h\right). \tag{4.100}$$

Fix $\varepsilon > 0$. Apply Hölder's and Young's inequalities to (4.100) to get

$$\alpha\delta^2 ||\nabla \boldsymbol{\phi}_j^h||^2 + ||\boldsymbol{\phi}_j^h||^2 \leq \alpha\delta^2 ||\nabla \boldsymbol{\eta}_j||^2 + ||\boldsymbol{\eta}_j||^2 + \varepsilon\alpha\delta^2 ||\nabla \mathbf{e}_{j-1}||^2 + \frac{1}{\varepsilon}\alpha\delta^2 ||\nabla \boldsymbol{\phi}_j^h||^2. \tag{4.101}$$

Taking $\varepsilon = 1$ and $\varepsilon = 2$ in (4.101) gives

$$||\boldsymbol{\phi}_j^h||^2 \leq \alpha\delta^2 ||\nabla \boldsymbol{\eta}_j||^2 + ||\boldsymbol{\eta}_j||^2 + \alpha\delta^2 ||\nabla \mathbf{e}_{j-1}||^2. \tag{4.102}$$

$$\alpha\delta^2 ||\nabla \boldsymbol{\phi}_j^h||^2 + 2||\boldsymbol{\phi}_j^h||^2 \leq 2\alpha\delta^2 ||\nabla \boldsymbol{\eta}_j||^2 + 2||\boldsymbol{\eta}_j||^2 + 4\alpha\delta^2 ||\nabla \mathbf{e}_{j-1}||^2. \tag{4.103}$$

The triangle inequality and estimate (4.102) give

$$||\mathbf{e}_j||^2 \leq 2\,||\boldsymbol{\eta}_j||^2 + \alpha\delta^2 ||\nabla \boldsymbol{\eta}_j||^2 + \alpha\delta^2 ||\nabla \mathbf{e}_{j-1}||^2.$$

Backward induction and properties of the L^2 projection then result in

$$\begin{aligned} ||\mathbf{e}_j||^2 \leq\ & \alpha\delta^2 (2 + 3\sum_{i=0}^{j} 4^i) \max_{0 \leq n \leq j} \inf_{\mathbf{v}^h \in X_h} ||\nabla (D_{\alpha,n} A^{-1}\mathbf{w} - \mathbf{v}^h)||^2 \\ & + 2(1 + \sum_{i=0}^{j} 4^i) \max_{0 \leq n \leq j} \inf_{\mathbf{v}^h \in X_h} ||D_{\alpha,n} A^{-1}\mathbf{w} - \mathbf{v}^h||^2 \end{aligned} \tag{4.104}$$

and estimate (4.98) follows. □

Corollary 4.6.5 (Convergence estimate)**.** *Under the assumptions of Corollary 4.5.2, suppose further that, for some $J = 0, 1, \ldots$, that $G = A^{-1}$, $G^h = A_h^{-1}$, $D = D_{\alpha,J}$, $D^h = D_{\alpha,J}^h$. If $\Delta^{2J+2}\mathbf{u} \in L^2(\Omega)$, then*

$$\begin{aligned} & ||\mathbf{u}_M - \mathbf{w}_M^h||^2 + Re^{-1}\Delta t \sum_{n=0}^{M-1} ||\nabla(\mathbf{u}_{n+1/2} - \mathbf{w}_{n+1/2}^h)||^2 \\ & \qquad \leq C_* Re(4^J(h^2 + \alpha\delta^2)h^{2k} + h^{2k} + h^{2s+2} + \Delta t^4 + (\alpha\delta^2)^{2J+2}). \end{aligned} \tag{4.105}$$

Proof. Apply estimates for $c_{1,j}$, $c_{2,j}$ from (4.94), resulting from Propositions 4.6.3, 4.6.4. □

4.6.2 Numerical results

This section presents two numerical examples. The first is the calculation of a flow with an exact solution to verify the convergence rates of the algorithm. The second examines the flow of a fluid over a step with recirculation. FreeFEM++ [72] was used to run the simulations.

Example 4.6.6 (Taylor-Green vortex)**.**

The convergence rates are tested against the Taylor-Green vortex problem [17,48,67,100]. We use a domain of $\Omega = [0,1] \times [0,1]$ and take $\mathbf{u} = (u_1, u_2)$ where

$$\begin{aligned} u_1(x,y,t) &= -\cos(n\pi x)\sin(n\pi y)e^{-2n^2\pi^2 t/\tau} \\ u_2(x,y,t) &= \sin(n\pi x)\cos(n\pi y)e^{-2n^2\pi^2 t/\tau} \\ p(x,y,t) &= -\frac{1}{4}(\cos(n\pi x) + \cos(n\pi y))e^{-2n^2\pi^2 t/\tau}. \end{aligned}$$

The pair $(\mathbf{u}, p)$ is a solution the two-dimensional NSE when $\tau = Re$ and $\mathbf{f} = 0$.

We used Crank-Nicolson discretization in time and P2-P1 elements in space according to Problem 4.3.1. That is, we used continuous piecewise quadratic elements for the velocity and continuous piecewise linear elements for the pressure. We chose the spatial discretization elements and parameters $n = 1$, $T = 0.5$, $\chi = 0.1$ and $Re = 10,000$ to correspond to a previous experiment in [67]. We chose $h = \frac{1}{m}$, $dt = \frac{1}{4}h$, $\delta = \sqrt[4]{h}$ and $\alpha = \sqrt{h}$ where m is the number of mesh divisions per side of $[0,1]$. These were chosen so that 4.6.5 reduces to

$$||\mathbf{u}_M - \mathbf{w}_M^h|| + \left[Re^{-1}\Delta t \sum_{n=0}^{M-1} ||\nabla(\mathbf{u}_{n+1/2} - \mathbf{w}_{n+1/2}^h)||^2 \right]^{1/2} \leq C(h^2 + h^{J+1}). \tag{4.106}$$

We summarize the results in Tables 6 and 7. Table 6 shows that not iterating the deconvolution, corresponding to choosing $J = 0$ in Definition 4.2.13. This choice of α and δ gives to convergence rates of $\|u - w^h\|_{\infty,0}$ and $\|\nabla(u - w^h)\|_{2,0}$ to be $\mathcal{O}(h)$ as predicted. Table 7 shows that iterating the deconvolution once, corresponding to choosing $J = 1$ in Definition 4.2.13. This choice of α and δ gives convergence rates of $\|u - w^h\|_{\infty,0}$ and $\|\nabla(u - w^h)\|_{2,0}$ to be $\mathcal{O}(h^2)$ as predicted.

Example 4.6.7 (Flow over a step)**.**

Table 6: Error and convergence rates for Leray-deconvolution with $J = 0$ for the Taylor-Green vortex with Re = 10,000, $\alpha = \sqrt{h}$, and $\delta = \sqrt[4]{h}$. Note the convergence rate is approaching 1 as predicted by (4.106).

m (=1/h)	$\|u - w^h\|_{\infty,0}$	Rate	$\|\nabla(u - w^h)\|_{2,0}$	Rate
20	0.038975		1.651230	
40	0.024334	0.680	1.468510	0.169
60	0.017751	0.778	1.159840	0.582
80	0.013854	0.862	0.935247	0.748
100	0.011255	0.931	0.774285	0.846

Table 7: Error and convergence rates for Leray-deconvolution with $J = 1$ for the Taylor-Green vortex with Re = 10,000, $\alpha = \sqrt{h}$, and $\delta = \sqrt[4]{h}$. Note the convergence rate is approaching 2 as predicted by (4.106).

m (=1/h)	$\|u - w^h\|_{\infty,0}$	Rate	$\|\nabla(u - w^h)\|_{2,0}$	Rate
20	0.023384		1.070400	
40	0.009739	1.264	0.640360	0.741
60	0.004997	1.646	0.357779	1.436
80	0.002899	1.892	0.212560	1.810
100	0.001915	1.858	0.136724	1.977

Our second example examines the shedding of eddies over a step [49, 67]. We use a parabolic inflow and outflow condition of $u_2 = y(10-y)/25$ on the left (inflow) and right (outflow) sides of a channel with dimensions 10×60. We also set the velocity $\mathbf{u} = 0$ along the top, bottom, and around the step. We discretized this with P2-P1 elements in space and Crank-Nicolson in time. The parameters chosen for this experiment are the same as [67], $Re = 750$, $\delta = 1.5$, $dt = 0.0025$, $\alpha = 0.01$ and $\chi = 0.01$. The mesh satisfied the properties of $h_{min} = 0.110753$, $h_{max} = 1.50497$, and had a total of 17688 degrees of freedom.

We calculated the velocity using Problem 4.3.1 with the deconvolution step using $J = 0$ and $J = 1$ steps in Definition 4.2.13. Recirculation regions form past the step, and for a critical Reynolds number, the eddies detach from the step and move downstream [67]. We expect to see the eddies detach more frequently for the $J = 1$ deconvolution compared to $J = 0$ because the regularization term stabilizes the flow, but the $J = 1$ iteration step regains accuracy. Figures 11, 12, and 13 for time levels of $T = 10$, $T = 20$, and $T = 30$ respectively show that eddies form and separate more frequently for the $J = 1$ case.

4.7 CONCLUSION

It is infeasible to resolve all persistent and energetically significant scales down to the Kolmogorov microscale of $\mathcal{O}(Re^{-3/4})$ for turbulent flows in complex domains using direct numerical simulations in a given time constraint. Regularization methods are used to find approximations to the solution. The modification of iterated Tikhonov-Lavrentiev to the modified iterated Tikhonov-Lavrentiev deconvolution in Definition 4.2.13 is a highly accurate method of solving the deconvolution problem in the Leray-deconvolution model, with errors $\mathbf{u} - D_{\alpha,0}\overline{\mathbf{u}} = \mathcal{O}((\alpha\delta^2)^{J+1})$ when applied to the differential filter. We use this result to show that under a regularity assumption, the error between the solutions to the NSE and to the Leray deconvolution model with time relaxation using the modified iterated Tikhonov-Lavrentiev deconvolution and discretized with Crank-Nicolson in time and finite elements in space are $\mathcal{O}(h^k(h + \sqrt{\alpha\delta^2}) + h^{s+1} + \Delta t^2 + (\alpha\delta^2)^{J+1})$.

We also examined two numerical examples using Problem 4.3.1 with the deconvolution in

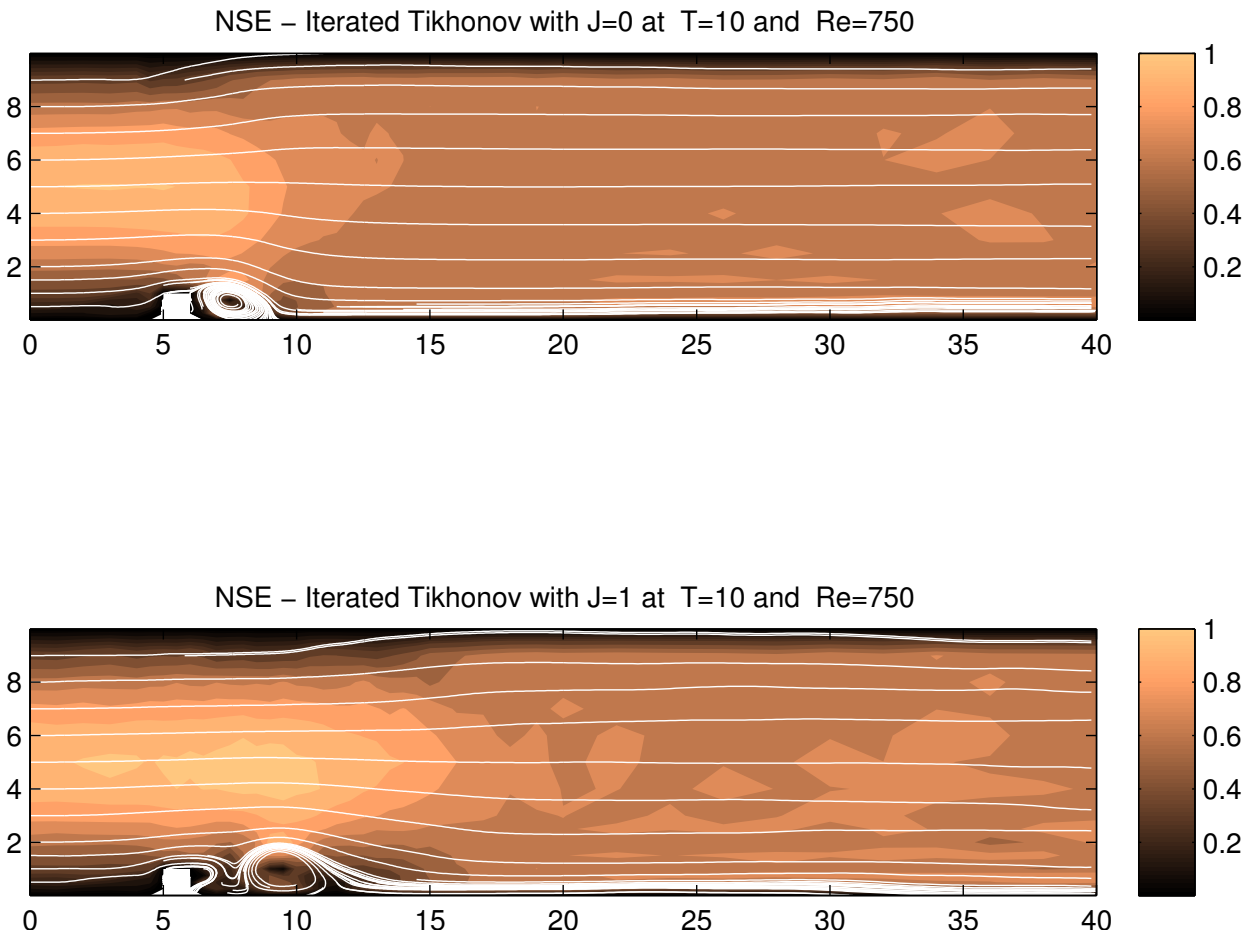

Figure 11: Leray-Tikhonov ($J = 0$) and Leray-iterated Tikhonov ($J = 1$) deconvolution models for flow over a step. Note the slower eddy formation and separation in the $J = 0$ case when compared to the $J = 1$ case.

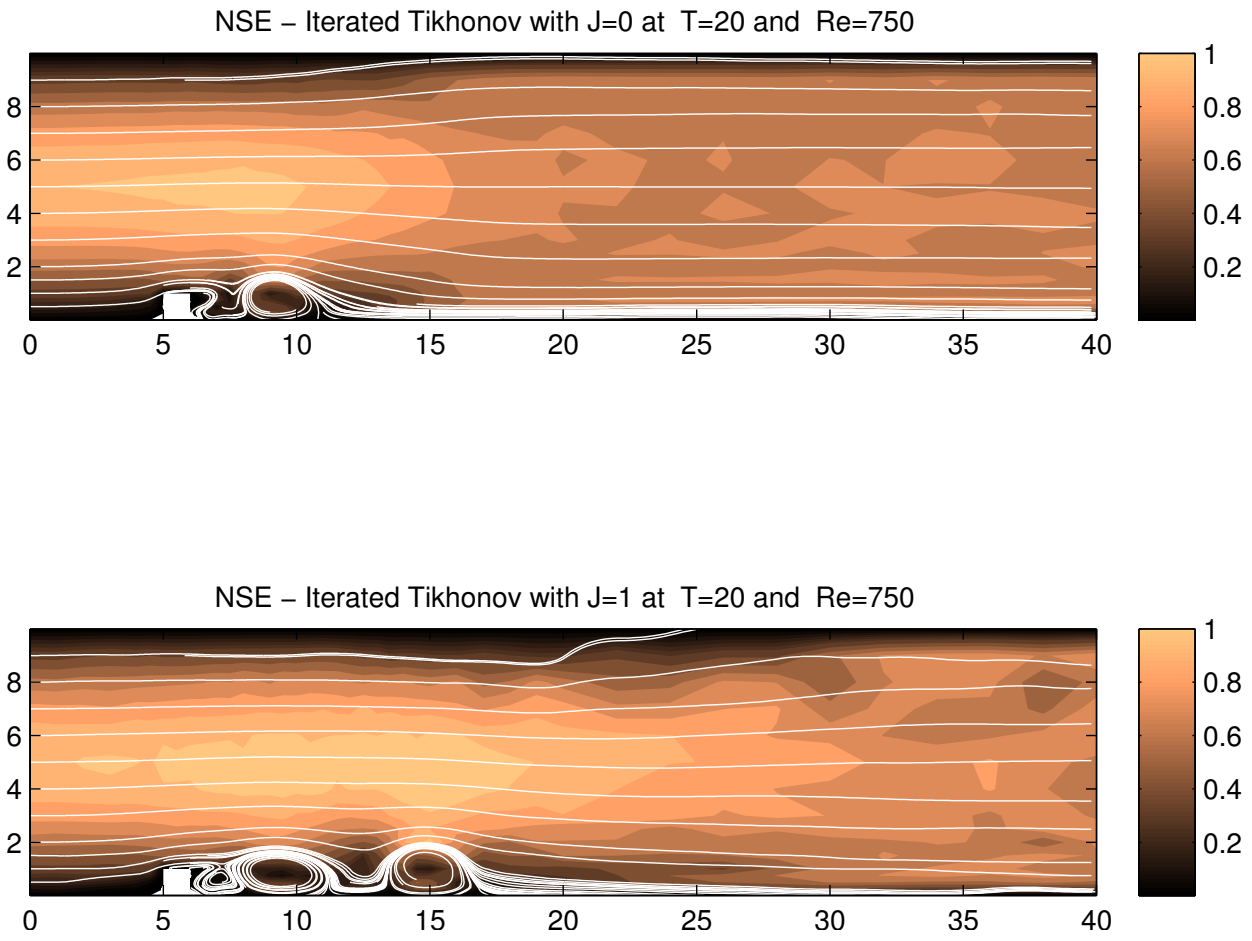

Figure 12: Leray-Tikhonov ($J = 0$) and Leray-iterated Tikhonov ($J = 1$) deconvolution models for flow over a step. Note the slower eddy formation and separation in the $J = 0$ case when compared to the $J = 1$ case.

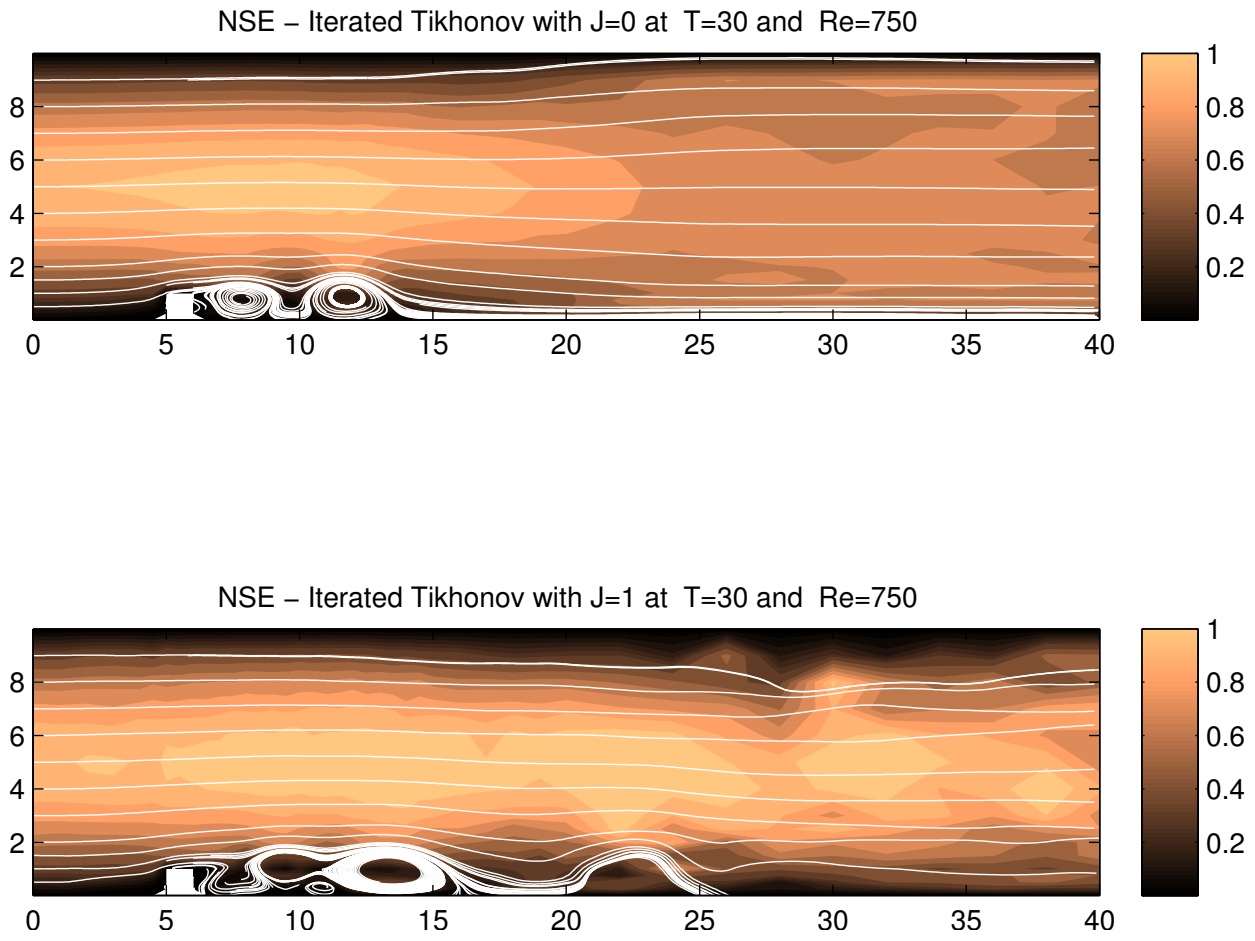

Figure 13: Leray-Tikhonov ($J = 0$) and Leray-iterated Tikhonov ($J = 1$) deconvolution models for flow over a step. Note the slower eddy formation and separation in the $J = 0$ case when compared to the $J = 1$ case.

Definition 4.2.13. The first one was the Taylor-Green vortex problem. We use this problem because it has an exact analytic solution to the NSE. The regularization parameters α and δ were chosen so that the convergence of the approximate solution to the error would be $\mathcal{O}(h^{J+1})$ for $J = 0$ and $J = 1$. The convergence rates calculated corresponded to those predicted rates, that is $\mathcal{O}(h^1)$ for $J = 0$ and $\mathcal{O}(h^2)$ for $J = 1$.

The second experiment demonstrated the use of the Leray deconvolution method with the modified iterated Tikhonov-Lavrentiev deconvolution for $J = 0$ and $J = 1$ to examine the qualitative features of a fluid flow. The parameters were chosen so that the flow would not be steady and would create eddies [67]. We saw shedding of eddies past a step for both the $J = 0$ and $J = 1$ cases, however the case of $J = 1$ appeared to have less numerical diffusion as evidenced by forming and shedding eddies more rapidly.

5.0 APPLICATION OF TIKHONOV REGULARIZATION TO BRAIN MAPPING

"We must make it our goal to find a method of solution of all problems... by means of a single simple method." (D'Alembert)

Slowing gait and difficulty walking are major and common problems of older adults; they worsen with age, and they are associated with greater risk of disability, hospitalization and death [55, 71, 81]. Efforts to understand the mechanisms underlying maintenance of mobility in late life can have tremendous implications for cost savings and prevention of disability. With 4 million people age 85 and older in the United States [52], the sheer number of old adults experiencing disability and requiring care results in great personal, societal and public health financial expenses [50, 68]. Slower gait is known to be associated with smaller volume of the brain both cross sectionally [9, 35, 76, 77, 79, 80, 96, 110] and longitudinally [5, 6, 9, 96, 101, 111]. Most neuroimaging studies of gait slowing in older age have examined measures of overall brain atrophy, and few studies have quantified the spatial distribution of gray matter atrophy in relationship with gait. Recent works indicate that slower gait is associated with less gray matter in the prefrontal cortex and posterior parietal lobule, as well as in the putamen and cerebellum [76, 77]. However, these initial findings have not been replicated in other large cohorts of community dwelling older adults and have mostly relied on least square regression models approaches.

The least square regression model does not entirely address the challenges of neuroimaging analysis. Firstly, there is noise (experimental noise or observational error) of unknown levels in both gait and neuroimaging data. In the presence of noise/observational errors in the measurements the modeling problem could have no solution. Secondly, there is a

high level of correlation between the brain regions measurements, thus the problem that must be solved to produce the association sought between the neuroimaging data and the gait data is ill-conditioned. This approximate co-linearity causes amplification of the noise to produce significant errors in the solution [23]. Specifically, small perturbations or small observational errors in the data of the walking speed data can lead to large changes in our regression coefficients. The results of least squares regression are sensitive to scaling, selection, and normalization of variables for statistical interpretations. Thirdly, there are a large number of potential predictors of slowing gait, including numerous brain regions and numerous health-related measures. Even when applying a selected number of regions based on á priori hypotheses, the number of variables would includes more than 30 regions of interest for each hemisphere, which yields a total of over 60 comparisons. Analysis of neuroimaging correlates of behavioral characteristics typically involve a very high number of comparisons and require conservative methods to correct for false positive results, for example Bonferroni or Sidak [91, 92]. However, the application of these conservative methods might also lead to a high number of false negative results. Lastly, these problems will increase in scale, as inevitably, a more precisely localized correlation of neuroimaging data with behavior is sought.

This paper gives an algorithm that addresses the four limitations of noise, high correlation, large number of predictors and scalability. The algorithm is adapted from a combination of iterated Tikhonov regularization with the L-curve method for optimal choice of the regularization parameters.

Definition 5.0.1 (Model problem)**.** *Assume that there is a linear relationship between the brain measurements (e.g. brain volume, cellular integrity, connectivity and blood flow) and the gait measurements (e.g. step width, step length, double support time, stance time and step time).*

For m participants, we define the i^{th} row of $A \in R^{m\times n}$ to be the brain measurements for a person i, the i^{th} row of $b \in R^{m\times k}$ to be the gait measurements of person i, and let $x \in R^{n\times k}$ be the correlation coefficients between the brain measurements and the gait measurements. The modeling problem is to determine the correlation coefficients x between the

brain measurements and gait measurements such that

$$Ax = b. \tag{5.1}$$

If there is noise (e.g. inevitable errors in data collection) in the right hand side data b, and the noise is not in the Range(A), then the modeling problem as stated in Definition 5.0.1 would have no solution. In that case, we seek an approximate solution. Even if a solution does exist, if A is severely ill-conditioned, then we show in Section 5.2 that a small amount of noise (10%) added to the right hand side data b leads to a large error (9,324,000%) in the least squares calculated solution.

To calculate an approximate solution, we first develop the Brain-Gait Correlator, a self-adaptive "black box" correlation algorithm for simultaneous correlations between all regions of interest (ROIs) and time to walk (Section 5.1). In Section 5.2, we validate the correlation algorithm with two problems. The first is a problem with real brain volume measurements and a synthetic walking speed (created from a hypothesized correlation), and the second is a synthetic problem to determine how the algorithm handles noisy measurement. Lastly, in Section 5.3, we apply the Brain-Gait Correlator to real brain volume measurement and real walking speeds using data obtained from two different cohorts of older adults.

Data were obtained from participants of two ongoing population-based, longitudinal studies, the Cardiovascular Health Study (CHS) and the Health Aging Body Composition Study (Healthy Brain Project). The CHS is a study of coronary heart disease and stroke risk in older adults. Details about the study design of the original cohort are published elsewhere [24]. Briefly, 5888 community-dwelling older adults were identified between 1987 and 1993 from Medicare eligibility lists in four clinical centers (Forsyth County, NC, Sacramento County, CA, Washington County, MD and Pittsburgh, PA) and were recruited if they were age 65 or older at time of recruitment, non-institutionalized, not wheelchair bound or undergoing active cancer treatment, able to give informed consent, and expected to remain in the area for 3 years. These 5888 participants have had annual clinic examinations through 1998-99, including information for all hospitalizations, a review of medical records, and selected laboratory and clinical evaluations. Brain MRIs were acquired in 523 participants in Pittsburgh in 1997-99 [65]. Compared to the parent population who had a brain MRI,

these participants were younger, more likely to have more years of education, and with lower prevalence of cardiovascular diseases and cerebrovascular findings [77, 79]. In 2003-04, a random sample of 327 brain MRIs from the 523 participants were re-read [76–78, 80]. No significant difference was observed between the 327 and the 196 participants with regard to demographics or health related factors.

The Healthy Brain Project began in 1997-1998 as a longitudinal, observational cohort study of 3,075 well-functioning older white and black men and women, from Pittsburgh, PA and Memphis, TN [93]. Participants were enrolled if they were 70-79 years old and reported no difficulty walking a quarter of a mile (400 m), climbing 10 steps, or performing activities of daily living; were free of life-threatening cancers with no active treatment within the prior 3 years; and had planned to remain within the study area for at least 3 years. In 2006-2007, 314 Healthy Brain Project participants from the Pittsburgh site who were interested and eligible for a brain 3T MRI and who were able to walk 20 meters, received a brain MRI in addition to the personal Healthy Brain Project assessments. Both studies have been approved by the institutional review boards of the University of Pittsburgh.

The participants of this study were all able to walk. Gait speed was assessed by measuring the time to walk at usual pace on a 15-foot course (for the CHS) and on a 20 meter course (for the Healthy Brain Project) at usual pace after starting from a standstill position [99].

Brain MRI assessments included volumetric measures of gray matter of individual regions and of total brain for both the CHS and the Healthy Brain Project MRIs. The brain MRI protocol for the CHS carried out in 1997-99 has been described elsewhere [114]. Briefly, sagittal T1-weighted localizer sequences and axial spin-echo spin-density-weighted, spin-echo T2-weighted and T1-weighted images were acquired. All MRI data were interpreted at a central MRI Reading Center using a standardized protocol [15,114]. The brain MRI protocol for the Healthy Brain Project was performed on a 3T Siemens Tim Trio MR scanner and a Siemens 12-channel head coil at the MR Research Center of the University of Pittsburgh. Magnetization-prepared rapid gradient echo (MPRAGE) T1-weighted images were acquired in the axial plane: TR=2300 ms; TE=3.43 ms; TI=900 ms; Flip angle= 9 deg; Slice Thickness= 1mm; FOV= 256×224 mm; voxel size= 1mm×1mm; matrix size= 256×224; and number of slices=176. A radiologist checked the MR images used in this study and excluded

any unexpected findings from the study.

Voxel counts of the gray matter were obtained for individual regions of interest and for the whole brain using a procedure previously described [78, 105, 113, 115]. After skull and scalp stripping [94], and after segmentation of gray matter, white matter and cerebrospinal fluid, the brain atlas and the individual subject brain are aligned and intensity normalization is done on each subjects structural image (SPGR for the CHS and MPRAGE for the Healthy Brain Project images) as well as on the template colin27, to give each subject the same orientation and image intensity distribution as the template and to improve the registration accuracy. For the 3Tesla images, the segmentation was done using the FAST - FMRIB's Automated Segmentation Tool [115]. The registration procedure uses a fully deformable automatic algorithm [102] which does not warp or stretch the individual brain and thus minimizes measurement inaccuracies [113]. Volumes were converted from number of voxels to cubic centimeters.

The regions of interest are gray matter volumes obtained for each hemisphere for the regions that are known to be associated with mobility control. The regions of interest were previously drawn on the MNI colin27 template brain according to the AAL neuroanatomical atlas [105, 112]. We examined a total of 32 ROIs (Figure 14). In addition to motor regions (primary motor cortex, sensorimotor cortex, supplementary motor cortex, basal ganglia and cerebellum), we also measured gray matter volume of associative cortices important for visuospatial attention and to relate perception of self with surrounding environment and with intended actions (superior parietal lobe and the inferior parietal lobule of the posterior parietal cortex), as well as regions important for working-memory/executive control function (dorsolateral prefrontal cortex), memory-related regions (hippocampus) and motor imagery-related regions (precuneus, parahippocampal gyrus, posterior cingulate cortex) [47]. The primary motor cortex included the precentral gyrus, and it was limited rostrally by the precentral sulcus and caudally by the Rolandic sulcus [105]. The dorsolateral prefrontal cortex (dLPFC) included the middle frontal gyrus. The posterior cingulate cortex was limited by the corpus callosum rostrally and the subparietal sulcus caudally. The basal ganglia included pallidum, putamen, caudate and thalamus. The hippocampus was defined on the sagittal views as the gray matter around the ventricles horns limited caudally by the

parahippocampal ramus.

Participants from the CHS study were 78.3 ± 4.1 years old, 57% women, 72% white and their gait speed was 0.9 ± 0.2 m/sec. Participants from the Healthy Brain Project study were 81.9 ± 2.7 years old, 55% women, 61% white and their gait speed was 1.0 ± 0.3 m/sec.

The paper is presented in the following fashion. Section 5.1 develops the self-adaptive "black box" Brain-Gait Correlator for simultaneous and correlation of all ROIs with complete gait data. Section 5.2 validates the Brain-Gait Correlator with two problems. The first problem has real brain volume measurements and a synthetic walking speed (created from a hypothesized correlation). The second is a purely synthetic problem to determine how the algorithm handles noisy measurements. Section 5.3 applies the Brain-Gait Correlator to real brain volume measurements and real walking speeds.

5.1 THE BRAIN-GAIT CORRELATOR ALGORITHM

This section gives a detailed presentation of a reliable algorithm to produce precise brain-gait correlations even in cases when least squares regression fails. The algorithm is built using five component sub-algorithms (described in Algorithm 5.1.1 below). Important aspects are the introduction of an iterated Tikhonov regularization parameter α to control for approximate co-linearity and a number of iteration steps J to stop convergence to a noisy solution. The regularization parameter is selected self-adaptively by the L-curve method to balance optimally the needs of high precision and control of noise amplification. The number of iteration steps is selected by our stopping criterion (Algorithm 5.1.9). Algorithm 5.1.1 reverts to ordinary least squares when regularization parameter $\alpha = 0$.

Algorithm 5.1.1 (Brain-Gait Correlator)**.** *The Brain-Gait Correlator is a collection of Algorithms 5.1.3, 5.1.4, 5.1.5, 5.1.9 and 5.1.10 to calculate the approximate solution, confidence intervals and p-values for the modeling problem* (5.1).

1. *Apply Algorithm 5.1.3 to statistically normalize the measured data.*
2. *Apply Algorithm 5.1.5 to choose a regularization parameter α by the L-curve method.*

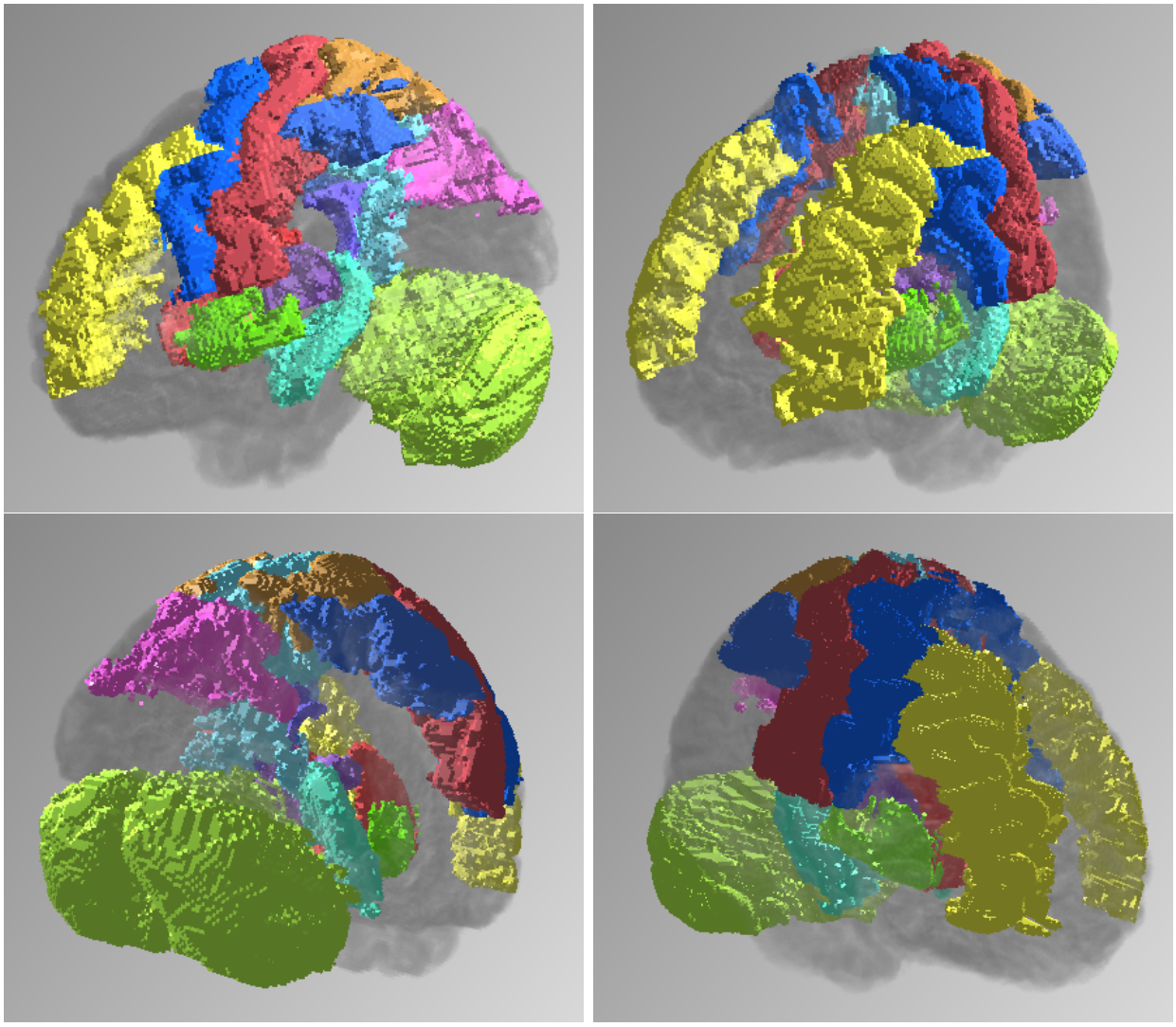

Figure 14: Multiple orientations of the brain displaying the colored ROIs that are studied in Problem 5.2.1 and Section 5.3

3. *Apply Algorithm 5.1.4 to calculate the approximate solution for (5.1) via iterated Tikhonov regularization.*
4. *If an estimate of the noise is known, apply Algorithm 5.1.9 to choose a stopping condition, otherwise take J in Algorithm 5.1.4 to be small.*
5. *Apply Algorithm 5.1.10 to approximate confidence intervals for our solution and p-values using a bootstrap by adding variations of noise to the data b and recalculating the solution using steps 1 - 4.*

Definition 5.1.2. *The statistical normalization of a vector $\vec{v}$ is defined to be the vector*

$$normalization(\vec{v}) = \frac{\vec{v} - average(\vec{v})}{stdev(\vec{v})}, \tag{5.2}$$

where $average(\vec{v})$ for a vector with n components is $\frac{1}{n-1}\sum_{i=1}^{n} v_i$ and

$$stdev(\vec{v}) = \sqrt{\frac{1}{n}\sum_{i=1}^{n}(\vec{v}_i - average(\vec{v}))^2}.$$

Statistical normalization is standard practice, see [8, 43, 44, 69]. Boolean data, such as male/female or black/white, should not be normalized.

Algorithm 5.1.3 (Statistical Normalization)**.** *Denote the i^{th} column of a matrix A by $A_{\cdot,i}$. For a set of columns C of matrix A, the statistical normalization $\tilde{A}$ is the matrix calculated by*

$$\tilde{A}_{\cdot,i} = \begin{cases} normalization(A_{\cdot,i}) & : i \in C \\ A_{\cdot,i} & : i \notin C \end{cases} \tag{5.3}$$

The foundation of the Brain-Gait Correlator for calculating the regression coefficients is iterated Tikhonov regularization.

Algorithm 5.1.4 (Iterated Tikhonov regularization)**.** *Choose regularization parameter $\alpha \geq 0$ and $J \geq 1$. For $j = 0, ..., J$, calculate the iterated Tikhonov approximations to problem (5.1) by solving for x_j which satisfies*

$$(A^*A + \alpha I)x_0 = A^*b, \qquad (A^*A + \alpha I)(x_j - x_{j-1}) = A^*(b - Ax_{j-1}) \tag{5.4}$$

Define $x_J = x_J(\alpha)$ to be the J^{th} iterated Tikhonov approximation of problem (5.1).

This introduces two parameters that need to be chosen for calculations, the regularization parameter α and the stopping parameter J. The first is calculated using the L-curve method developed by Hansen [40] for discrete ill-posed problems and further studied by Hansen and O'Leary [42]. When the magnitude of the noise is known, the stopping parameter is chosen by the Stopping Criterion in Algorithm 5.1.9. When the magnitude of the noise is not known, we chose J to be 1.

Previous work [76] has studied using least squares regression to calculate regression coefficients. Applying the L-curve method in Algorithm 5.1.1 Step 2, allows for the case when $\alpha = 0$ if that solution is the best balance of stability and accuracy. However, if another parameter will give a better balance, then the L-curve method will choose that parameter.

Algorithm 5.1.5 (The L-curve Method)**.** *For a fixed J in iterated Tikhonov regularization, select a set of regularization parameters $\{\alpha_i\}$ and plot the parametric graph of the norm of the solution $\|x_J(\alpha)\|$ versus the norm of the residual $\|Ax_J(\alpha) - b\|$.*

1. *For each regularization parameter α_i, calculate the Tikhonov approximation $x_J(\alpha_i)$ using (5.4).*
2. *Plot the parametric graph of $\|x_J(\alpha)\|$ versus $\|Ax_J(\alpha) - b\|$ on a log-log scale.*
3. *Find the corner of this graph, i.e. the point of maximum curvature.*
4. *The α that is the maximizer of the curvature is taken to be the regularization parameter.*

We use following definition for curvature from [23].

Definition 5.1.6. *The curvature of the L-curve graph at a point α is defined to be*

$$\kappa(\alpha) = \frac{\xi''(\alpha)\eta'(\alpha) - \xi'(\alpha)\eta''(\alpha)}{(\xi'(\alpha)^2 + \eta'(\alpha)^2)^{3/2}}, \tag{5.5}$$

where $\xi(\alpha) = \log(\|b - Ax_J(\alpha)\|)$ and $\eta(\alpha) = \log(\|x_J(\alpha)\|)$.

We calculate the curvature for 60 different values of α across 12 orders of magnitude and select the α that gives the largest curvature. Next, we develop a stopping criteria for iterated Tikhonov regularization. Start by decomposing the gait data as $b = y + \varepsilon$ where y is the true gait measurement and ε is the noise/observational error of the problem. Then the model problem (5.1) is decomposed as

$$Ax = y + \varepsilon. \tag{5.6}$$

Least squares regression for (5.6) is equivalent to the minimization problem

$$x_{LS} = \text{minimizer}_{v\in\mathbb{R}^n}\ E_\varepsilon(v)\ \text{, where } E_\varepsilon(v) := \frac{1}{2}(A^*Av, v) - (A^*(y+\varepsilon), v).$$

We are using $(\cdot,\cdot)$ to denote the usual Euclidean inner product and $||\cdot||$ to denote the Euclidean norm. Given x_j, the $j+1th$ iterated Tikhonov is the unique minimizer of

$$x_{j+1} = \text{minimizer}_{v\in X}\ E_\varepsilon(v) + \frac{\alpha}{2}||v - x_j||^2.$$

The next theorem is a novel contribution that elucidates when the iterated Tikhonov approximations $x_0, x_1, \cdots$ form a minimizing sequence for the functional $E_0(\cdot) := E_\varepsilon(\cdot)|_{\varepsilon\equiv 0}$ associated with the (unknown) noise free data.

Theorem 5.1.7. *Let $\alpha > 0$. Then the iterated Tikhonov approximations form a minimizing sequence for E_ε. In particular,*

$$E_\varepsilon(x_j) - E_\varepsilon(x_{j+1}) = \frac{1}{2}((A^*A + 2\alpha I)(x_{j+1} - x_j), x_{j+1} - x_j) \geq 0. \tag{5.7}$$

Thus

$$E_\varepsilon(x_{j+1}) < E_\varepsilon(x_j),\ \textit{unless } x_{j+1} = x_j.$$

Moreover, as $j \to \infty$ for fixed α, $||A^*b - A^*Ax_j|| \to 0$.

Proof. We have

$$\begin{aligned}
E_\varepsilon(x_j) - E_\varepsilon(x_{j+1}) &= \frac{1}{2}\left(A^*Ax_j, x_j\right) - \frac{1}{2}\left(A^*Ax_{j+1}, x_{j+1}\right) \\
&\quad - \left(A^*(y+\varepsilon), x_j - x_{j+1}\right) \\
&= \frac{1}{2}\left(A^*Ax_j, x_j\right) - \frac{1}{2}\left(A^*Ax_{j+1}, x_{j+1}\right) - \left(A^*Ax_j, x_j - x_{j+1}\right) \\
&\quad - \left((A^*A + \alpha I)(x_{j+1} - x_j), x_j - x_{j+1}\right) \\
&= -\frac{1}{2}\left(A^*Ax_j, x_j\right) + \frac{1}{2}\left(A^*Ax_j, x_{j+1}\right) \\
&\quad + \frac{1}{2}\left(A^*Ax_j, x_{j+1}\right) - \frac{1}{2}\left(A^*Ax_{j+1}, x_{j+1}\right) \\
&\quad - \left((A^*A + \alpha I)(x_{j+1} - x_j), x_j - x_{j+1}\right) \\
&= \frac{1}{2}\left(A^*Ax_j, x_{j+1} - x_j\right) + \frac{1}{2}\left(A^*Ax_{j+1}, x_j - x_{j+1}\right) \\
&\quad - \left((A^*A + \alpha I)(x_{j+1} - x_j), x_j - x_{j+1}\right) \\
&= \frac{1}{2}\left(A^*A(x_j - x_{j+1}), x_{j+1} - x_j\right) \\
&\quad - \left((A^*A + \alpha I)(x_{j+1} - x_j), x_j - x_{j+1}\right) \\
&= \frac{1}{2}\left((A^*A + 2\alpha I)(x_{j+1} - x_j), x_{j+1} - x_j\right)
\end{aligned}$$

Since the right hand side of (5.7) is positive unless $x_{j+1} = x_j$, it immediately follows that $E_\varepsilon(x_{j+1}) < E_\varepsilon(x_j)$, unless $x_{j+1} = x_j$ as claimed.

To show that $||A^*b - A^*Ax_j|| \to 0$, note that $E_\varepsilon(\cdot)$ is bounded since $A^*A \geq 0$. Hence, the monotonically decreasing numbers $E_\varepsilon(x_j)$ are convergent. The RHS of equation (5.7) then implies that $||x_{j+1} - x_j|| \to 0$ as $j \to \infty$. From the form of the updates, $x_{j+1} = x_j$ only if $A^*Ax_j = A^*y$, see (5.4). Finally, the RHS of the iterated Tikhonov algorithm (5.4) implies that the residual $||A^*b - A^*Ax_j|| \to 0$. □

Since the problem we seek to solve is the noise-free one

$$A^*Ax_{true} = A^*y,$$

and this is equivalent to finding the minimizer of the noise free functional $E_0(v)$, Theorem 5.1.8 shows under what conditions the updates reduce the noise-free functional

$$E_0(v) := \frac{1}{2}(A^*Av, v) - (A^*y, v).$$

Theorem 5.1.8. *Let $\alpha > 0$ and $||\varepsilon|| \leq \varepsilon_0$. Then the iterated Tikhonov approximations satisfy*

$$E_0(x_j) - E_0(x_{j+1}) = -(\varepsilon, x_{j+1} - x_j) + \frac{1}{2}((A^*A + 2\alpha I)(x_{j+1} - x_j), x_{j+1} - x_j). \tag{5.8}$$

They are a descent sequence for the noise-free functional $E_0(\cdot)$ as long as

$$\alpha \geq \frac{\varepsilon_0}{||x_{j+1} - x_j||}. \tag{5.9}$$

Moreover, the termination criterion to stop when (5.9) is violated is equivalent to the discrepancy principle [23] of stopping when

$$||A^*Ax_{j+1} - A^*b|| \geq \varepsilon_0. \tag{5.10}$$

Proof. Equation (5.8) follows from noting that $E_\epsilon(v) = E_0(v) - (A^*\epsilon, v)$ and substituting this into (5.7). Then the Cauchy-Schwartz inequality implies that

$$|(\epsilon, x_{j+1} - x_j)| \leq \|\epsilon\|\|x_{j+1} - x_j\|.$$

If (5.9) holds, then

$$\begin{aligned} 0 &\leq \|\epsilon\|\|x_{j+1} - x_j\| - |(\epsilon, x_{j+1} - x_j)| \\ &\leq \alpha\|x_{j+1} - x_j\|^2 - |(\epsilon, x_{j+1} - x_j)| \\ &\leq \frac{1}{2}((A^*A + 2\alpha I)(x_{j+1} - x_j), x_{j+1} - x_j) - (\epsilon, x_{j+1} - x_j) \end{aligned}$$

The last line of this inequality follows from

$$(A^*A(x_{j+1} - x_j), x_{j+1} - x_j) \geq 0 \text{ and } (\epsilon, x_{j+1} - x_j) \leq |(\epsilon, x_{j+1} - x_j)|.$$

The equivalence to the discrepancy principle comes from subtracting (5.4) for x_j from (5.4) for x_{j+1} to obtain

$$(A^*A + \alpha I)((x_{j+1} - x_j) - (x_j - x_{j-1})) = -A^*A(x_j - x_{j-1}).$$

Simplifying this yields

$$A^*(b - Ax_j) = \alpha(x_j - x_{j-1}).$$

Taking the norm of the equation gives the result.

□

Theorem 5.1.8 shows that in the early steps, where larger updates are expected, x_j moves closer to the noise-free solution as j increases. As the updates become smaller, x_j converges to the noisy solution by Theorem 5.1.7. If the inequality in (5.9) is violated for some j, then Theorem 5.1.8 suggests either stopping the updates at that point or increasing α to permit further updating to potentially obtain a better approximation to the noise-free problem. This gives Algorithm 5.1.9, a new stopping condition for iterated Tikhonov regularization.

Algorithm 5.1.9 (Stopping Criterion)**.** *Given data* $b + \varepsilon$*, Suppose* $\varepsilon_0 \geq ||\varepsilon||$*. Select* α*.*

Solve for x_0*:* $(A^*A + \alpha I)\, x_0 = A^*b$*.*

For $j = 1, 2, \cdots$ *and while* $\alpha \geq \frac{\varepsilon_0}{||x_j - x_{j-1}||}$ *solve for* x_j *:* $(A^*A + \alpha I)[x_j - x_{j-1}] = A^*b - A^*A\, x_{j-1}$.

If $\alpha < \frac{\varepsilon_0}{||x_j - x_{j-1}||}$ *then compute as above* $x_j - x_{j-1}$ *and solve for* x_j*.*

Next, we estimate p-values to quantify the certainty of our solution. P-values are the probability (due to distributional noise as well as correlations in A and b) of obtaining data-derived coefficients x_J that exceed the calculated original dataset x_J coefficients under the assumption that the true (no noise) coefficients x_J are 0. In this probability framework, the original (A, b) is considered as one realization from an underlying joint distribution of possible (A, b). P-vales less than 0.05 are interpreted as unusual or sufficiently improbable enough (assuming that x_J is 0) that the data are actually providing evidence that the true x_J is not 0. In this case, the result is declared statistically significant. With Gaussian noise, p-values can be computed exactly using the closed-form of the multivariate normal distribution together with the closed-form sampling distributions of the variances and correlations of the columns of A and b [85,87]. In the general case, the bootstrap method, presented in Algorithm 5.1.10, can be used to obtain approximate p-values without having to make specific distributional assumptions [20, 108].

Algorithm 5.1.10 (Bootstrap)**.** *For a given number of ROI* n*, fix* $T > n$*, the number of bootstrap calculations, and* $\alpha > 0$*, the regularization parameter.*

- *Using iterated Tikhonov regularization (5.4), calculate the solution* x_J *and the residual* $e = b - Ax_J$*.*
- *Scale* e *by a factor of* $\sqrt{\frac{T}{T-n}}$*.*

- *For* $t = 1, 2, \ldots, T$
  - *Create an artificial noise term by choosing terms randomly with replacement from the scaled* e *and call this* $\tilde{e}_t$.
  - *Calculate pseudo-data* $\tilde{b}_t$ *by taking* $\tilde{b}_t = Ax_J + \tilde{e}_t$.
  - *Calculate the Tikhonov approximation* x_J^t *via (5.4) using pseudo-data* $\tilde{b}_t$.
  - *Save each* x_J^t.

We obtain statistical information from the statistical properties of the x_J^t.

Definition 5.1.11 (Confidence interval and p-value)**.** *Denote* $x_J(i)$ *to be the* i*th term in* x_J*. Similarly* $x_J^t(i) = x^t(i)$ *will denote the* i*th term of* x_J^t*. For every* i*, order the coefficients* $x^t(i)$ *in increasing order. The endpoints of the 95% confidence interval for* $x_J(i)$ *are the 2.5th percentile and the 97.5th percentile of* $x^t(i)$*.*

The p-value for $x_J(i)$ *is calculated by finding the first* k *such that the ordered* $x_J^k(i)$ *changes signs, if* $x_J^t(i)$ *does not change signs, then we define* $k = 1$ *by convention. Then the p-value is calculated as* $p = \frac{2k}{T}$ *if* $k < \frac{T}{2}$ *or* $p = \frac{2(k - T/2)}{T}$ *otherwise.*

In step 1 of Algorithm 5.1.1, we statistically normalize the data. Definition 5.1.12 defines this in a matrix operator sense.

Definition 5.1.12 (Column average)**.** *The column average of a matrix* $A \in R^{n \times m}$*, is a matrix* $\overline{A} \in R^{n \times m}$ *defined column-wise. Each entry in column* i *of* $\overline{A}$ *is*

$$\overline{A}_{j,i} = average(A_{\cdot,i}), \quad \forall i \in 1, \cdots, m, \ \forall j \in 1, \cdots, n. \tag{5.11}$$

Lemma 5.1.13. *If* $\tilde{x}$ *is the ordinary least squares (OLS) solution to* $Ax = b$*, then* $\tilde{x}$ *is the OLS solution to* $(A - \overline{A})x = b$ *if and only if* $\overline{A}^*(b - A\tilde{x}) = 0$.

Proof. The OLS $\tilde{x}$ satisfies

$$A^*A\tilde{x} = A^*b$$

by writing $A = A - \overline{A} + \overline{A}$ and collecting terms, we get that $\tilde{x}$ satisfies

$$(A - \overline{A})^*(A - \overline{A})\tilde{x} = (A - \overline{A})^*b + \overline{A}^*(b - A\tilde{x}) - (A - \overline{A})^*\overline{A}\tilde{x}.$$

However, $(A - \overline{A})^* \overline{A} = 0$, so the previous line is true if and only if

$$(A - \overline{A})^*(A - \overline{A})\tilde{x} = (A - \overline{A})^* b + \overline{A}^*(b - A\tilde{x})$$

□

Lemma 5.1.13 shows that if the residual of the OLS solution is in the nullspace of the $\overline{A}^*$ operator, that is, the sum of the residuals is 0, then the solution of the modified problem is equivalent to the solution to the original problem.

5.2 VALIDATION OF THE BRAIN-GAIT CORRELATOR

We validate the Brain-Gait Correlator through two problems in this section. For both, we create an exact solution mimicking the type of behavior we expect to see in the correlation of real brain measurements to gait measurements, that is a few coefficients that are significant and the rest having no correlation. We calculate the right hand side data b by multiplying the matrix A with the created dependencies x, and noise is then added to this data. The system is solved using the Brain-Gait Correlator algorithm. Since the exact solution is known, the error between the true solution of the noise free problem and the computed solution of the noisy problem with the Brain-Gait Correlator can be computed.

A successful algorithm will produce a solution with an error on the order of the noise input and a small confidence interval containing the noise free solution. The successful algorithm will also produce a solution with small p-values for all significant variables and have a near optimal choice for the regularization parameter. The optimal regularization parameter (generally unknowable) is defined as the regularization parameter that minimizes the error between the approximated solution and the true solution.

The first problem uses real brain volume measurements of the ROIs and synthesized walking speeds by taking a hypothesized correlation equation and determining what speeds correspond to each set of brain measurements. The second problem is a synthetic example where the matrix A is highly co-linear.

5.2.1 Brain measurement data with synthetic gait data

For this validation the data is created by taking actual brain measurements and correlation coefficients from actual data using a least squares solution of the Healthy Brain Project data. These are the target coefficients listed in Table 8. We add normally distributed noise (with mean 0 and standard deviation 0.87) to the right hand side, our simulated gait variable. This variation in noise corresponds to the variation of the actual gait measurements from the Healthy Brain Project data in Section 5.3. The regression calculation only uses the data from the measurements of the variables listed in Table 8. In this experiment, there were 97 subjects and 10 coefficients to calculate. Brain measurements were selected by first using a regression analysis of the Healthy Brain Project data and choosing the most significant regions.

The calculation is run using 1000 bootstrap steps and is summarized in Table 8. Table 8 shows that all ROIs are reported significant and there is only one brain variables (total_gm) that is not considered statistically significant in this calculation, but the calculated value is close to the true value. Also to note is that the age and log pallidum measurements are statistically significant, but the true coefficients fall outside the 95% confidence interval. The total gray matter and baseline constant terms are within the confidence range. Algorithm 5.1.1 and least squares regression (the case where $\alpha = 0$) both determine five out of the six brain variables are significant. The regularization parameter chosen was 2.395e-07 signifying a small amount of regularization is needed.

Next we add measurements of the other 23 measured gray matter volume variables that do not occur in the exact regression equation. That is, the true coefficients for each term should be zero. The Brain-Gait Correlator applied to the entire data reports that two out of the six brain variables are significant with a third that is nearly significant. Least squares gives comparable results with three of the brain variables reported as significant. These results are sorted in order of increasing p-values and summarized in Table 9 for the Brain-Gait Correlator and Table 11 for least squares regression.

Table 8: True values used to simulate the data and regression coefficients calculated using Algorithm 5.1.1 on problem 5.2.1 (the synthetic gait test) using 5 ROIs, only the regions used to create the data. All 5 of the brain ROI calculated coefficients are reported as statistically significant.

Variable	True Coef	In CI	Reg. Coef	95% Conf Int	p-value
Constant	-3.0e-6	yes	-0.020	(-0.076 , 0.039)	0.484
black	-0.20	yes	-0.148	(-0.203 , -0.096)	0.002
male	0.26	yes	0.235	(0.177 , 0.297)	0.002
age	-0.28	no	-0.220	(-0.272 , -0.161)	0.002
gray matter (total)	-0.05	yes	-0.076	(-0.168 , 0.008)	0.080
putamen (left)	0.21	yes	0.155	(0.080 , 0.235)	0.002
cingulum post (right)	-0.13	yes	-0.162	(-0.224 , -0.102)	0.002
cuneus (right)	0.15	yes	0.127	(0.059 , 0.197)	0.002
dLPFC (left)	0.12	yes	0.146	(0.078 , 0.216)	0.002
log pallidum (left)	-0.21	no	-0.096	(-0.176 , -0.017)	0.012

Table 9: Regression coefficients using the Brain-Gait Correlator on the problem 5.2.1 (the synthetic gait test) using all 33 available brain volumes from ROI and demographic variables. Note that the calculated coefficients for all ROI lie in the 95% confidence interval.

Variable	True Coef	In CI	Reg. Coef	95% Conf Int	p-value
Constant	3.0e-6	yes	-0.019	(-0.084 , 0.039)	0.492
black	-0.20	yes	-0.178	(-0.250 , -0.104)	0.002
male	0.26	yes	0.234	(0.158 , 0.302)	0.002
age	-0.28	yes	-0.232	(-0.303 , -0.156)	0.002
gray matter (total)	-0.05	yes	0.003	(-0.276 , 0.258)	0.992
cingulum post (right)	-0.13	yes	-0.147	(-0.249 , -0.040)	0.006
dLPFC (left)	0.12	yes	0.132	(0.032 , 0.232)	0.008
cuneus (right)	0.15	yes	0.122	(-0.011 , 0.239)	0.072
putamen (right)	0.00	yes	0.114	(-0.036 , 0.266)	0.108
precuneus (left)	0.00	yes	-0.079	(-0.206 , 0.032)	0.174
postcentral (left)	0.00	yes	0.095	(-0.042 , 0.239)	0.180
parietal sup (left)	0.00	yes	0.067	(-0.037 , 0.162)	0.214
precuneus (right)	0.00	yes	-0.066	(-0.186 , 0.060)	0.286
postcentral (right)	0.00	yes	-0.058	(-0.225 , 0.095)	0.396

Table 10: Continuation of Table 9.

Variable	True Coef	In CI	Reg. Coef	95% Conf Int	p-value
log pallidum (left)	-0.21	yes	-0.057	(-0.219 , 0.098)	0.506
parietal inf (right)	0.00	yes	0.034	(-0.069 , 0.134)	0.522
cuneus (left)	0.00	yes	0.035	(-0.081 , 0.139)	0.528
caudate (right)	0.00	yes	0.030	(-0.089 , 0.133)	0.586
log pallidum (right)	0.00	yes	-0.043	(-0.195 , 0.102)	0.610
hippocampus (right)	0.00	yes	-0.027	(-0.139 , 0.087)	0.622
putamen (left)	0.21	yes	0.044	(-0.134 , 0.216)	0.664
precentral (right)	0.00	yes	-0.024	(-0.163 , 0.127)	0.754
dLPFC (right)	0.00	yes	-0.020	(-0.137 , 0.091)	0.762
precentral (left)	0.00	yes	-0.019	(-0.169 , 0.132)	0.768
parietal inf (left)	0.00	yes	-0.019	(-0.145 , 0.105)	0.818
cerebellum (right)	0.00	yes	-0.020	(-0.203 , 0.161)	0.824
cingulum post (left)	0.00	yes	0.015	(-0.097 , 0.120)	0.856
cerebellum (left)	0.00	yes	-0.018	(-0.259 , 0.215)	0.870
parietal sup (right)	0.00	yes	-0.011	(-0.146 , 0.113)	0.872
thalamus (left)	0.00	yes	0.012	(-0.233 , 0.276)	0.916
hippocamus (left)	0.00	yes	-0.007	(-0.124 , 0.114)	0.934
thalamus (right)	0.00	yes	0.013	(-0.218 , 0.246)	0.944
caudate (left)	0.00	yes	0.001	(-0.121 , 0.123)	0.998

Table 11: Regression coefficients using ordinary least squares regression on Problem 5.2.1 (the synthetic gait test). The solution is similar to Algorithm 5.1.1 and reported in Table 9, because least squares regression gives a stable result.

Variable	Reg. Coef	95% Conf Int	p-value
Constant	-0.019	(-0.079 , 0.043)	0.552
black	-0.178	(-0.253 , -0.100)	0.002
male	0.234	(0.163 , 0.303)	0.002
Age	-0.232	(-0.311 , -0.158)	0.002
gray matter (total)	0.003	(-0.261 , 0.258)	0.954
Cingulum post (right)	-0.147	(-0.257 , -0.039)	0.006
Middle frontal gyrus (left)	0.132	(0.035 , 0.231)	0.010
Cuneus (right)	0.122	(-0.009 , 0.242)	0.070
Putamen (right)	0.114	(-0.031 , 0.267)	0.112
Parietal Sup (left)	0.067	(-0.038 , 0.180)	0.188
Postcentral (left)	0.095	(-0.054 , 0.233)	0.192
Precuneus (left)	-0.079	(-0.202 , 0.041)	0.200
Precuneus (right)	-0.066	(-0.191 , 0.069)	0.364
Postcentral (right)	-0.058	(-0.208 , 0.096)	0.426

Table 12: Continuation of Table 11.

Variable	Reg. Coef	95% Conf Int	p-value
Cuneus (left)	0.035	(-0.068 , 0.147)	0.512
Parietal inf (right)	0.034	(-0.069 , 0.147)	0.518
Log pallidum (left)	-0.057	(-0.209 , 0.114)	0.534
Log pallidum (right)	-0.043	(-0.196 , 0.096)	0.552
Hippocampus (right)	-0.027	(-0.132 , 0.076)	0.622
Caudate (right)	0.030	(-0.082 , 0.138)	0.632
Putamen (left)	0.044	(-0.136 , 0.208)	0.648
Middle frontal gyrus (right)	-0.020	(-0.128 , 0.091)	0.728
Parietal inf (left)	-0.019	(-0.140 , 0.096)	0.752
Precentral (right)	-0.024	(-0.178 , 0.125)	0.766
Cingulum post (left)	0.015	(-0.096 , 0.121)	0.792
Precentral (left)	-0.019	(-0.176 , 0.119)	0.796
Cerebellum (right)	-0.020	(-0.216 , 0.158)	0.822
Parietal sup (right)	-0.011	(-0.142 , 0.110)	0.834
Thalamus (right)	0.013	(-0.208 , 0.260)	0.866
Cerebellum (left)	-0.018	(-0.246 , 0.204)	0.910
Hippocampus (left)	-0.007	(-0.123 , 0.107)	0.912
Caudate (left)	0.001	(-0.129 , 0.125)	0.934
Thalamus (left)	0.012	(-0.244 , 0.264)	0.966

5.2.2 Synthetic problem with high approximate co-linearity

This validation used three variables (called x_1, x_2, and x_3) and a baseline (called Constant) that correlated with the outcome y. The outcome y had no correlation to the variables x_4 through x_{20}. The correlation used is

$$y = 0.1 + 1.0x_1 + 0.1x_2 + 0.1x_3. \tag{5.12}$$

We then created 100 sets of values for x_1 through x_{20} by forming five copies of a 20×20 Hilbert matrix, with entries $H_{i,j} = \frac{1}{i+j+1}$, joined together for a system that is 100×20. We calculate the y corresponding to the x via (5.12) and add 10% normally distributed noise to y ($\frac{\|noise\|}{\|y\|} = 0.10$). Table 13 reports the results of the Brain-Gait Correlator applied to this problem with 2000 bootstrap steps. Due to the definition of the correlation coefficients in (5.12), we do not normalize the system (step 1 in 5.1.1). This is not significant computationally as the normalization of this problem reduces the condition number from 4.7×10^{18} to 7.9×10^{16}. The stopping condition determined $J = 1$ to be optimal.

Table 13 also shows the 4 nonzero coefficients in the noise free solution, that is x_1, x_2, x_3 and the constant term, as significant. The x_4 term is also reported significant. Table 13 also shows that the true correlation coefficients for values of the constant term and x_3 lie within the calculated confidence intervals and the x_1 calculated solution is within 9% of the noise free solution. The x_2 calculated coefficient has the correct correlation direction, though it is more than twice the noise free solution.

The relative error of the approximated solution using the Brain-Gait Correlator is 16.87% which is the same order of magnitude as the noise (10%). The regularization parameter chosen by the Brain-Gait Correlator algorithm is $\alpha = 0.001$ which suggests that some regularization is necessary to accurately solve this problem. We calculate the actual optimal regularization parameter by finding the value of α that minimizes $\|x_{true} - x(\alpha)\|$. The optimal parameter is $\alpha = .0001887$ which is close to our chosen regularization parameter.

The results presented in Table 14 come from forcing $\alpha = 0$, corresponding to no regularization (least squares regularization). The relative error in this solution is $9,324,000\%$. Table 14 also shows that none of the variables are reported as significant.

Table 13: Solution using the Brain-Gait Correlator on problem 5.2.2. Note that all of the variables used to create the data ($x_1 - x_3$) and the constant term, as well as x_4, are reported as significant, and $x_5 - x_{20}$ are insignificant.

Variable	Reg. Coef	95% Conf Int	p-value
Constant	0.096	(0.060 , 0.119)	0.001
x_1	0.915	(0.772 , 0.973)	0.001
x_2	0.241	(0.217 , 0.332)	0.001
x_3	0.088	(0.056 , 0.181)	0.001
x_4	0.034	(0.000 , 0.118)	0.045
x_5	0.011	(-0.024 , 0.083)	0.309
x_6	0.001	(-0.036 , 0.063)	0.626
x_7	-0.004	(-0.041 , 0.050)	0.904
x_8	-0.007	(-0.043 , 0.041)	0.906
x_9	-0.008	(-0.042 , 0.035)	0.815
x_{10}	-0.008	(-0.041 , 0.029)	0.738
x_{11}	-0.008	(-0.040 , 0.025)	0.675
x_{12}	-0.008	(-0.039 , 0.023)	0.631
x_{13}	-0.007	(-0.037 , 0.021)	0.594
x_{14}	-0.007	(-0.035 , 0.019)	0.565
x_{15}	-0.007	(-0.033 , 0.017)	0.546
x_{16}	-0.006	(-0.031 , 0.016)	0.543
x_{17}	-0.006	(-0.030 , 0.015)	0.530
x_{18}	-0.005	(-0.028 , 0.014)	0.522
x_{19}	-0.005	(-0.027 , 0.013)	0.517
x_{20}	-0.005	(-0.025 , 0.012)	0.511

Table 14: Solution using least squares ($\alpha = 0$ in Algorithm 5.1.1) on Problem 5.2.2. Note that the ordinary least squares solution fails: 10% noise in the data is amplified to 9,000,000% error in the solution.

Variable	Reg. Coef	95% Conf Int	p-value
Constant	-5.318	(-72.131 , 46.932)	0.674
x_1	-457.425	(-856.118 , 493.905)	0.556
x_2	19459.666	(-18538.570 , 30817.381)	0.605
x_3	-192556.227	(-264417.095 , 177377.668)	0.693
x_4	684626.985	(-688145.101 , 869414.940)	0.790
x_5	-734336.274	(-926195.934 , 891065.970)	0.913
x_6	-556687.510	(-735565.866 , 560915.710)	0.783
x_7	448789.414	(-651855.744 , 568921.101)	0.954
x_8	1932993.526	(-2465071.196 , 2423511.588)	0.965
x_9	100072.993	(-126791.223 , 209479.022)	0.604
x_{10}	-3159960.633	(-4021219.077 , 4439855.858)	0.970
x_{11}	-932341.999	(-1212020.826 , 1205611.293)	0.952
x_{12}	1320998.037	(-1747726.667 , 1660887.956)	0.995
x_{13}	1325016.498	(-2014809.971 , 1693703.844)	0.933
x_{14}	5031673.344	(-6586852.012 , 6283665.792)	0.985
x_{15}	-6576167.402	(-8234187.248 , 8538522.537)	0.984
x_{16}	111471.992	(-694018.433 , 469540.741)	0.709
x_{17}	283431.407	(-576290.682 , 852003.799)	0.678
x_{18}	774668.858	(-1381401.472 , 1099715.404)	0.893
x_{19}	620896.589	(-751750.672 , 782239.520)	0.910
x_{20}	-500949.194	(-651349.658 , 751644.675)	0.935

This validation shows that in cases with high co-linearity of the measurements $(x_1 - x_{20})$ and noise in the observed data, regularization is necessary to obtain an accurate answer. The Brain-Gait Correlator provides the correct amount of regularization with no knowledge of the amount of noise added to the system.

These two experiments show that Algorithm 5.1.1 automatically selects whether or not least squares regression is optimal. If least squares regression is not the optimal method, it selects a method that gives a much more reliable solution.

5.3 APPLICATION OF THE BRAIN-GAIT CORRELATOR TO REAL MEASUREMENTS

The data used in this section comes from the Healthy Brain Project and the Cardiovascular Health Study (CHS) [77]. In the following experiment, we apply the Brain-Gait Correlator algorithm to this data. We have no á priori estimate of the noise level, so we pick a small value for the stopping criterion instead of using Algorithm 5.1.9. In this case, we select $J = 1$ and the number of bootstrap steps to be 1000.

5.3.1 Healthy Brain Project

When analyzing 302 participants and using 28 different brain ROIs and 5 demographic variables, the condition number of the system is 1.9×10^7. However after standardizing, the condition number of the system is 16, and the algorithm selects $\alpha = 1.74 \times 10^{-11}$. The variables used for this test are the demographic variables (age, race, and gender) and the gray matter volume of brain ROIs. We assigned a numerical gender variable of 0 if the participant is female and 1 if the participant is male. Similarly, a numerical race variable of 0 was assigned if the participant is black and 1 if the participant is white. The calculated coefficients are listed in order of increasing p-values in Table 15.

Table 15 shows that all of the personal demographic variables are reported as significant. Also, the right region of the cuneus, the left region of dlpfc and the total gray matter are

close to being 95% significant ($0.05 < p < 0.1$).

5.3.2 Cardiovascular Health Study

We study the correlation of gait to brain size and activity for the data set obtained by CHS. When we applied the Brain-Gait Correlator algorithm to CHS data, we found that 3 of the first 4 brain regions (with p-value < 0.2) that the algorithm identified (BA11 right, BA9 left, BA45 left) overlapped with those identified using correlation analysis of each region at a time (BA11 Right and Left, BA6, 9,45 and cerebellum in the left hemisphere, Precuneus Right and Left) [77].

Table 17 shows the correlations between the ROIs selected from [77] and the gait speed using the Brain-Gait Correlator algorithm. This shows the Brain-Gait Correlator algorithm's use in selecting important ROIs to study further without applying the tedious methods of individual analysis used in [77].

5.4 CONCLUSION

The Brain-Gait Correlator algorithm addresses the four limitations of current methods in neuroimaging: noise, high correlation, large number of predictors and scalability. The algorithm is a robust method of calculating brain parameters. The Brain-Gait Correlator algorithm is built using components of least squares regression, regularization for enhanced stability, and automatic parameter selection via the L-curve method. When least squares regression works, the Brain-Gait Correlator produces comparable results as shown in Section 5.2.1. However, when least squares regression fails, the Brain-Gait Correlator still produces reliable results as shown in Section 5.2.2.

The analysis of the HBP dataset in Section 5.3.1 shows that smaller gray matter volume of the left Dorsolateral prefrontal cortex was the brain MRI variable most strongly associated with slower gait. This finding is consistent with the previous analysis [77]. Section 5.3.2 shows an additional use of the Brain-Gait Correlator as an identifier of significant ROIs in

Table 15: Regression coefficients from the Healthy Brain Project dataset using 33 parameters. The middle frontal gyrus (left) and cuneus (right) regions are the most significant ROIs examined.

Variable	Reg. Coef	95% Conf Int	p-value
Constant	0.973	(0.929 , 1.014)	0.002
race	0.109	(0.062 , 0.155)	0.002
gender	0.119	(0.069 , 0.169)	0.002
age	-0.050	(-0.075 , -0.029)	0.002
gray matter (total)	-0.075	(-0.164 , 0.014)	0.090
Middle frontal gyrus (left)	0.029	(-0.005 , 0.061)	0.084
cuneus (right)	0.033	(-0.006 , 0.070)	0.096
log pallidum (left)	-0.034	(-0.079 , 0.009)	0.124
cingulum post (right)	-0.030	(-0.069 , 0.008)	0.140
thalamus (right)	-0.036	(-0.090 , 0.018)	0.174
precentral (left)	0.029	(-0.015 , 0.066)	0.184
parietal inf (left)	0.022	(-0.013 , 0.058)	0.234
parietal sup (left)	-0.019	(-0.053 , 0.016)	0.254
caudate (left)	0.022	(-0.014 , 0.058)	0.268
postcentral (right)	0.022	(-0.017 , 0.064)	0.274
putamen (right)	0.028	(-0.022 , 0.080)	0.276
putamen (left)	0.025	(-0.028 , 0.072)	0.300

Table 16: Continuation of Table 15.

Variable	Reg. Coef	95% Conf Int	p-value
log pallidum (right)	-0.023	(-0.067 , 0.020)	0.338
parietal sup (right)	-0.016	(-0.052 , 0.017)	0.340
hippocampus (right)	0.015	(-0.018 , 0.052)	0.368
cerebellum (right)	0.023	(-0.034 , 0.078)	0.388
hippocampus (left)	0.017	(-0.021 , 0.052)	0.424
cerebellum (left)	-0.021	(-0.074 , 0.031)	0.458
thalamus (left)	0.019	(-0.037 , 0.071)	0.476
precuneus (right)	0.013	(-0.030 , 0.052)	0.560
precentral (right)	-0.012	(-0.054 , 0.029)	0.568
Middle frontal gyrus (right)	-0.009	(-0.045 , 0.028)	0.586
parietal inf (right)	0.009	(-0.024 , 0.040)	0.622
postcentral (left)	0.010	(-0.033 , 0.048)	0.628
cuneus (left)	0.009	(-0.028 , 0.045)	0.660
precuneus (left)	-0.007	(-0.046 , 0.034)	0.776
caudate (right)	-0.004	(-0.038 , 0.033)	0.804
cingulum post (left)	-0.002	(-0.040 , 0.039)	0.888

Table 17: Regression coefficients from the CHS dataset using 31 parameters. In one calculation, Algorithm 5.1.1 chooses 3 of the 6 regions that were previously identified as significant by calculations of each individual parameter.

Variable	Reg. Coef	95% Conf Int	p-value
Constant	0.927	(0.905 , 0.950)	0.002
ba11_r_m	0.063	(0.011 , 0.114)	0.014
ba45_r_m	-0.056	(-0.101 , -0.013)	0.014
ba9_l_mn	0.030	(-0.011 , 0.069)	0.148
ba45_l_m	0.028	(-0.014 , 0.072)	0.182
cereb_l	0.026	(-0.015 , 0.064)	0.216
ba40_l_m	-0.025	(-0.068 , 0.014)	0.234
ba39_r_m	-0.025	(-0.066 , 0.020)	0.246
ba7_l_mn	0.033	(-0.028 , 0.091)	0.278
Thalamus_L	-0.031	(-0.083 , 0.026)	0.286
Caudate_R	-0.021	(-0.061 , 0.019)	0.338
ba6_l_mn	0.024	(-0.024 , 0.075)	0.338
ba9_r_mn	-0.016	(-0.057 , 0.024)	0.402
Putamen_R	0.018	(-0.033 , 0.068)	0.454

Table 18: Continuation of Table 17.

Variable	Reg. Coef	95% Conf Int	p-value
ParaHippocampal_R	0.013	(-0.021 , 0.046)	0.456
Precuneus_R	-0.019	(-0.081 , 0.038)	0.492
ba7_r_mn	0.016	(-0.041 , 0.073)	0.568
cereb_r	0.011	(-0.031 , 0.056)	0.576
ba6_r_mn	0.013	(-0.036 , 0.065)	0.580
ba39_l_m	0.011	(-0.030 , 0.052)	0.594
Precuneus_L	-0.017	(-0.082 , 0.051)	0.608
ba46_r_m	0.010	(-0.034 , 0.055)	0.674
Putamen_L	-0.010	(-0.062 , 0.042)	0.706
ba40_r_m	-0.008	(-0.049 , 0.034)	0.712
ba11_l_m	0.012	(-0.042 , 0.065)	0.720
ba4_l_mn	-0.011	(-0.058 , 0.038)	0.724
Caudate_L	-0.009	(-0.053 , 0.036)	0.726
ba47_l_m	-0.008	(-0.051 , 0.035)	0.744
ba47_r_m	-0.006	(-0.051 , 0.035)	0.796
Thalamus_R	0.006	(-0.047 , 0.064)	0.834
ba46_l_m	-0.006	(-0.041 , 0.034)	0.852
ba4_r_mn	-0.001	(-0.050 , 0.039)	0.890
ParaHippocampal_L	-0.001	(-0.035 , 0.032)	0.932

a more direct manner than the previous analysis in [77].

6.0 CONCLUSIONS AND FUTURE RESEARCH

"Each problem that I solved became a rule, which served afterwards to solve other problems." (René Descartes)

6.1 CONCLUSIONS

Inverse problems are an integral part of the sciences and deserve consideration. Tikhonov regularization is a versatile method of solving these problems.

Chapter 2 demonstrated a superconvergence result: in the case when a regularity condition for iterated Tikhonov regularization is not globally satisfied, then some projections of the error are significantly smaller than the theoretical predictions. We examined the sensitivity of iterated Tikhonov regularization to the choice of the regularization parameter chosen. We showed that higher order sensitivities correct for accuracy. We presented an algorithm that is simple to implement, and it calculates the iterated Tikhonov updates and the sensitivities to the regularization parameter at a small computational cost more than the standard iterated Tikhonov calculation. Our numerical experiments agree with the sensitivity and superconvergence theory.

Chapter 3 examined a new modification to iterated Tikhonov-Lavrentiev regularization for the specific application of deconvolution of the differential filter. We showed that this modification to iterated Tikhonov-Lavrentiev decreases the theoretical error bounds from $\mathcal{O}(\alpha(\delta^2+1))$ for Tikhonov-Lavrentiev regularization to $\mathcal{O}((\alpha\delta^2)^{J+1})$. This result was extended to a generic iterated deconvolution method satisfying minimal assumptions in Chapter 4. We then applied the deconvolution method to the Leray deconvolution model of fluid

flow. We discretized the problem with Crank-Nicolson in time and finite elements in space. We showed existence, uniqueness and optimal convergence CNFE rates with the addition of the deconvolution errors for this solution. The convergence rates were confirmed quantitatively with a Taylor-Green vortex flow calculation. We examined the solution qualitatively by calculating the flow of a fluid over a step and observing the shedding of eddies.

We also examined the combination of iterated Tikhonov regularization, the L-curve method, a new stopping criterion and a bootstrapping algorithm, which we call the "Brain-Gait Correlator" as a general solution method in brain mapping. This combination of methods overcomes the difficulties associated with brain mapping: uncertainty quantification, co-linearity of the data, and data noise. We verified the algorithm against two problems that illustrate different difficulties. The algorithm performed at least as well as the standard method in brain mapping (ordinary least squares) in the worst case, and in the best case, it performed significantly better. We used the Brain-Gait Correlator to estimate correlation coefficients between brain regions and average walking speed as well as identify regions of interest for future analysis.

6.2 FUTURE RESEARCH

The results presented in this paper can be extended by answering the following questions. Modified Iterated Tikhonov:

- The filtering function uses homogenous or periodic boundary conditions. This is an acceptable assumption for fluid flow because of the no-slip condition. However, when you have inflow and outflow, what is the appropriate boundary condition to enforce? Consider the problem of $u(x, y) = \cos(\pi x)\cos(\pi y)$ in the region $[0, 1]^2$. The differential filter will give the solution of $\overline{u} = \frac{1}{2\delta^2\pi^2+1}u$ in the interior. Continuity requires that we define $\overline{u} = \frac{1}{2\delta^2\pi^2+1}u$ on the boundary.
- The analysis of Theorem 3.4.2 requires $\alpha \leq \frac{1}{2}$ to guarantee that the minimization of the noisy energy functional is also minimizing the noise-free energy functional, and this condition is necessary in the analysis. An enforced boundary on α, such as $\alpha \leq 1/2$ for

the problem $Ax = b$ can be avoided by solving $\frac{1}{N}Ax = \frac{1}{N}b$. The condition number of this new problem is the same as the old problem, but the regularization parameter needs to be smaller by a factor of N to obtain the same results. The new α_N needed might be under $\frac{1}{2}$ and thus satisfy the minimization of noise-free energy criterion, but the original problem with α would not satisfy the criterion.

Brain Imaging:

- The ultimate goal was to obtain reliable and repeatable numerical relations between gait speed and ROI data. The next step to take is to extend the analysis and numerical calculations to enforce sparsity conditions. This will look for the few regions that give the largest results. One sparsity enforcing method is to use ℓ^p norms in the minimization formulation of Tikhonov regularization. That is, in the space of acceptable regularization coefficients Ω and for $1 \leq p \leq 2$,

$$x_{\alpha,p} = \arg\min_{x\in\Omega} \|Ax - b\|^2 + \alpha\|x\|_{\ell^p}^p. \tag{6.1}$$

  The minimization calculation puts a larger weight on small components of x with smaller values of p compared to $p = 2$, especially for the limiting case $p = 1$. An iterative threshold algorithm for this problem is presented in [18]. Further examples of sparse solves can be found in [74]

- The Brain-Gait Correlator uses a statistical normalization. Lemma 5.1.13 gives a condition for when the ordinary least squares solution before normalization and after normalization are equivalent. Can we quantify the amount of change in the solution due to the normalization? For instance, if $\tilde{x}$ is the OLS solution of the original problem and $x^\dagger$ is the OLS solution of the normalized problem, then it can be shown (using $(A-\overline{A})^*\overline{A} = 0$) that the difference between the two is

$$\tilde{x} - x^\dagger = (A^*A)^{-1}\overline{A}^*(b + \overline{A}x^\dagger).$$

  Does this equation lead to estimates to how the condition numbers of A compare to $A - \overline{A}$ (which will tell us about the amount of regularization needed)?

- The statistical normalization step in step 1 of Algorithm 5.1.1 is a standard process in statistics [8, 43, 44, 69]. Applying ordinary least squares (OLS) regularization with an infinite precision computer and a finite (but possibly large) condition number before normalization and then normalizing the results afterward gives the exact same results as normalization before OLS. The normalization process before regularization helps due to its reduction of the condition number and the finiteness of computer arithmetic. Tikhonov regularization (and iterated Tikhonov regularization) will have a different result because of the meaning of αI before and after normalization. Is there a benefit in waiting to normalize after applying Tikhonov regularization?
- The problem in Chapter 5 is to analyze the equation $Ax = b$ when error is in the observed right hand side gait data. However, the measurements of A come from brain MRI scans. These scans are then transformed into a standard brain template to analyze the amounts of brain volume and activity in a given section. These measurements and transformations are potentially noisy, so there will be noise in the operator A. The next step to analyzing this problem is to extend the current analysis to use total least squares (TLS) [32], as opposed to ordinary least squares which only assumes noise in the right hand side. This generalizes to Tikhonov regularization of the TLS [7, 31]. This can be further extended to iterated Tikhonov regularization in the same method as Chapter 5.
- The data analyzed in this problem comes from real measurements. Currently, if one of those measurements is missing, then the algorithm (in the select valid participants step) eliminates that participant's data from the analysis. In one case, about half of the participants were missing one particular measurement, and the number of valid participants dropped from approximately 300 to approximately 150. The operator had to screen the data before the analysis could begin to eliminate the problem measurements. The next question to answer is what can be done algorithmically for missing data.

BIBLIOGRAPHY

[1] A. Alekseev and I. Navon, *The analysis of an ill-posed problem using multi-scale resolution and second order adjoint techniques*, C.M.A.M.E., 190 (2001), pp. 1486–1496.

[2] M. Anitescu and W. Layton, *Sensitivities in large eddy simulation and improved estimates of turbulent flow functionals*, SIAM J. Scientific Computing, 29 (2007), pp. 1650–1667.

[3] F. Anselmet, Y. Gagne, E. J. Hopfinger, and R. A. Antonia, *High-order velocity structure function in turbulent shear flows*, J. Fluid Mech., 140 (1984), pp. 63–89.

[4] A. Bakushinsky and M. Y. Kokurin, *Iterative methods for approximate solution of inverse problems*, Kluwer, Dordrecht, the Netherlands, 2004.

[5] R. Baloh, S. Ying, and K. Jacobson, *A longitudinal study of gait and balance dysfunction in normal older people*, Arch Neurol, 60 (2003), pp. 835–9.

[6] R. Baloh, Q. Yue, T. Socotch, and K. Jacobson, *White matter lesions and disequilibrium in older people. I. case-control comparison*, Arch Neurol, 52 (1995), pp. 970–4.

[7] A. Beck and A. Ben-Tal, *On the solution of the Tikhonov regularization of the total least squares problem*, SIAM J. on Optimization, 17 (2006), pp. 98–118.

[8] D. A. Belsley, E. Kuh, and R. E. Welsch, *Regression Diagnostics: Identifying Influential Data and Sources of Collinearity*, vol. 546, Wiley, Hoboken, NJ, 1980.

[9] R. Benson, C. Guttmann, X. Wei, S. Warfield, C. Hall, J. Schmidt, R. Kikinis, and L. Wolfson, *Older people with impaired mobility have specific loci of periventricular abnormality on MRI*, Neurology, 58 (2002), pp. 48–55.

[10] L. Berselli, T. Iliescu, and W. Layton, *Mathematics of Large Eddy Simulations of Turbulent Flows*, Springer, Berlin, 2006.

[11] M. Bertero and B. Boccacci, *Introduction to Inverse Problems in Imaging*, Institute of Physics Publishing Ltd, Bristol, UK, 1998.

[12] J. Borggaard and J. Burns, *A PDE sensitivity equation method for optimal aerodynamic design*, J.C.P, 136 (1997), pp. 366–384.

[13] S. Brenner and L. R. Scott, *The Mathematical Theory of Finite Element Methods*, Springer-Verlag, New York, 1994.

[14] C. Brezinski, M. Redivo-zaglia, G. Rodriguez, and S. Seatzu, *Extrapoloation techniques for ill-conditioned linear systems*, J. Approx. Theory, 49 (1998), pp. 1–29.

[15] R. Bryan, S. Wells, T. Miller, A. Elster, C. Jungreis, V. Poirier, B. Lind, and T. Manolio, *Infarct like lesions in the brain: Prevalence and anatomic characteristics at MR imaging of the elderly-data from the cardiovascular health study*, Radiology, 202 (1997), pp. 47–54.

[16] H. Choi and P. Moin, *Effects of the computational time step on numerical solutions of turbulent flow*, J. Comp. Physics, 113 (1994), pp. 1–4.

[17] A. J. Chorin, *Numerical solution of the Navier-Stokes equations*, Math. Comp., 22 (1968), pp. 745–762.

[18] I. Daubechies, M. Defrise, and C. D. Mol, *An iterative thresholding algorithm for linear inverse problems*, Communications on Pure and Applied Mathematics, 57 (2004), pp. 1413–1457.

[19] A. Dunca, *Space avereged Navier-Stokes equations in the presence of walls*, Ph.D. Thesis, University of Pittsburgh, (2004).

[20] B. Efron and R. J. Tibshirani, *An Introduction to the Bootstrap*, Chapman and Hall, New York, 1993.

[21] H. Engl, *On the choice of the regularization parameter for iterated Tikhonov regularization of inverse problems*, J. Approx. Theory, 49 (1987), pp. 55–63.

[22] H. Engl, C. Flamm, P. Kügler, J. Lu, S. Müller, and P. Schuster, *Inverse problems in systems biology*, Inverse Problems, 25 (2009), p. 123014.

[23] H. Engl, M. Hanke, and A. Neubauer, *Regularization of inverse problems*, Kluwer, Dordrecht, the Netherlands, 1996.

[24] L. Fried and N. Borhani, *The cardiovascular health study: design and rationale*, Ann Epidemiol, 1 (1991), pp. 263–76.

[25] G. Galdi, *An Introduction to the Mathematical Theory of the Navier-Stokes Initial-Boundary Value Problem*, Birkhauser, Basel, New York, 2000.

[26] M. Germano, *Differential filters for the large eddy numerical simulation of turbulent flows*, Phys. Fluids, 29 (1986), pp. 1755–1757.

[27] ——, *Differential filters of elliptic type*, Phys. Fluids, 29 (1986), pp. 1757–1758.

[28] B. Geurts, *Inverse modeling for large eddy simulations*, Phys. Fluids, 9 (1997), p. 3585.

[29] H. Gfrerer, *An a posteriori parameter choice for ordinary and iterated Tikhonov regularization leading to optimal convergence rates*, Math. Comp., 49 (1987), pp. 507–522.

[30] V. Girault and P. Raviart, *Finite Element approximation of the Navier-Stokes equations*, Springer-Verlag, New York-Berlin, 1979.

[31] G. H. Golub, P. C. Hansen, and D. P. O'Leary, *Tikhonov regularization and total least squares*, SIAM J. Matrix Anal. Appl, 21 (1997), pp. 185–194.

[32] G. H. Golub and C. F. V. Loan, *An analysis of the total least squares problem*, SIAM Journal on Numerical Analysis, 17 (1980), pp. 883–893.

[33] H. Grant, R. Stewart, and A. Moilliet, *Turbulence spectra from a tidal channel*, J. Fluid Mech., 12 (1962), pp. 241–263.

[34] M. D. Gunzburger, *Perspectives in Flow Control and Optimization*, Society for Industrial and Applied Mathematics, Philadelphia, PA, USA, 2002.

[35] X. Guo, B. Steen, M. Matousek, L. Andreasson, L. Larsson, S. Palsson, V. Sundh, and I. Skoog, *A population-based study on brain atrophy and motor performance in elderly women*, J Gerontol A Biol Sci Med Sci, 56 (2001), pp. M633–7.

[36] U. Hämarik, R. Palm, and T. Raus, *Use of extrapolation in regularization methods*, J. Inverse and Ill-Posed Problems, 15 (2007), pp. 277–294.

[37] U. Hämarik, R. Palm, and T. Raus, *Extrapolation of Tikhonov and Lavrentiev regularization methods*, Journal of Physics: Conference Series, 135 (2008), p. 012048.

[38] U. Hamarik and U. Tautenhahn, *On the monotone error rule for parameter choice in iterative and continuous regularization methods*, BIT, 41 (2001), pp. 1029–1038.

[39] M. Hanke and C. Groetsch, *Nonstationary iterated Tikhonov regularization*, J. Optim. Theory and Appl., 98 (1998), pp. 36–53.

[40] P. Hansen, *Analysis of discrete ill-posed problems by means of the L-curve*, SIAM Review, 34 (1992), pp. 561–580.

[41] ——, *Regularization tools: A Matlab package for analysis and solution of discrete ill-posed problems*, Numer. Algorithms, 6 (1994), pp. 1–35.

[42] P. C. Hansen and D. P. O'Leary, *The use of the L-curve in the regularization of discrete ill-posed problems*, SIAM J. Sci. Comput., 14 (1993), pp. 1487–1503.

[43] A. E. Hoerl and R. W. Kennard, *Ridge regression: Applications to nonorthogonal problems*, Technometrics, 12 (1970), pp. pp. 69–82.

[44] ——, *Ridge regression: Biased estimation for nonorthogonal problems*, Technometrics, 42 (2000), pp. pp. 80–86.

[45] B. Hoffman, *Regularization for Applied Inverse and Ill-Posed Problems*, Teubner, Leipzig, 1986.

[46] R. Horn and C. Johnson, *Matrix Analysis*, Cambridge University Press, New York, 1985.

[47] K. Jahn, A. Deutschländer, T. Stephan, M. Strupp, M. Wiesmann, and T. Brandt, *Brain activation patterns during imagined stance and locomotion in functional magnetic resonance imaging*, Neuroimage, 22 (2004), pp. 1722–1731.

[48] V. John and W. J. Layton, *Analysis of numerical errors in large eddy simulation*, SIAM J. Numer. Anal., 22 (2002), pp. 995–1020.

[49] V. John, W. J. Layton, and N. Sahin, *Derivation and analysis of near wall models for channel and recirculating flows*, Comput. Math. Appl., 48 (2004), pp. 1135–1151.

[50] A. Jorm and D. Jolley, *The incidence of dementia: a meta-analysis*, Neurology, 51 (1998), pp. 728–33.

[51] J. King and D. Chillingworth, *Approximation of generalized inverses by iterated regularization*, Numer. Functional Anal. and Optim., 1 (1979), pp. 499–513.

[52] K. Kinsella and V. A. Velkoff, *An Aging World: 2001*, US Bureau of the Census, Washington, DC, 2001.

[53] A. Kirsch, *An Introduction to the Mathematical Theory of Inverse Problems*, Springer, New York, 2011.

[54] A. Kolmogorov, *The local structure of turbulence in incompressible viscous fluids at very large Reynolds numbers*, Dokl. Akad. Nauk. SSSR, 30 (1941), pp. 301–305.

[55] L. Kuller, A. Arnold, W. Longstreth Jr., T. Manolio, D. O'Leary, G. Burke, L. Fried, and A. Newman, *White matter grade and ventricular volume on brain MRI as markers of longevity in the cardiovascular health study*, Neurobiol Aging, 28 (2007), pp. 1307–15.

[56] A. Labovskiy and C. Trenchea, *Approximate deconvolution models for magnetohydrodynamics*, Numerical Functional Analysis and Optimization, 31 (2010), pp. 1362–1385.

[57] M. Lavrentiev, *Some improperly posed problems in mathematical physics*, Nauka, Moscow, second ed., 1979.

[58] W. Layton, *Introduction to the Numerical Analysis of Incompressible Viscous Flows*, SIAM, Philadelphia, 2008.

[59] W. Layton and R. Lewandowski, *Residual stress of approximate deconvolution large eddy simulation models of turbulence*, Journal of Turbulence, 46 (2006), pp. 1–21.

[60] W. Layton and M. Neda, *Truncation of scales by time relaxation*, JMAA, 325 (2006), pp. 788–807.

[61] W. Layton and L. Tobiska, *A two-level method with backtracking for the Navier-Stokes equations*, SIAM J. Numer. Anal., 35 (1998), pp. 2035–2054.

[62] A. Leonov, *On the accuracy of Tikhonov regularizing algorithms and quasioptimal selection of of a regularization parameter*, Soviet Math. Dokl., 44 (1992), pp. 711–716.

[63] J. Leray, *Sur le movement d'un fluide visqueux emplissant l'espace*, Acta Math, 63 (1934), pp. 193–248.

[64] J. Liu, *A sensitivity analysis for least squares ill-posed problems using the Haar basis*, SINUM, 31 (1994), pp. 1486–1496.

[65] O. Lopez, W. Jagust, C. Dulberg, J. Becker, S. DeKosky, A. Fitzpatrick, J. Breitner, C. Lyketsos, B. Jones, C. Kawas, M. Carlson, and L. Kuller, *Risk factors for mild cognitive impairment in the cardiovascular health study cognition study: Part 2*, Arch Neurology, 60 (2003), pp. 1394–1399.

[66] C. Manica and S. K. Merdan, *Convergence analysis of the finite element method for a fundamental model in turbulence*, Technical Report Server, Mathematics Department, University of Pittsburgh, http://www.mathematics.pitt.edu/documents/0612.pdf, (2006).

[67] C. Manica and I. Stanculescu, *Numerical analysis of Leray-Tikhonov deconvolution models of fluid motion*, Comput. Math. Appl., 60 (2010), pp. 1440–1456.

[68] K. Manton, L. Corder, and E. Stallard, *Chronic disability trends in elderly United States populations: 1982-1994*, Proc Natl Acad Sci, 94 (1997), pp. 2593–8.

[69] D. W. Marquardt, *A critique of some ridge regression methods: Comment*, Journal of the American Statistical Association, 75 (1980), pp. pp. 87–91.

[70] F. Natterer, *Error bounds for Tikhonov regularization in Hilbert scales*, Appl. Anal., 18 (1984), pp. 262–270.

[71] S. Perera, S. Studenski, J. Chandler, and J. Guralnik, *Magnitude and patterns of decline in health and function in 1 year affect subsequent 5-year survival*, J. Gerontol A Biol Sci Med Sci, 60 (2005), pp. 894–900.

[72] O. Pironneau, F. Hecht, and J. Morice, *FreeFEM++, http://www.freefem.org.*

[73] S. Pope, *Turbulent Flows*, Cambridge Univ. Press, Cambridge, 2000.

[74] R. Ramlau and G. Teschke, *A Tikhonov-based projection iteration for nonlinear ill-posed problems with sparisty constraints*, Numer. Math., 104 (2006), pp. 177–203.

[75] W. Rheinboldt, *On measures of ill-conditioning for nonlinear equations*, Mathematics of Computation, 30 (1976), pp. 104–111.

[76] C. Rosano, H. Aizenstein, J. Brach, A. Longenberger, S. Studenskiand, and A. Newman, *Gait measures indicate underlying focal gray matter atrophy in the brain of older adults*, Journal of Gerontology: Medical Sciences, 63A (2008), pp. 1380–1388.

[77] C. Rosano, H. Aizenstein, S. Studenski, and A. Newman, *A regions-of-interest volumetric analysis of mobility limitations in community-dwelling older adults*, Journal of Gerontology: Medical Sciences, 62A (2007), pp. 1048–1055.

[78] C. Rosano, J. Becker, O. Lopez, P. Lopez-Garcia, C. Carter, A. Newman, L. Kuller, and H. Aizenstein, *Morphometric analysis of gray matter volume in demented older adults: exploratory analysis of the cardiovascular health study brain MRI database*, Neuroepidemiology, 24 (2005), pp. 221–229.

[79] C. Rosano, J. Brach, W. Longstreth Jr, and A. Newman, *Quantitative measures of gait characteristics indicate prevalence of underlying subclinical structural brain abnormalities in high-functioning older adults*, Neuroepidemiology, 26 (2006), pp. 52–60.

[80] C. Rosano, J. Brach, S. Studenski, W. Longstreth Jr., and A. B. Newman, *Gait variability is associated with subclinical brain vascular abnormalities in high-functioning older adults*, Neuroepidemiology, 29 (2007), pp. 193–200.

[81] C. Rosano, A. Newman, R. Katz, C. Hirsch, and L. Kuller, *Association between lower digit symbol substitution test score and slower gait and greater risk of mortality and of developing incident disability in well-functioning older adults*, J Am Geriatr Soc, 56 (2008), pp. 1618–25.

[82] S. G. Saddoughi, *Local isotropy in complex turbulent boundary layers at high Reynolds number*, Journal of Fluid Mechanics, 348 (1997), pp. 201–245.

[83] S. G. Saddoughi and S. V. Veeravalli, *Local isotropy in turbulent boundary layers at high Reynolds number*, Journal of Fluid Mechanics, 268 (1994), pp. 333–372.

[84] P. Sagaut, *Large Eddy Simulation for Incompressible Flows*, Springer, Berlin, 2001.

[85] A. R. Sampson, *A tale of two regressions*, Journal of the American Statistical Association, 69 (1974), pp. 682–689.

[86] T. Schuster, *The Method of Approximate Inverses*, Springer, Berlin, 2007.

[87] G. A. F. Seber, *Multivariate Observations*, John Wiley & Sons, Inc., Hoboken, NJ, 2008.

[88] L. G. Shapiro and G. C. Stockman, *Computer Vision*, Prentence Hall, Upper Saddle River, NJ, 2001.

[89] C. Shaw Jr., *Improvements of the resolution of an instrument by numerical solution of an integral equation*, J. Math. Anal. Appl., 37 (1972), pp. 83–112.

[90] E. Shock, *Constructive methods for the practical treatment of integral equations*, Birkhauser, Basel, 1985.

[91] Z. Sidak, *On multivariate normal probabilities of rectangles: Their dependence on correlations*, Ann. Math. Statist., 39 (1968), pp. 1425–1434.

[92] ——, *On probabilities of rectangles in multivariate normal student distributions: their dependence on correlations*, Ann. Math. Statist., 42 (1971), pp. 169–175.

[93] E. M. Simonsick, A. B. Newman, M. C. Nevitt, S. B. Kritchevsky, L. Ferrucci, J. M. Guralnik, and T. Harris, *Measuring higher level physical function in well-functioning older adults: expanding familiar approaches in the Health ABC study*, J Gerontol A Biol Sci Med Sci, 56 (2001), pp. M644–9.

[94] S. Smith, *Fast robust automated brain extraction*, Hum Brain Mapp, 17 (2002), pp. 143–155.

[95] L. Stanley and D. Stewart, *Design sensitivity analysis: Computational issues of sensitivity equation methods*, vol. 25, Frontiers in Applied Math, SIAM, Philadelphia, 2002.

[96] J. Starr, S. Leaper, A. Murray, H. Lemmon, R. Staff, I. Deary, and L. Whalley, *Brain white matter lesions detected by magnetic resonance imaging are associated with balance and gait speed*, J. Neurol. Neurosurg. Psychiatry, 74 (2003), pp. 94–98.

[97] H. Stetter, *The defect correction principle and discretization methods*, Numer. Math., 29 (1978), pp. 425–443.

[98] S. Stolz, N. Adams, and L. Kleiser, *The approximate deconvolution model for large-eddy simulations of compressible flows and its application to shock-turbulent-boundary-layer interaction*, Physics of Fluids, 13 (2001), pp. 997–1015.

[99] S. Studenski, S. Perera, K. Patel, C. Rosano, K. Faulkner, M. Inzitari, J. Brach, J. Chandler, P. Cawthon, E. B. Connor, M. Nevitt, M. Visser, S. Kritchevsky, S. Badinelli, T. Harris, A. B. Newman, J. Cauley, L. Ferrucci, and J. Guralnik, *Gait speed and survival in older adults*, J. American Medical Association, 305 (2011), pp. 50–8.

[100] D. Tafti, *Comparison of some upwind-biased high-order formulations with a second-order central-difference scheme for time integration of the incompressible Navier-Stokes equations*, Computers & Fluids, 25 (1996), pp. 647–665.

[101] G. Tell, D. S. Lefkowitz, P. Diehr, and A. D. Elster, *Relationship between balance and abnormalities in cerebral magnetic resonance imaging in older adults*, Arch. Neurol., 55 (1998), pp. 73–9.

[102] J. Thirion, *Image matching as a diffusion process: an analogy with Maxwell's demons*, Med Image Anal, 2 (1998), pp. 243–260.

[103] A. Tikhonov and V. Arsenin, *Solution of Ill-Posed Problems*, Halsted Press, New York, 1977.

[104] ——, *Methods of solving ill-posed problems in Hilbert spaces*, Nauka, Moscow, 1979.

[105] N. Tzourio-Mazoyera, B. Landeaub, D. Papathanassioua, F. Crivelloa, O. Etarda, N. Delcroixa, B. Mazoyerc, and M. Joliota, *Automated anatomical labeling of activations in SPM using a macroscopic anatomical parcellation of the MNI MRI single-subject brain*, Neuroimage, 15 (2002), pp. 273–289.

[106] G. Vainikko, *Solution methods for linear ill-posed problems in Hilbert spaces*, Nauka, Moskow, 1982.

[107] G. Vainikko and A. Y. Veretennikov, *Iterative procedures in ill-posed problems*, Nauka, Moskow, 1982.

[108] H. Vinod, *Double bootstrap for shrinkage estimators*, Journal of Econometrics, 68 (1995), pp. 287–302.

[109] C. Vogel, *Computational Methods for Inverse Problems*, SIAM publications, Philadelphia, 2002.

[110] G. T. Whitman, T. Tang, A. Lin, and R. W. Baloh, *A prospective study of cerebral white matter abnormalities in older people with gait dysfunction*, Neurology, 57 (2001), pp. 990–994.

[111] L. Wolfson, X. Wei, C. Hall, V. Panzer, D. Wakefield, R. Benson, J. Schmidt, S. Warfield, and C. Guttmann, *Accrual of MRI white matter abnormalities in elderly with normal and impaired mobility*, J Neurol Sci, 232 (2005), pp. 23–27.

[112] R. P. Woods, S. T. Grafton, J. D. G. Watson, N. L. Sicotte, and J. C. Mazziotta, *Automated image registration: II. intersubject validation of linear and nonlinear models*, J Comput Assist Tomogr, 22 (1998), pp. 153–165.

[113] M. Wu, O. Carmichael, P. Lopez-Garcia, C. Carter, and H. Aizenstein, *Quantitative comparison of AIR, SPM, and the fully deformable model for atlas-based*

segmentation of functional and structural MR images, Hum Brain Mapp, 27 (2006), pp. 747–754.

[114] N. Yue, A. Arnold, W. Longstreth Jr, A. Elster, C. Jungreis, D. O'Leary, V. Poirier, and R. Bryan, *Sulcal, ventricular, and white matter changes at MR imaging in the aging brain: data from the cardiovascular health study*, Radiology, 202 (1997), pp. 33–39.

[115] Y. Zhang, M. Brady, and S. Smith, *Segmentation of brain MR images through a hidden Markov random field model and the expectation maximization algorithm*, IEEE Trans on Medical Imaging, 20 (2001), pp. 45–57.